Computational studies of the photophysical properties of Zn(II)-CAAC complexes

---

Master Thesis

by

Markus Putscher

January 2023

Institute for Theoretical and Computational Chemistry
Faculty of Mathematics and Natural Sciences
Heinrich-Heine University Düsseldorf

Reviewer	Prof. Dr. Christel M. Marian
Co-Reviewer	Prof. Dr. Christian Ganter

Abstract

In this work the photophysical and thermally activated delayed fluorescence (TADF) emitter properties of ^{Menth}CAAC-Zn(II)-BDT (Zn-BDT) and ^{Menth}CAAC-Zn(II)-BDO (Zn-BDO) were investigated. It was discovered that both molecules have several conformers that are energetically close and only differ in the position of their ligands towards each other. However, these conformers show little differences in their photophysical properties. All conformers of both molecules have low-lying singlet and triplet ligand-to-ligand charge-transfer (LLCT) states that qualify as emissive states. The spin–orbit couplings between these states are low, yet high (reverse) Intersystem Crossing rates are achieved in combination with tiny energy gaps. The phosphorescence rates are so low that only emission from the singlet state is expected. The fluorescence rates from the singlet LLCT states are high. The emission of Zn-BDT produces yellow light, while that of Zn-BDO is in the infrared region. Experimental results of Zn-BDT agreed well with the computational data. Both molecules are considered suitable as TADF-emitter materials, characterized by the emission of light of different wavelengths.

Zusammenfassung

Im Rahmen dieser Arbeit wurden zwei Moleküle, ^{Menth}CAAC-Zn(II)-BDT (Zn-BDT) und ^{Menth}CAAC-Zn(II)-BDO (Zn-BDO), auf ihre photophysikalischen und thermisch aktivierte verzögerte Fluoreszenz (TADF)-Emitter-Eigenschaften untersucht. Dabei zeigt sich für beide Moleküle, dass mehrere energetisch nah beieinander liegende Konformere auftreten, die sich durch die Stellung der Liganden zueinander unterscheiden. Diese zeigen in Bezug auf ihre photophysikalischen Eigenschaften jedoch kaum Unterschiede. Alle Konformere beider Moleküle besitzen tief liegende Singulett und Triplett ligand-to-ligand charge-transfer (LLCT) Zustände, die als emissive Zustände in Frage kommen. Die Spin-Bahn-Kopplungen zwischen diesen Zuständen sind niedrig. Jedoch können in Kombination mit winzigen Energielücken hohe (reverse) Intersystem Crossing Raten erreicht werden. Die Phosphoreszenzraten sind so niedrig, dass ausschließlich Emission aus dem Singulett-Zustand zu erwarten ist. Die Fluoreszenzraten aus den Singulett LLCT Zuständen sind hoch. Die Emission des Zn-BDT erzeugt gelbes Licht, die des Zn-BDO liegt im infraroten Bereich. Experimentelle Ergebnisse des Zn-BDTs zeigen eine gute Übereinstimmung mit den computergestützen Berechnungen. Beide Moleküle eigenen sich als TADF-Emitter-Material und sind durch Emission von Licht unterschiedlicher Wellenlänge gekennzeichnet.

Contents

List of Abbreviations

BDO	Benzene-1,2-Diol
BDT	Benzene-1,2-Dithiol
CAAC	Cyclic Alkyl Amino Carbene
CI	Configuration Interaction
CISD	Configuration Interaction Singles Doubles
COSMO	Conductor-Like Screening Model
CSF	Configurational State Function
DCBH	Dirac-Coulomb-Breit-Hamiltonian
DFT	Density Functional Theory
FC	Franck-Condon
GGA	Generalized Gradient Approximation
HF	Hartree-Fock
IC	Internal Conversion
ISC	Intersystem Crossing
IQE	Internal Quantum Efficiency
KS	Kohn-Sham
LE	Locally Excited
LDA	Local Density Approximation
LLCT	Ligand-to-Ligand Charge-Transfer
MC	Metal-Centered
MLCT	Metal-to-Ligand Charge-Transfer
MRCI	Multireference Configuration Interaction
MRSOCI	Multireference Spin–Orbit Configuration Interaction
OLED	Organic Light Emitting Diode
PCM	Polarizable Continuum Model
rISC	reverse Intersystem Crossing
RMSD	Root-Mean-Square Deviation
SAS	Solvent-Accesible Suface
SES	Solvent-Excluded Surface
SOC	Spin–Orbit Coupling
SOCME	Spin–Orbit Coupling Matrix Element
SOMF	Spin–Orbit Mean-Field
TADF	Thermally Activated Delayed Fluorescence
TDA	Tamm-Dancoff-Approach
TDDFT	Time-Dependent Density Functional Theory
vdW	van der Waals
VR	Vibrational Relaxation
Zn-BDO	^{Menth}CAAC-Zn(II)-BDO
Zn-BDT	^{Menth}CAAC-Zn(II)-BDT

1 Introduction

Organic light-emitting diodes (OLED)s are thin-film devices made of organic semiconductor material that emit light when an electric current is applied. They are commonly used primarily in display technology and can be found in many smartphones and televisions. OLEDs are popular due to their high contrast ratio, which gives the impression of higher brightness, fast response times, which contribute to the sharper display of moving objects, and the fact that they do not require background radiation resulting in lower electricity costs. In addition, OLEDs are flexible and can be mounted on flexible surfaces due to their non-crystalline nature. [1]

The efficiency of OLEDs is a topic of interest, and scientist are still searching for more efficient emitter materials. The internal quantum efficiency (IQE) is a significant factor in the overall efficiency, and it is closely linked to the exciton yield. In OLEDs, excitons are formed by recombination of an electron-hole pair. Electrons and holes are injected through the anode and cathode, respectively, when a voltage is applied. The (quasi-)particles of the resulting electron-hole pair move towards each other until they recombine. The resulting excitons can be divided into singlets and triplets based on their spin multiplicity and occur statistically in a ratio of 1:3. To maximize IQE, both singlet and triplet excitons should contribute to light generation. This can occur through two different mechanisms, resulting in either phosphorescence or fluorescence. [2]
Phosphorescent emitters, also called second-generation OLED emitters, have a high base IQE, because 75 % of the excitations are created in the triplet state after recombination. The remaining singlet excitons can be transferred to the triplet state through intersystem crossing (ISC) in suitable emitter molecules. Therefore, low fluorescence rates as well as high ISC and phosphorescence rates ensure that all excitions can be harvested in a single decay channel. [3]

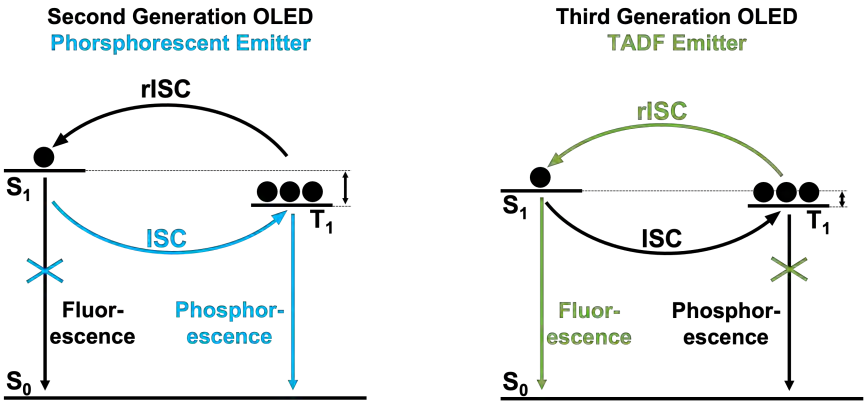

Fig. 1.1: Illustration of the mechanisms of second- and third-generation OLED emitters.

Suitable molecules for emitter materials are transition metal complexes. For second-generation OLED emitters, iridium(III) or platinum(II) are often chosen as the central transition metal atoms. They are usually characterized by low-lying metal-to-ligand charge-transfer (MLCT) states and large spin–orbit coupling (SOC) elements, which favour fast ISC and high phosphorescence rates. However, finding blue phosphorescent emitters is challenging, due to operational instability caused by low-lying metal-centered (MC) states, which initiate dissociation of the metal-ligand bonds.
Thermally activated delayed fluorescence (TADF), a mechanism that utilizes all excitons and thus helps to achieve 100 % IQE, converts triplet excitons to singlet excitons through rISC. From there, the excitons are converted into light through fluorescence. An optimal TADF emitter, also known as a third-generation OLED emitter, is characterized by the absence of any competitive processes. [4]
For metal organic third-generation OLED emitters, copper(I) has been addressed in many recent investigations. [5–8] Cu(I) complexes whose lowest singlet and triplet states have ligand-to-ligand charge-transfer (LLCT) character appear to favour TADF. [9] Corresponding LLCT states have a small energetic splitting of their singlet and triplet states (ΔE_{S-T}), but also small SOC. While a small ΔE_{S-T} favours fast (r)ISC rates, SOC is still required to convert singlet to triplet states. However, the small SOC can be counteracted by adding MLCT character to the LLCT state wave function. The advantages of copper complexes over second-generation emitters are the better and cheaper availability of copper, as well as the absence of low-lying MC states due to the fully occupied d-shell of the metal atom, which counteracts dissociation instability.
Some of the aforementioned advantages also apply to zinc(II) complexes: its high earth abundance makes zinc a cheap metal and low-lying MC states are absent, since ligand-centered (LC), intraligand charge-transfer (ILCT) or LLCT excitations are predominant. As with copper, the problem of small SOC elements arises, but by choosing suitable ligands, SOC can be enhanced. However, zinc(II) complexes are scarcely investigated in the field of TADF emitters. [10,11]

Lüdtke et al. recently investigated the photophysical properties of Zn(II) complexes (see left side figure 1.2). [11] Using quantum chemical calculations, they found a molecule with excellent TADF emitter properties: small ΔE_{S-T}s , fast (r)ISC rates, high fluorescence, and low phosphorescence rates. The molecule is called ^{Me}CAAC-Zn(II)-BDT. In it, a zinc atom is surrounded by two ligands, a cyclic alkyl amino carbene (CAAC) and a benzene-1,2-dithiol (BDT).
However, in experiments, it was shown that dimerization takes place even in the solid state. It is accompanied by a strong bending of the BDT ligand which lowers the fluorescence rate constant. Thus, the probability of competitive reactions is increased. The authors speculate that introducing a bulkier residue on the CAAC ligand may prevent the bending of the BDT ligand and thus dimerization. Replacing the two methyl groups with

a menthyl residue is suggested. The absence of dimerization would allow access to the excellent TADF properties of the monomer.
The influence of the sulfur atom on the properties of the complex is also of interest. In the paper, a molecule that carries a benzene-1,2-diol (BDO) ligand instead of BDT, meaning an exchange of the sulfur atoms with oxygen, was also studied. The compound with oxygen showed similar properties with a red-shifted emission.

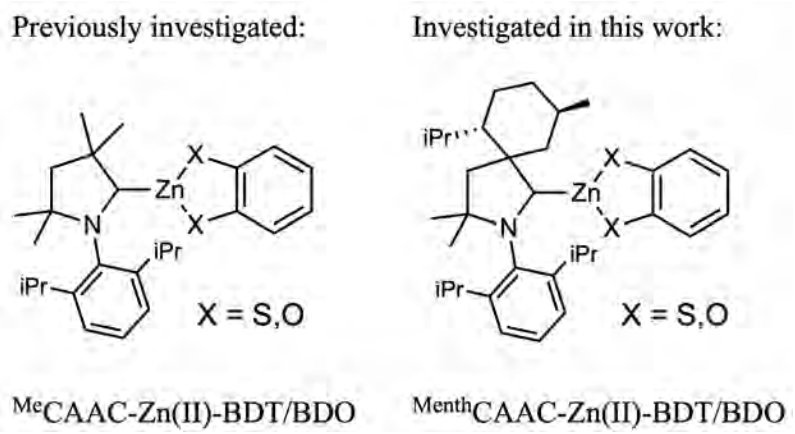

Fig. 1.2: Molecular structures of the investigated complexes.

In this master thesis, a quantum chemical investigation of the ^{Menth}CAAC-Zn(II)-BDT (Zn-BDT) and ^{Menth}CAAC-Zn(II)-BDO (Zn-BDO) (see right side figure 1.2) concerning their TADF emitter properties is performed. The geometries of the ground and excited states are optimized, excitation energies are calculated, absorption and emission spectra are constructed, and rate constants are investigated.

2 Theory

2.1 Photophysical Processes

An understanding of the most important photophysical processes is essential for the characterization of a TADF emitter. These processes are absorption, vibrational relaxation (VR), internal conversion (IC), ISC, rISC, fluorescence, and phosphorescence. All of these processes can be well described by looking at the Jablonski diagram presented in figure 2.1.

Beginning from the ground state (S0), photophysical processes in molecules start with the absorption of energy, which leads to the promotion to an excited state. The energy can be supplied in different ways. In OLEDs, electroluminescence takes place, wherein an electric current or an electric field provides the energy for the excitation. Another way is the absorption of photons. In both cases the energy absorption leads to an excited molecule with the desire to fall back into an energetically lower state, which is usually the ground state. The way back to this state can take place in different manners.

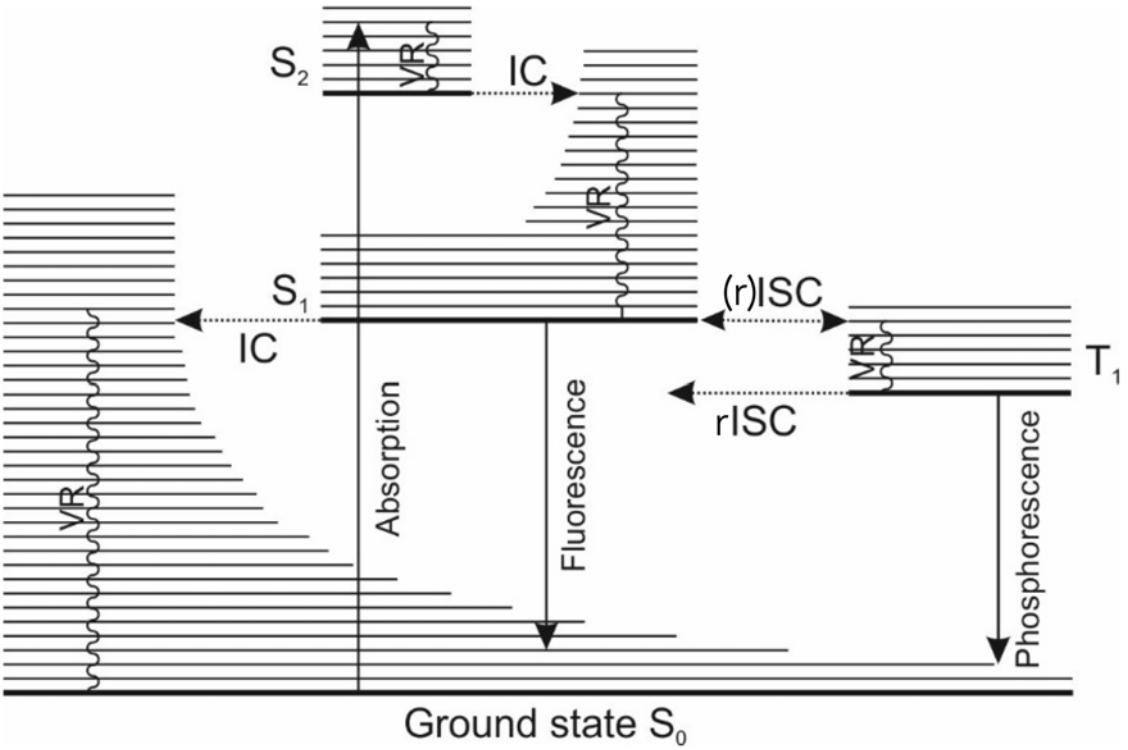

Fig. 2.1: Drawing of the Jablonski diagram.[12]

After excitation into a higher electronic state, the relaxation process starts by following Kasha's rule.[13] It states that molecules in an upper state of a specific multiplicity fall into the state with the same multiplicity with the lowest energy above the ground state (S1/T1). This happens though VR and IC. VR is the relaxation from a higher vibrational

state to the vibrational ground state of the respective electronic state and is visualized by wavy arrows in the Jablonski diagram. IC is the transition from the vibrational ground state of an electronic state to a lower electronic state of the same multiplicity and drawn as dotted arrows. VR and IC are so fast for higher excited states that no competition processes occur.
Starting from S1, three different paths to the S0 are possible. The first one is a repetition of the previous step; the molecule falls into the ground state through IC followed by VR. This is a radiationless process. The second path is the relaxation to the ground state by emitting a photon, which results in the emergence of light. This process is called fluorescence and drawn as a straight line in the Jablonski diagram. The third option involves the lowest excited triplet state (T1). It begins with the transition from the singlet to triplet state, a process called ISC, which involves a change of multiplicity. The relaxation following from T1 can be, once again, split into three paths: either rISC back to the S1 state, rISC to the singlet ground state (another radiationless process) or phosphorescence. Phosphorescence is a similar phenomenon as fluorescence; a photon is emitted, but this time accompanied by a change of multiplicity from T1 to S0. It is highlighted in the Jablonski diagram as a straight line.[14]

2.2 Density Functional Theory

Density functional theory (DFT) is the basis of the most widely used computational methods in quantum chemistry. It differs fundamentally from wave function-based methods such as Hartree Fock. Instead of a suitable wave function, the calculation of the energy of a system is based on the electron density. The big advantage lies in an immense decrease of relevant coordinates and therefore less computational effort. Wave functions refer to 3N coordinates, electron densities to only 3.[15]

Basis of the DFT are two theorems established by Hohenberg and Kohn. The first theorem states that the ground state energy of a system is related to the one-electron density of the system by a universal functional. If the exact one-electron density is known, the exact energy can be derived via the functional. The second theorem states that the variational principle is applicable to the one-electron density. Thus, by inserting any one-electron density into the functional, the true energy of the system cannot be undercut. This allows an iterative improvement of the energy by adjusting the electron density. However, the big challenge of DFT is, that the connecting universal functional is not known.[16]

Instead, the functional can be approximated using a HF-like approach, thus reintroducing orbitals, i.e., one-electron wave functions. Within the Born-Oppenheimer approximation, the functional of the electron density $\boldsymbol{E}[\boldsymbol{\rho}]$ contains three terms: the functional for the kinetic energy of the electrons $\boldsymbol{T_e}[\boldsymbol{\rho}]$, the nuclear-electron attraction $\boldsymbol{E_{en}}[\boldsymbol{\rho}]$ and the

electron-electron interaction $\boldsymbol{E_{ee}[\rho]}$, where the latter can be divided into a Coulomb $\boldsymbol{J[\rho]}$ and an exchange $\boldsymbol{K[\rho]}$ term.

$$\boldsymbol{E[\rho]} = \boldsymbol{T_e[\rho]} + \boldsymbol{E_{en}[\rho]} + \boldsymbol{E_{ee}[\rho]} \tag{2.1}$$

$$= \boldsymbol{T_e[\rho]} + \boldsymbol{E_{en}[\rho]} + \boldsymbol{J[\rho]} + \boldsymbol{K[\rho]} \tag{2.2}$$

The nuclear-electron attraction $\boldsymbol{E_{en}[\rho]}$ and the Coulomb term $\boldsymbol{J[\rho]}$ can be calculated according their classic formulas. The challenge lies in the description of the kinetic energy $\boldsymbol{T_e[\rho]}$ and the exchange term $\boldsymbol{K[\rho]}$. Since the kinetic energy contribution is the largest unknown term, a very accurate approximation of its functional is crucial for good results.

In the Kohn-Sham (KS) formalism most of the kinetic energy is calculated through a reference system of non-interacting electrons. To describe this reference system, KS orbitals $\boldsymbol{\phi_i(r)}$ are generated from the KS equation.

$$\left(-\frac{\hbar^2}{2m}\boldsymbol{\nabla^2} + \upsilon_{\text{eff}}(\boldsymbol{r})\right)\phi_i(\boldsymbol{r}) = \varepsilon_i\phi_i(\boldsymbol{r}) \tag{2.3}$$

Here $\boldsymbol{\upsilon_{\text{eff}}(r)}$ is the KS potential in which the non-interacting particles move. The resulting KS orbitals can be used to derive the one-electron density of the reference system.

$$\boldsymbol{\rho(r)} = \sum_{\boldsymbol{i}}^{\boldsymbol{N}} |\phi_i(\boldsymbol{r})|^2 \tag{2.4}$$

Likewise, the energy of the reference system can be determined via the KS orbitals as well. Only a single Slater determinant is necessary for that.

$$\boldsymbol{T_s} = \sum_{\boldsymbol{i=1}}^{\boldsymbol{N}} \left\langle \phi_i(\boldsymbol{r}) \left| -\frac{\boldsymbol{1}}{\boldsymbol{2}}\boldsymbol{\nabla^2} \right| \phi_i(\boldsymbol{r}) \right\rangle \tag{2.5}$$

Due to the independent-particle approximation, a correction term $\boldsymbol{(T_e[\rho] - T_s[\rho])}$ must be introduced to account for the missing part of the kinetic energies. This is combined with the exchange term $\boldsymbol{K[\rho]}$, which has also not yet been taken into account, to form the exchange correlation term $\boldsymbol{E_{xc}}$.

$$\boldsymbol{E_{xc}} = \boldsymbol{(T_e[\rho] - T_s[\rho])} + \boldsymbol{K[\rho]} \tag{2.6}$$

Thus, the following expression is obtained for the functional of the electronic energy within the KS formalism:[17]

$$\boldsymbol{E[\rho]} = \boldsymbol{T_s[\rho]} + \boldsymbol{E_{ek}[\rho]} + \boldsymbol{J[\rho]} + \boldsymbol{E_{xc}[\rho]} \tag{2.7}$$

The exchange correlation term is the only unknown term of the above mentioned equation and approximated by a density functional. Meanwhile, there is a variety of density functionals that differ in their accuracy and applicability. They can be divided into five categories: the local density approximations (LDA), generalized gradient approximations (GGA), meta-GGAs, hybrids and double hybrids. Their precision increases from left to right.[18]

The density functional used in this work with the name BH-LYP[19,20] belongs to the hybrids. Its exchange term is split up into 50 % HF and 50 % LDA/B88 exchange in addition to a LYP correlation term.

$$\boldsymbol{E_{xc} = 0,5 E_x^{HF} + 0,5 E_x^{LDA/B88} + E_c^{LYP}} \tag{2.8}$$

2.3 Time-dependent Density Functional Theory

Phenomena such as molecular excitations are time-dependent, since a change in the external potential must be taken into account. Classical DFT is a time-independent method and only suitable for calculations of systems in the ground state. For the determination of excited molecules, one may use the time-dependent density functional theory (TDDFT). Just like classical DFT, it uses the electron density to determine molecular properties.

The basis of TDDFT is the Runge-Gross theorem, which can be seen as a time-dependent analogue of the first Hohenberg-Kohn theorem. It states that there exists a one-to-one mapping between the electron density and the external potential.[21]
For time-independent systems, the electron density can be obtained by minimizing the total energy. For the time-dependent case, this is no longer possible. The variational principle is not applicable to the total energy, since it is no longer a conserved quantity. Instead, in TDDFT, the quantum mechanical action integral $\boldsymbol{A[\rho]}$ is used, by whose minimization the exact one-electron density can be obtained.

$$\boldsymbol{A[\rho] = \int_{t_0}^{t_1} dt \left\langle \Psi[\rho](r,t) \left| i\frac{\delta}{\delta t} - \hat{H}(r,t) \right| \Psi[\rho](r,t) \right\rangle} \tag{2.9}$$

Similar to time-independent DFT, the one-electron density is calculated by a fictitious reference system of non-interacting electrons. Once again the reference system is derived from KS orbitals $\boldsymbol{\phi_i(r,t)}$, which can be calculated by the KS equation.

$$\left(-\frac{1}{2}\nabla_i^2 + v_{\text{eff}}(r,t) + \frac{\delta J[\rho]}{\delta p(r,t)} + \frac{\delta A_{\text{xc}}[\rho]}{\delta p(r,t)} \right) \phi_i(r,t) = i\frac{\delta}{\delta t}\phi_i(r,t) \tag{2.10}$$

These in turn can be used to determine the one-electron density.

$$\rho(r,t) = \sum_{i}^{N} |\phi_i(r,t)|^2 \tag{2.11}$$

The so-called TDDFT equation can be derived from the time-dependent KS equation.

$$\begin{bmatrix} A & B \\ B^* & A^* \end{bmatrix} \begin{bmatrix} X \\ Y \end{bmatrix} = \omega \begin{bmatrix} 1 & 0 \\ 0 & -1 \end{bmatrix} \begin{bmatrix} X \\ Y \end{bmatrix} \tag{2.12}$$

This non-Hermitian eigenvalue equation allows the determination of the excitation energies.[22]
However, it should be mentioned that the description of charge-transfer states often causes substantial errors in calculations with TDDFT. Especially the description of long-range interactions is problematic, which can lead to a significant underestimation of excitation energies. This error increases as the proportion of non-local exchange terms contained in the functional is smaller. The BH-LYP functional has 50 % HF exchange and is therefore very well suited to counteract this error.[23]

For the calculation of triplet geometries, it is worthwhile to resort to the Tamm-Dancoff-Approach (TDA). It promises lower computational costs and a more accurate description for molecules with triplet instabilities.[24] By neglecting the matrix B from the TDDFT equation, a Hermitian eigenvalue equation of the following form is obtained:[22]

$$AX = \omega X \tag{2.13}$$

2.4 Multireference Configuration Interaction

Due to the mean-field approximation of HF, the HF energy does not correspond to the exact value. The difference between the HF energy and the exact energy is called electron correlation. It constitutes only a small part of the total energy, but lies in the order of magnitude of binding energies and thus cannot be neglected. The correlation energy must also be described as accurately as possible when calculating electronic excitations.

Several post-HF methods are suitable for determining the correlation energy, including the configuration interaction (CI) method. The CI method is a multi-determinant method, where several Slater determinants are created by occupying virtual orbitals. Slater determinants created by considering single excitations are called singles, in case of double excitations doubles and so on. Their linear combination forms a CI wave function.

$$|\Psi_{\mathrm{CI}}\rangle = c_0 |\Psi_0\rangle + \sum_{a,r} c_a^r |\Psi_a^r\rangle + \sum_{a,b,r,s} c_{ab}^{rs} |\Psi_{ab}^{rs}\rangle + \sum_{a,b,c,r,s,t} c_{abc}^{rst} |\Psi_{abc}^{rst}\rangle + \ldots \tag{2.14}$$

If all possible excitations are taken into account, the so-called full CI wave function is obtained. A full-CI provides the exact energy for the time-independent Schrödinger equation, taking into account the Born-Oppenheimer approximation and neglecting relativistic effects. However, a full-CI is associated with an enormous computational effort and is therefore not practical for larger molecules.
Often, in addition to the reference determinant, only single and double excitations are considered in a CI expansion (CISD). This promises an acceptable computational effort and provides good results for ground state calculations. For excited states, however, determinants of higher excitations should be included in the expansion.

An extension of the CI method is the multi-reference CI (MRCI). Here, excitations are no longer considered with respect to only one, but several reference determinants.

$$|\Psi_{\mathrm{MRCI}}\rangle = \sum_{I} \left(c_I |\Psi_I\rangle + \sum_{a,r} c^r_{I,a} |\Psi^r_{I,a}\rangle + \sum_{a,b,r,s} c^{rs}_{I,ab} |\Psi^{rs}_{I,ab}\rangle + ... \right) \tag{2.15}$$

To keep the number of determinants and the computational effort within limits, a configuration selection is performed. This may take place over a perturbation theoretical approach. Only configurations with a considerable contribution are taken into account for the development of the MRCI wave function.[25,26]

2.5 DFT/MRCI

The DFT/MRCI method[27,28] combines the advantages of DFT and MRCI. It ensures a good description of the electron correlation at low computational cost and is thus particularly suitable for the investigation of molecule's spectral properties.
The method is based on a DFT calculation followed by an MRCI calculation. In this process, DFT KS orbitals are generated, which are used to form configurational state functions (CSF)s, from which the CI wave function is finally constructed.
The dynamic correlation is already well captured by DFT, whereas the MRCI provides a good description of the static correlation. However, since the MRCI also captures dynamic correlation, empirical corrections in the Hamiltonian matrix are employed to prevent double counting of the dynamic correlation, which makes it a semi-empirical method.[27]
Starting from the Original Hamilonian, it has been evolved several times to make improvements and adapt to specific systems. In this work, the Hamiltonian R2018 is used, which is particularly suitable for the calculation of transition metal complexes.[29] Its matrix elements can be divided into three categories: diagonal elements, off-diagonal elements with the same spacial but different spin part, and off-diagonal elements with different spacial and spin part.

In the diagonal elements, the HF orbital energies are replaced by KS orbital energies.

$$\langle w\omega|\hat{\boldsymbol{H}}^{\boldsymbol{DFT}} - \boldsymbol{E}^{\boldsymbol{HF}}|w\omega\rangle = \langle w\omega|\hat{\boldsymbol{H}}^{\boldsymbol{DFT}} - \boldsymbol{E}^{\boldsymbol{HF}}|w\omega\rangle - \sum_{i\in c}^{n_{exc}} (\boldsymbol{F}_{ii}^{\boldsymbol{HF}} - \boldsymbol{F}_{ii}^{\boldsymbol{KS}}) \tag{2.16}$$

$$+ \sum_{i\in a}^{n_{exc}} (\boldsymbol{F}_{ii}^{\boldsymbol{HF}} - \boldsymbol{F}_{ii}^{\boldsymbol{KS}}) + \boldsymbol{\Delta E_{coul}} - \boldsymbol{\Delta E_{exch}} \tag{2.17}$$

with $\boldsymbol{w}$ representing the spin-dependent part of the CSF, $\boldsymbol{\omega}$ the spatial part, $\boldsymbol{E}^{\boldsymbol{HF}}$ the total HF energy evaluated from the KS orbitals, $\boldsymbol{n}^{\boldsymbol{exc}}$ the number of excitations, $\boldsymbol{F}_{\boldsymbol{ii}}^{\boldsymbol{HF}}$ the Fock matrix element using the non-interacting KS orbitals, $\boldsymbol{F}_{\boldsymbol{ii}}^{\boldsymbol{KS}}$ the KS orbital energy and $\boldsymbol{c}$ and $\boldsymbol{a}$ created/annihilated electrons.
The coulomb $\boldsymbol{\Delta E_{coul}}$ and exchange $\boldsymbol{\Delta E_{exch}}$ integrals are scaled by two empirical parameters, a spin-independent Coloumb scaling $\boldsymbol{p_J}$ and an exchange scaling $\boldsymbol{p_X}$.

$$\boldsymbol{\Delta E_{coul}} - \boldsymbol{\Delta E_{exch}} = \boldsymbol{p_J} \left(- \sum_{\substack{i,j\in c \\ i>j}}^{n_{exc}} \boldsymbol{V}_{ijij} - \sum_{\substack{i,j\in a \\ i>j}}^{n_{exc}} \boldsymbol{V}_{ijij} + \sum_{i\in c}^{n_{exc}} \sum_{i\in a}^{n_{exc}} \boldsymbol{V}_{ijij} \right) \tag{2.18}$$

$$- \boldsymbol{p_X} \left(\frac{\mathbf{1}}{\mathbf{2}} \sum_{i\in c}^{n_{exc}} \sum_{i\in a}^{n_{exc}} \boldsymbol{V}_{ijji} + \sum_{\substack{i,j\in o \\ i>j}}^{\boldsymbol{N_o}} \boldsymbol{V}_{ijji} \boldsymbol{\eta}_{\boldsymbol{ij}}^{\boldsymbol{ji}} \right) \tag{2.19}$$

with $\boldsymbol{V}$ representing the exchange/Coulomb integrals and $\boldsymbol{\eta}_{\boldsymbol{ij}}^{\boldsymbol{ji}}$ the spin-coupling.[30]
The off-diagonal elements with the same spatial but different spin parts are also scaled by the $\boldsymbol{p_X}$ parameter.

$$\langle w\omega|\hat{\boldsymbol{H}}^{\boldsymbol{DFT}}|w'\omega\rangle = \langle w\omega|\hat{\boldsymbol{H}}|w'\omega\rangle(\mathbf{1} - \boldsymbol{p_X}) \tag{2.20}$$

The off-diagonal elements with different spatial and spin parts are modified by a damping function.

$$\langle w\omega|\hat{\boldsymbol{H}}^{\boldsymbol{DFT}}|w'\omega'\rangle = \langle w\omega|\hat{\boldsymbol{H}}|w'\omega'\rangle \cdot \boldsymbol{f_{damping}} \tag{2.21}$$

The damping function of the R2018 Hamiltonian contains a scaling $\boldsymbol{p_1}$ and a damping parameter $\boldsymbol{p_2}$.

$$\boldsymbol{f_{damping}} = \boldsymbol{p_1} \cdot \boldsymbol{e}^{-\boldsymbol{p_2}\cdot\boldsymbol{\Delta E}_{\omega\omega'}^{\mathbf{6}}} \tag{2.22}$$

The parameters are optimized for the BH-LYP functional. The DFT/MRCI method yields a root-mean-square deviation (RMSD) of 0.15 eV for transition metal complex excited state energies, when employing the R2018 Hamiltonian.[29]

2.6 Spin–Orbit Coupling

In non-relativistic quantum chemistry, electronic transitions between states of different multiplicity are formally forbidden. To describe processes like ISC, rISC, and phosphorescence, the interaction between spin and orbital angular momentum, known as spin-orbit coupling (SOC), must be taken into account. The consequence of SOC is that states no longer have pure spin character, but are composed as a mixed state with both singlet and triplet spin character. Hamiltonians that consider SOC can be derived from either the Dirac equation or the Schrödinger equation.

The Dirac equation is a fully relativistic one-particle theory for spin 1/2 systems from which SOC naturally arises. For chemical applications, this one-electron theory must be extended to a many-body theory. The difference from the non-relativistic case is that instantaneous processes cannot take place due to the finite speed of light. Therefore, the interaction between two electrons cannot be described simply by a Coulomb term; it must be extended by a so-called retardation term. Together with a magnetic interaction term, these terms are summarized as the Breit interaction, which leads to the Dirac-Coulomb-Breit-Hamiltonian (DCBH). The DCBH is usually divided approximately into a spin-free and spin-dependent part for easier application. However, a significant disadvantage of the DCBH remains: algorithms and computational techniques are significantly more demanding in the spinor basis that arises from the Dirac equation.[31]

Starting from the Schrödinger equation of a molecule in an external electric and magnetic field, the Breit-Pauli-Spin-Orbit-Hamiltonian can be derived by assuming that the scalar potential is Coulombic and the magnetic field arises from the electronic spin.

$$\hat{H}_{SO}^{BP} = \frac{1}{2m_e^2c^2} \sum_i \sum_I \frac{Z_I}{\hat{r}_{iI}^3} (\hat{r}_{iI} \times \hat{p}_i) \cdot \hat{s}_i \tag{2.23}$$

$$- \frac{1}{2m_e^2c^2} \sum_i \sum_{j \neq i} \frac{Z_I}{\hat{r}_{iI}^3} (\hat{r}_{iI} \times \hat{p}_i) \cdot (\hat{s}_i + 2\hat{s}_j) \tag{2.24}$$

Here, m_e is the mass of an electron, c is the speed of light, i and l are the labels of an electron, I is the label of a nucleus, and Z is the charge of the nucleus. The upper part of the equation describes the interaction of the spin magnetic moment of an electron i with the magnetic moment that results from the electron orbiting the nucleus I. The lower part of the equation describes the spin-same-orbit term, which relates to the motion of one electron in the field of another, and the spin-other-orbit terms, which relates to the coupling between the spin magnetic and orbital magnetic moments of two electrons.[32]
Since the calculation of the two-electron terms contained in the Breit-Pauli Hamiltonian is computationally very expensive and requires a lot of memory, the spin-orbit mean-field approximation (SOMF) is applied. In the SOMF, many-electron integrals are averaged similarly to how they are in the HF theory.[33]

The Pauli-Breit Hamiltonian is the most widely used SOC operator. Nevertheless, it should be employed with caution in combination with variational methods because there is no lower limit.[32]

2.7 Rate Constants

ISC Rates

Rate constants of non radiative processes $\boldsymbol{k_{NR}}$ can be calculated using Fermi's golden rule:

$$\boldsymbol{k_{NR} = \frac{2\pi}{\hbar} \sum_{f} |\hat{H}_{if}^{(1)}|^2 \delta(E_i - E_f)} \tag{2.25}$$

Here $\boldsymbol{\hat{H}_{if}^{(1)}}$ is a perturbation operator coupling the initial state $\boldsymbol{i}$ with a set of final states $\boldsymbol{f}$. A small interaction energy of these states compared to their adiabatic energy difference and a high density of the final vibrational state at the energy of the initial state are necessary conditions for the validity of equation 2.25.
By neglecting spin-vibronic interaction terms the ISC rate $\boldsymbol{k_{ISC}}$ is given by:

$$\boldsymbol{k_{ISC} = \frac{2\pi}{\hbar} \sum_{a} \sum_{k} |\langle \Psi_{Sa}, v_{aj} | \hat{H}_{SO} | \Psi_{Tb}^{\alpha}, v_{bk} \rangle|^2 \delta(E_{aj} - E_{bk})} \tag{2.26}$$

In the Condon approximation only direct SOC is taken into account. Therefore electronic and vibrational contributions can be separated and the ISC rate $\boldsymbol{k_{ISC}^{FC}}$ is given by:[32]

$$\boldsymbol{k_{ISC}^{FC} = \frac{2\pi}{\hbar} \sum_{a} |\langle \Psi_{Sa} | \hat{H}_{SO} | \Psi_{Tb}^{\alpha} \rangle|_{q_0}^2 \sum_{k} |\langle v_{aj} | v_{bk} \rangle|^2 \delta(E_{aj} - E_{bk})} \tag{2.27}$$

By assuming a Boltzmann distribution for the population of the vibrational levels not only the vibrational ground states are populated. This is especially relevant for the calculation of rISC rate constants, since the process usually does not start from a vibrational ground state. This lead to the following equation:[34]

$$\boldsymbol{k_{ISC} = \frac{1}{Z} \sum_{j} e^{-\frac{E_{aj}}{k_B T}} k_{ISC}^{FC}} \tag{2.28}$$

When calculating rISC rates the initial state becomes the final state and vice versa and a factor of 1/3 needs to be added, since three triplet states instead of only one singlet state need to be taken into account.

Emission Rates

According to Fermi's golden rule, the rate constant of a radiative decay k_R can be calculated via the following formula:

$$k_R = \frac{4e^2}{3c^3\hbar^4}(E_i - E_f)^3|\langle f|\vec{r}|i\rangle|^2 \tag{2.29}$$

By expressing the rate constant k_R in units of 1/s, the energy difference of initial an final state $(E_i - E_f)$ in 1/cm and the dipole moment $\mu_{el} = \langle f|\vec{r}|i\rangle$ in atomic units, the prefactor becomes $2.0261 \cdot 10^{-6}$. By choosing S1 as the initial state and S0 as the final state, one can obtain the formula for the calculation of the fluorescence rate.

$$k_F = \frac{4e^2}{3c^3\hbar^4}(E_{S_1} - E_{S_0})^3|\mu_{el}(S_1 \rightarrow S_0)|^2 \tag{2.30}$$

Phosphorescence rates $k_{P,\zeta}$ from the triplet sublevels $\zeta = x, y, z$ can be obtained by inserting spin–orbit mixed wave functions of S0 and T1 into the initial and final state.[35]

$$k_{P,\zeta} = \frac{4e^2}{3c^3\hbar^4}(E_{T_1} - E_{S_0})^3|\mu_{el}(T_{1,\zeta} \rightarrow S_0)|^2 \tag{2.31}$$

The fine-structure sublevels of the T1 state are energetically close and equally populated at room temperature. In this case, the total phosphorescence rate $\bar{k}_P$ can be obtained from the average of the sublevel phosphorescence components.[36]

$$\bar{k}_P = \frac{1}{3}(k_{P,x} + k_{P,y} + k_{P,z}) \tag{2.32}$$

2.8 Adiabatic and Vertical Hessian Method

In this work, non-radiative rate constants were calculated using the Adiabatic Hessian Method (AH). The AH method requires the equilibrium geometries of the initial and final states. Within the VIBES program[37], the normal modes and frequencies of the two states are used to quantify the probability of vibronic transitions and calculate non-radiative rate constants.

To calculate emission spectra, the Vertical Hessian (VH) method was used.[38,39] For VH only the optimized geometry of the initial state is required. The gradients and Hessian matrix of the final state at this geometry are used to extrapolate the equilibrium geometry and normal modes of the final state. Modes with imaginary frequencies are removed for both states.

Large Cartesian displacements between the initial and final states can sometimes lead to significantly broadened spectra. In some cases, it is therefore advisable to remove modes with large displacements in addition to imaginary modes. This is a valid procedure as long as these modes are not responsible for the shape of the spectrum.[39] However, this approach should be viewed with caution. If additional modes have been removed, it will

be mentioned in this work.
The significant advantage of the VH method is that reasonable spectra and rate constants can even be determined for vibronic transitions where large structural changes occur. Additionally, optimization of the final state reduces the computational cost.

2.9 Solvent Models

Molecular geometries, energies, and properties are heavily influenced by solvent-solute interactions. Adding explicit solvent molecules to take these effects into account is a rather costly matter. A less time-consuming approach is to use an implicit continuum solvent model. In this approach, the solute molecule is placed inside a cavity that is surrounded by a dielectric continuum with a given permittivity that mimics the solvent.
The cavity can be built by overlapping spheres surrounding the atoms of the solute molecule. The size of the spheres is determined by the van der Waals (vdW) radii of the associated atoms. This resulting area is also referred to as the solvent-excluded surface (SES). Inside the SES, the permittivity is set to one, while outside it, a solvent-specific value is assigned. Together with spheres surrounding the solvent molecules, whose size also depends on their respective vdW radii, another layer occurs: the solvent-accessible area (SAS). It should be noted that the construction of the cavity and SAS can be done in different ways, depending on the selected model. [40]

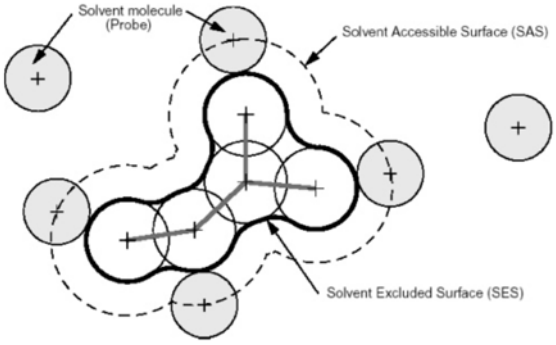

Fig. 2.2: Illustration of SES and SAS built by vdW radii of the solute and solvent atoms. [40]

The effects of the solvent-solute interaction are applied to the Schrödinger equation by adding an effective potential.

$$\left[\hat{\boldsymbol{H}}_{\mathbf{0}} + \hat{\boldsymbol{V}}_{\boldsymbol{int}}(\boldsymbol{\rho})\right] \boldsymbol{\Psi} = \boldsymbol{E}\boldsymbol{\Psi} \tag{2.33}$$

Here, $\hat{\boldsymbol{H}}_{\mathbf{0}}$ refers to the Hamiltonian of the solute in vacuum, and $\hat{\boldsymbol{V}}_{\boldsymbol{int}}(\boldsymbol{\rho})$ refers to the effective potential that depends on the charge distribution of the solute molecule. Through this dependence, a variational solution of the equation above can be obtained by minimizing the Gibbs free energy. [41]

The Gibbs energy can be divided into five different parts:

$$\boldsymbol{G = G_{el} + G_{cav} + G_{dis} + G_{rep} + G_{mm}} \tag{2.34}$$

Where $\boldsymbol{G_{el}}$ describes the electrostatic interactions, $\boldsymbol{G_{cav}}$ the energy that is necessary to form the cavity, $\boldsymbol{G_{dis}}$ the dispersion energy, $\boldsymbol{G_{rep}}$ the repulsion energy and $\boldsymbol{G_{mm}}$ the thermal motions.[42]
The most widely used continuum models are the polarizable continuum model (PCM)[43] and the conductor-like screening model (COSMO)[44]. They mostly differ in the boundary condition used to calculate the polarizable charge density. In PCM, exact dielectric conditions are applied, while in COSMO, empirically scaled conductor boundary conditions are used. In this work, the PCM is utilized, and the solvent, DCM, is described with a permittivity of $\boldsymbol{\epsilon = 8.93}$.

3 Computational Details

The Gaussian 16 program package[45] was employed for all geometry optimizations and vibrational frequency analyses. Electrostatic solvent-solute interactions were taken into account by utilizing the PCM[43] model. Equilibrium geometries of the electronic ground states were determined with KS DFT using the BH-LYP[19,20] functional. For triplet and singlet excited-state geometries (TDA-)TDDFT calculations were performed. Hydrogen, carbon, nitrogen and oxygen atoms were represented by the def2-SV(P)[46] basis set. Sulfur was described by def2-SVPD[47]. For the zinc ion an effective core potential (ECP10MDF) was added, combined with the associated basis set (10-mdf 6s5p3d)[48].

Excitation energies were calculated applying the DFT/MRCI method[27,28] using the R2018 Hamiltonian[29] with a short parameter set and a selection threshold of 0.8 E_h. For every geometry the first 21 singlet and 20 triplet roots were calculated. Solvent-solute interactions were taken into account through exported PCM point charges.

The SPOCK program[49,50] was used for the determination of spin–orbit coupling matrix elements (SOCME)s. The phosphorescence lifetimes were calculated using the variational multireference spin-orbit configuration interaction (MRSOCI)[51] method. The rate constants for ISC and reverse ISC (rISC) as well as emission spectra were obtained in the Franck-Condon (FC) approximation with the VIBES program[37] (16384 or 32768 grid points, interval of 300 fs, damping of 100 cm^{-1}, temperatures of 77 and 298 K). For the (r)ISC rates internal coordinates were used. Emission spectra were calculated via vertical Hessian.

4 Results and Discussion

4.1 Zn-BDT

4.1.1 Ground State

Ground State Minima

A relaxed scan with fixed dihedral angle built up by N-C-Zn-S (compare figure 4.1) was conducted to understand the potential energy surface and identify relevant conformers of Zn-BDT. All calculations were performed in DCM utilizing the PCM model. The chosen dihedral angle affects the position of the ligands relative to each other. Starting at an angle of 0 degrees (planar alignment of the ligands), stationary points were optimized at intervals of 10 degrees until an angle of 90 degrees (orthogonal alignment of the ligands) was reached. The geometries of the stationary points obtained from the scan were used to determine the corresponding S0 energies using DFT/MRCI calculations. The result of this scan is shown in figure 4.1. In addition to the S0 energies of the stationary points (black dots), the figure also plots the S0 energies of the minima (red bars) that were obtained from regular geometry optimizations.

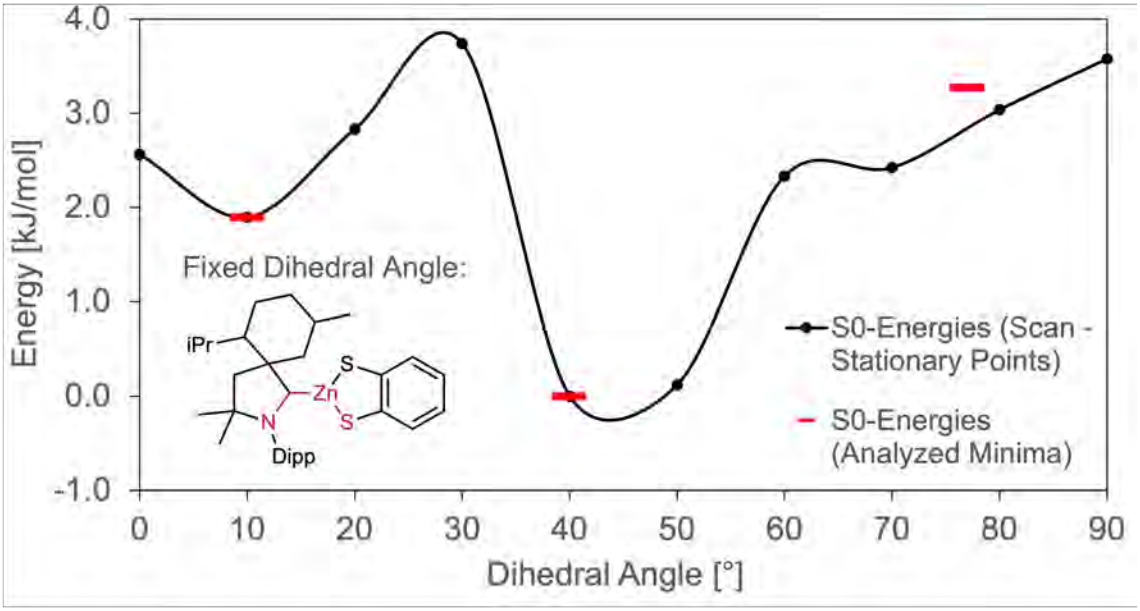

Fig. 4.1: Relative DFT/MRCI energies of Zn-BDT with different ligand orientation obtained from the relaxed scan. The stationary points are marked as black dots, and the calculated minima are marked as red bars.

The scan reveals three relevant conformers, one with a planar orientation of the ligands (10°), another one at an angle of 40° (referred to as the queer conformer in this work), and the last conformer at an orthogonal ligand orientation with an angle of 70°. Based on the stationary points found through the scan, minima were optimized, the relative energies of

which are also plotted in figure 4.1. The conformer designations of the minima, as well as the precise dihedral angles and S0 energies, are summarized in table 4.1.

Table 4.1: Summary of the conformer names, dihedral angles, and S0-DFT/MRCI energies of the optimized minima of Zn-BDT, as well as the energy difference compared to the most favourable conformer.

Conformer Name	Dihedral Angle	S0-Energy [Hartree]	Δ E [kJ/mol]
planar	10	-2361.826428	1.9
queer	40	-2361.827149	0
ortho	77	-2361.825903	3.3

The queer minimum is the lowest in energy, but is only 2-3 kJ/mol below the energies of the planar and orthogonal conformers. The calculated stationary points with dihedral angles in between the minima are also not significantly higher in energy. Overall, all conformers are within a range of 4 kJ/mol. This suggests that the rotational barrier between the conformers is low and that the ligands can rotate freely at room temperature in solution, allowing all three minima to be present. Crystal structures measured by Mrózek and Steffen et al. from TU Dortmund also show the presence of different conformers with dihedral angles of 5, 49 and 62 degrees.

Excitations

At the ground state geometry of all three conformers, the first excited singlet state is a $\pi\pi^*$-state (S-LLCT ($\pi\pi^*$)). It is characterized by a charge transfer from the BDT ligand to the carbene carbon atom of the CAAC ligand. The first excited triplet (T1) is also a $\pi\pi^*$ state (T-LLCT ($\pi\pi^*$)), with the same orbitals involved in the transition as the S1. The difference densities of both of these states at the geometry of the queer conformer are shown in figure 4.2.

The S2 and T2(planar)/T3(queer and ortho) are also LLCT ($\pi\pi^*$) states with the same character as the S1 and T1. The energy difference of these states is about 0.6 eV. The S1 and T1 excitation occurs from the HOMO to the LUMO, whereas the S2 and T2/T3 excitation occurs from the HOMO-1 to the LUMO. Since the order and character of the LLCT states never change, the energetically higher ones are not mentioned further in the evaluation.

Locally excited (LE) states are significantly higher in energy at the ground state geometries of the three conformers. This is illustrated in figure 4.3. The lowest LE is a triplet state that is characterized by a redistribution of charge on the benzoldithiol ligand. It is 0.70 to 0.55 eV above the T1-LLCT ($\pi\pi^*$). The lowest locally excited singlet state is even higher, with a distance of 1.28 to 1.14 eV. Pictures of the difference densities of these two states are in figure 4.2.

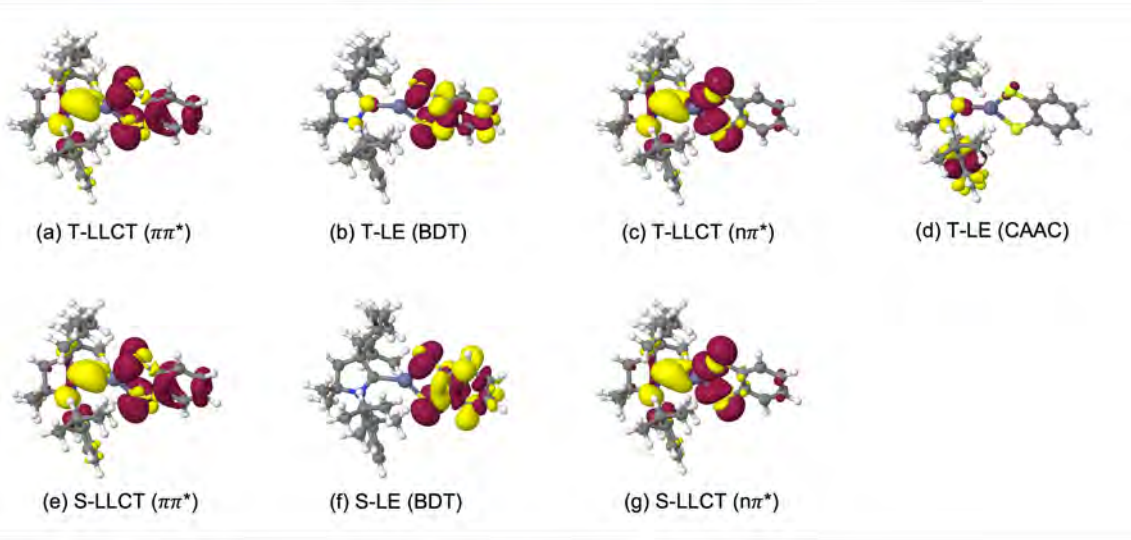

Fig. 4.2: DFT/MRCI difference densities (±0.001) of low-lying excited states at the ground state geometry of the queer conformer of Zn-BDT. Red indicates a loss and yellow indicates an increase in electron density.

The lowest state with a local excitation on the CAAC ligand is also a triplet state with an energy distance of 1.07 to 0.97 eV from the lowest triplet state (T1-LLCT ($\pi\pi^*$)). The corresponding singlet state is not within the first 10 excited states and is therefore not listed further.

A LLCT state involving a non-bonding orbital is also among the low excitations. The triplet and singlet LLCT ($n\pi^*$) are 1.03 to 1.04 eV and 1.06 to 1.11 eV, respectively, above the lowest excited triplet state.

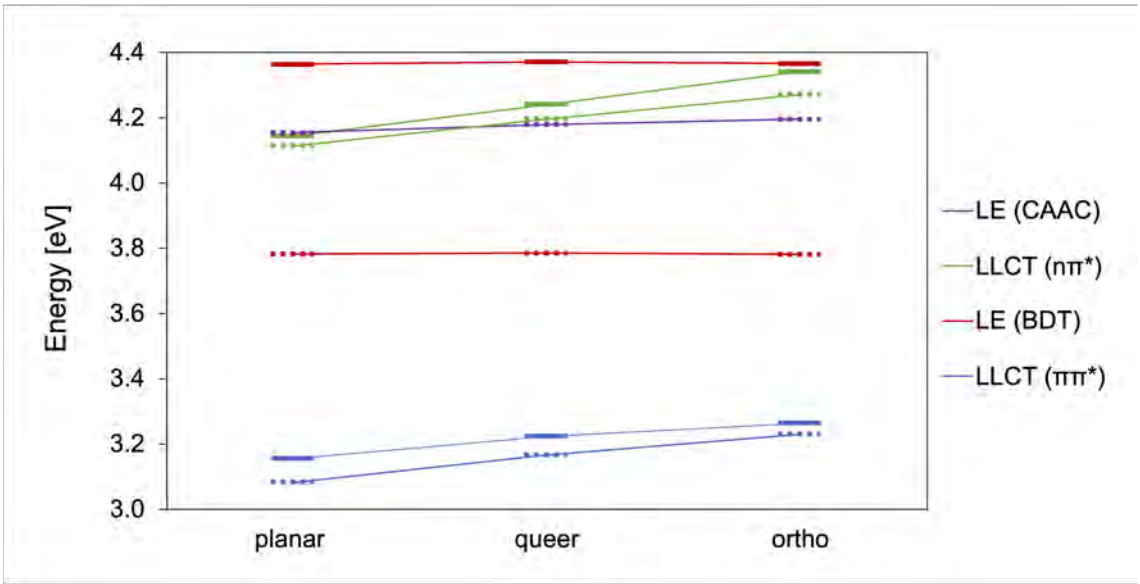

Fig. 4.3: Plot of the vertical excitation energies based on the ground state geometry of each conformer of Zn-BDT. Singlet states are represented by solid lines, triplet states by dashed lines.

There are no significant differences in the excitation energies of the conformers among themselves. Compared to each other, LLCT states are slightly more favourable at the planar geometry, while the orthogonal alignment favours LE states.

Noticeably, there are no LMCT states among the first excitations. For the planar and queer conformers, there are no LMCT transitions among the first ten single and triplet excitations. For the orthogonal conformer, the first LMCTs are S6 and T9. This is due to the electronic properties of zinc. The fully occupied d-shell of the d^{10} metal results in a low desire to absorb electrons. Therefore, the zinc atom is not involved in the low excitations and charge transfer to the unoccupied p-orbitals only occurs at high excitation energies.

Absorption

The absorption spectra of all three conformers have a similar shape and contain four major peaks, where one band is particularly pronounced. For the first two bands, differences between the conformers in terms of shape and height are noticeable, while the last two bands are almost exactly the same for all conformers.

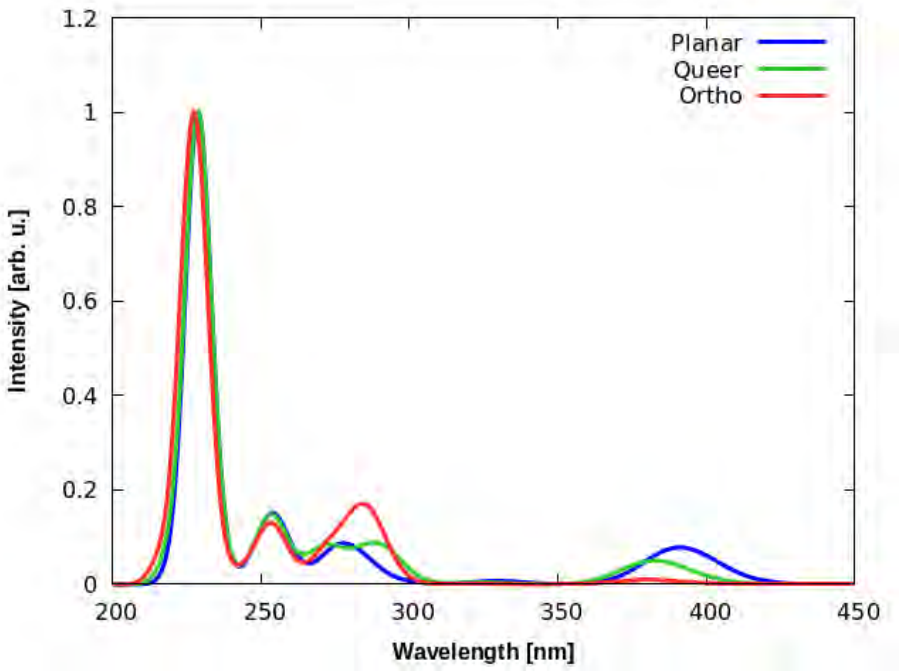

Fig. 4.4: Absorption spectra of the three Zn-BDT conformers.

The first band with a maximum at approximately 385 nm is caused by the S1 excitation for all three conformers and is therefore of CT character. Its intensity decreases from the planar over to the queer to the orthogonal conformer. The band of the orthogonal conformers is hardly visible any more.

For the next band which is in the range of 270-300 nm deviations between the conformers can be seen as well. This band is most pronounced for the orthogonal conformer and is caused by a CT state with $n\pi^*$ character. In the spectrum of the queer conformer, there are two peaks visible in this range, which are characterized by a further CT and by a local excitation. For the planar conformer, only one peak is visible again, which is due to an LE state.
The third band has a very similar high and shape for all conformers. The maximum is at around 254 nm and is caused by a local excitation on the BDT. The last band with a maximum at approximately 227 nm is the most pronounced. It is very similar for all conformers as well and is also caused by a local excitation on the BDT ligand.

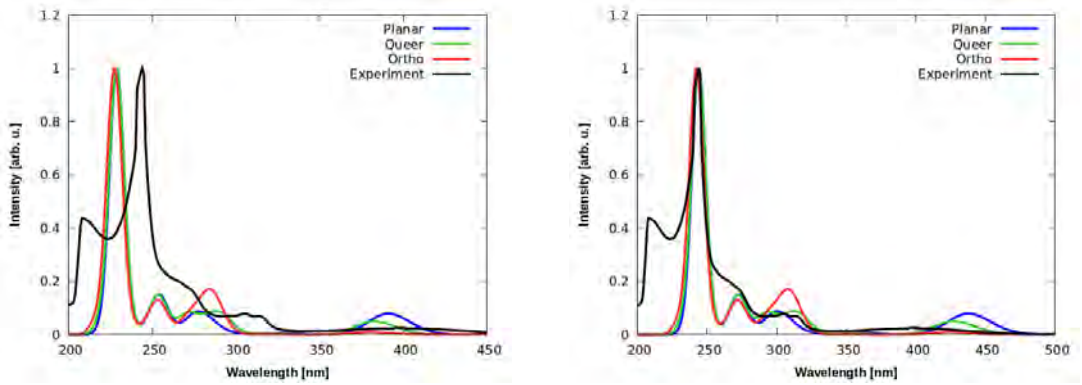

Fig. 4.5: Absorption spectra of the three Zn-BDT conformers and the experiment. On the left side is the untouched experimental spectrum on the right side the calculated spectra are shifted by 0.34 eV for a maximum overlap with the experimental spectrum. The experimental spectrum was measured in DCM by Mrózek and Steffen et al. from TU Dortmund. Results have not been published yet.

The calculated spectra are blue-shifted compared to the experimental one. The peaks of the most pronounced, highest-energy bands deviate by 15 nm. By shifting the calculated spectra so that there is a maximum overlap for these band, it can be seen that the shapes of the spectra are very similar.
The shape of the highest-energy band, caused by a local excitation on the BDT ligand, is almost identical for the calculated and experimental spectra. The second highest-energy peak, also caused by an LE, is more pronounced in the experimental spectrum, but has a similar shape. For the band with the third highest energy, three small, closely spaced peaks are visible in the experiment. These three peaks can be caused by the superposition of the peaks of the individual conformers, which suggests that different conformers are present in the experiment. The lowest-energy band also may be caused by the superposition of the spectra of the three conformers. The experimental band is less intense than the spectra of the planar and queer conformers, but more pronounced than that of the orthogonal one.

4.1.2 Excited States

Optimized Geometries

In order to further characterize the photophysical properties, structures of the lowest excited states were optimized. A total of two singlets (LLCT ($\pi\pi^*$) and LLCT ($n\pi^*$)) and four triplets (LLCT ($\pi\pi^*$), LLCT ($n\pi^*$), LE (BDT) and LE (CAAC)) were found. In the following, the differences between the geometries of the excited and ground states will be discussed. A detailed summary of the dihedral angles, energies, and energy differences can be found in table 4.2.

Comparison to the Ground State Geometries

For the singlet and triplet LLCT ($\pi\pi^*$) states, three energetically close conformers are relevant again. Their geometries differ only slightly from the ground state ones. The largest deviations occur with respect to the position of the ligands relative to each other. There are differences of 1-7 degrees for the dihedral angles of the ground state geometries compared to the LLCT ($\pi\pi^*$) state geometries (compare 4.1 and 4.2).
The geometry of the optimized local excitation on the BDT ligand is similar to the orthogonal conformer of the ground state geometry. However, there is a geometric change on the BDT ligand. The sulfur atoms and the benzene ring are no longer in the same plane, which results in a twist of the BDT ligand. This difference is illustrated in figure 4.6.

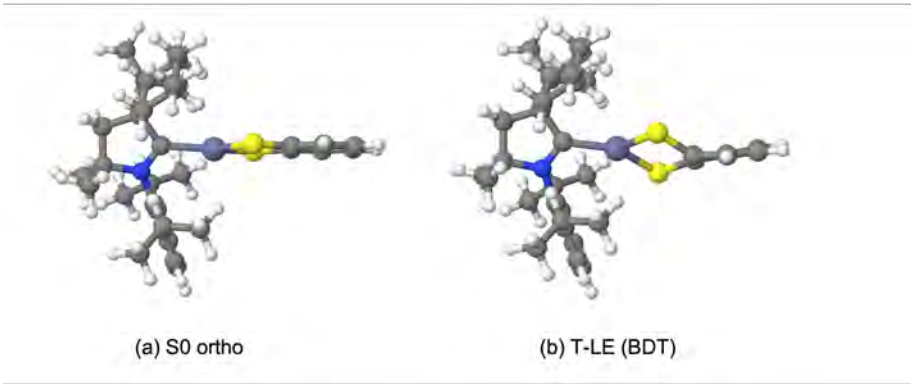

Fig. 4.6: Comparison of the geometry of the orthogonal conformer of the ground state to that of T-LE (BDT) for Zn-BDT.

The geometry of the T-LE (CAAC) is similar to the queer conformer in the ground state. With a dihedral angle of 36° for the T-LE (CAAC) and a dihedral angle of 40 degrees for the queer ground state conformer, the ligand orientations are pretty much the same. However, there are geometric differences on the CAAC ligand due to the loss of planarity of the Dipp moiety. This occurs due to anti bonding orbitals being occupied on the Dipp moiety resulting from the excitation.

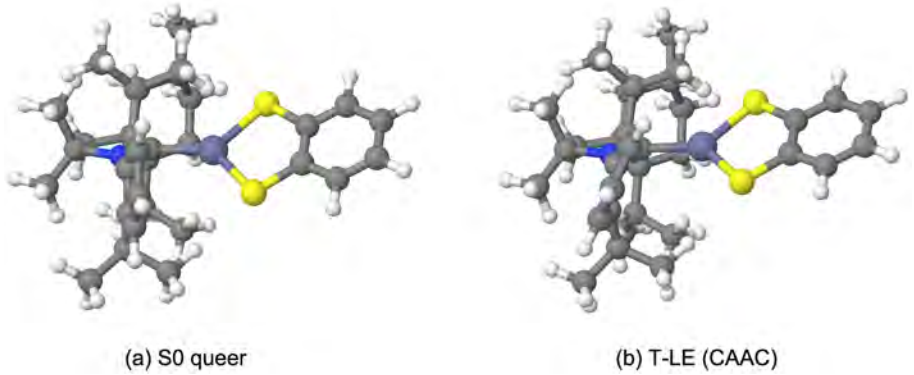

Fig. 4.7: Comparison of the geometry of the queer conformer in the ground state to that of T-LE (CAAC) for Zn-BDT.

The single and triplet LLCT ($n\pi^*$) states show the largest geometric deviations compared to the ground state geometries. The optimized ($n\pi^*$) is characterized by a bent BDT ligand. Due to the sterically demanding groups on both sides of the CAAC ligand, the bend is most energetically favourable in the planar position of the ligands towards each other. The geometric differences between the singlet and triplet LLCT ($n\pi^*$) states themselves are minimal. Therefore, in the following figure, the planar ground state is only compared with the singlet LLCT ($n\pi^*$) state.

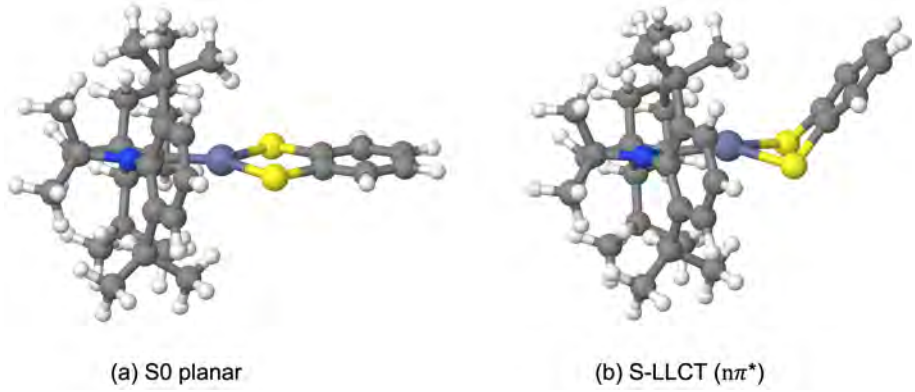

Fig. 4.8: Comparison of the geometry of the planar conformer of the ground state to that of S-LLCT ($n\pi^*$) for Zn-BDT.

Comparison of the Energies of the Excited State Geometries

The dihedral angles of all excited state geometries are summarized in table 4.2. The table also includes the S0 energies of all optimized excited states geometries and their energy difference compared to the most favourable S0 energy (T-LLCT ($\pi\pi^*$) ortho).

The orthogonal conformer of the T-LLCT ($\pi\pi^*$) geometry has the most favourable S0 energy, closely followed by the S0 erngey of the queer S-LLCT ($\pi\pi^*$) geometry, which is only 1 kJ/mol higher. In general, the S0 energys of all conformers of the singlet and triplet LLCT ($\pi\pi^*$) geometries are very close to each other. The distance of the S0 energies of the locally excited state geometries to the most favourable S0 energy is already significantly higher with 39 and 42 kJ/mol and increases further to 46 and 44 kJ/mol for the singlet and triplet LLCT ($n\pi^*$) state geometries.

Table 4.2: Dihedral angles, S0 energies and energy differences compared to the most favourable S0 energy (T-LLCT ($\pi\pi^*$) ortho) of the optimized excited state geometries of Zn-BDT.

Optimized State	Angle (Orientation)	Δ E [kJ/mol]
S-LLCT ($\pi\pi^*$)	17° (planar)	1.7
	39° (queer)	1.0
	76° (ortho)	1.8
S-LLCT ($n\pi^*$)	(planar - bend)	45.7
T-LLCT ($\pi\pi^*$)	13° (planar)	6.2
	36° (queer)	3.6
	80° (ortho)	0
T-LLCT ($n\pi^*$)	(planar - bend)	44.1
T-LE (BDT)	(ortho - twisted)	38.8
T-LE (CAAC)	36° (queer)	41.8

Adiabatic Excitation Energies

In the diagram below, the excitation energies of relevant states are plotted for all six optimized excited state geometries and the ground state. Of particular interest are the adiabatic excitation energies, which in this case are always the lowest excited states at the corresponding geometries.

The singlet and triplet LLCT ($\pi\pi^*$) excitations that lie lowest in the ground state undergo a decrease in energy of more than 0.6 eV at their optimized state geometry. As shown in figure 4.9, these two states remain the adiabatically lowest. Upon optimization the LLCT ($n\pi^*$) states are stabilised by more than 1.5 eV. Thus, the adiabatic distance between the LLCT $\pi\pi^*$ and $n\pi^*$ states is only 0.2 eV. Due to this small distance, all four states (S- and T-LLCT ($\pi\pi^*$) and S- and T-LLCT ($n\pi^*$)) may be involved in relaxation processes after e.g. photo excitation.

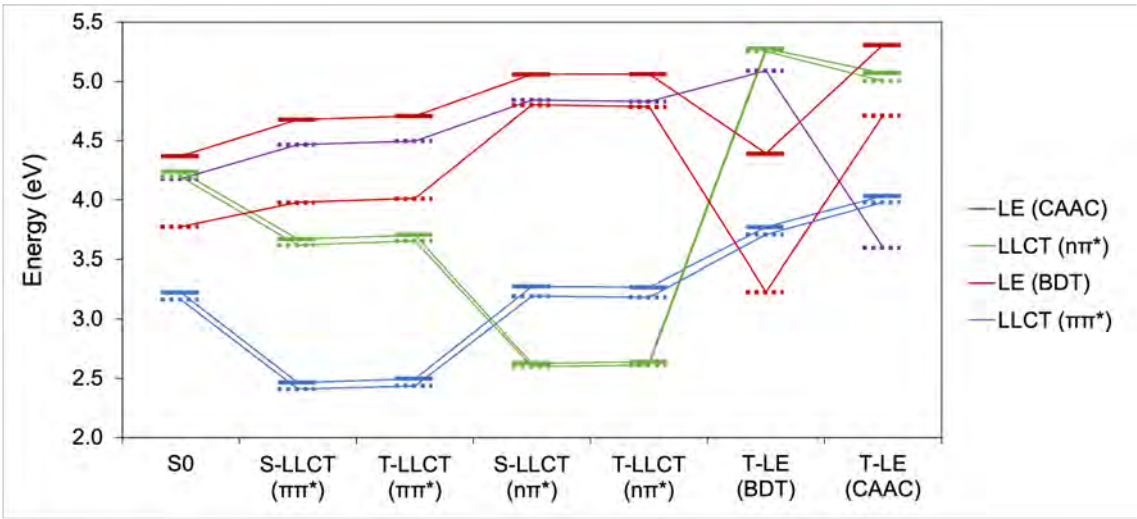

Fig. 4.9: Excitation energies for all optimized state geometries of Zn-BDT. For the S0, S- and T-LLCT ($\pi\pi^*$) geometries the results of the queer conformers are shown. Similar diagrams for the other conformers hardly differ and can be taken from the appendix. Singlet states are represented by solid lines, triplet states by dashed lines.

The locally excited states are not lowered as much in energy upon optimization as the CT states. Their adiabatic energy level is significantly higher with 0.7 to 1.1 eV above the LLCT ($\pi\pi^*$) states. This suggests that the T-LEs are unimportant in terms of the Zn-BDT emission properties. Thus, it can be expected that the molecule will end up in one of the LLCT states after excitation.

figure 4.9 already indicates small ΔE_{S-T}s for the CT states. This is true for both the ($\pi\pi^*$) and ($n\pi^*$) states. With 223 cm^{-1} for the planar, 195 cm^{-1} for the queer and 157 cm^{-1} for the orthogonal conformer for the LLCT ($\pi\pi^*$)s and 134 cm^{-1} for the LLCT ($n\pi^*$)s, all ΔE_{S-T}s are tiny.

Table 4.3: ΔE_{S-T}s of the LLCT states of Zn-BDT.

LLCT State	$\pi\pi^*$			$n\pi^*$
Ligand Orientation	planar	queer	ortho	planar
ΔE_{S-T} [cm^{-1}]	223	195	157	134

4.1.3 Rate Constants

Fluorescence and Phosphorescence Rates

First, the fluorescence and phosphorescence rate constants are considered. A list of these is given for both the conformers of the $\pi\pi^*$ states and the $n\pi^*$ states in table 4.4.
The $\pi\pi^*$ states have a very pronounced fluorescence with rates in the range of $10^6 - 10^7$ s^{-1}. The planar and queer conformers have 8 to 5 times higher rates than the orthogonal conformer. For the $n\pi^*$ states, the fluorescence rates are about 2 orders of magnitude lower.
The phosphorescence rates are very low for all states. However, yet again the $\pi\pi^*$ states show more favourable TADF emitter properties concerning the phosphorescence rates and are therefore lower. Again the rates of the planar and queer conformer differ somewhat from the orthogonal conformer and are 470 to 30 times lower.
Therefore, a population of LLCT $\pi\pi^*$ states would be more favourable for the TADF behaviour of Zn-BDT due to the higher fluorescence and lower phosphorescence rates.

Table 4.4: Fluorescence and phosphorescence rates of the LLCT $\pi\pi^*$ and $n\pi^*$ states of Zn-BDT.

State	Ligand Orientation	k_F [s^{-1}]	k_P [s^{-1}]
LLCT ($\pi\pi^*$)	planar	$1.0{\cdot}10^7$	2
	queer	$7.8{\cdot}10^6$	31
	ortho	$1.3{\cdot}10^6$	939
LLCT ($n\pi^*$)	planar	$7.4{\cdot}10^4$	1570

ISC and rISC Rates - Same Character

Below, the ISC and rISC rates between singlet and triplet states of the same character (i.e., transition from S-LLCT $\pi\pi^*$ to T-LLCT $\pi\pi^*$ vice versa, and the same for the $n\pi^*$ states) will be discussed. First, a consideration of the SOCME:

Table 4.5: SOCMEs of the LLCT $\pi\pi^*$ and $n\pi^*$ states of Zn-BDT.

State	Ligand Orientation	$\sum$SOCME^2	
		S [cm^{-2}]	T [cm^{-2}]
LLCT ($\pi\pi^*$)	planar	3.1	1.8
	queer	21.6	20.1
	ortho	8.9	7.2
LLCT ($n\pi^*$)	planar	2.1	3.4

The Zn-BDT contains a rather weak SOC, which is sufficient, however, to induce (r)ISC. The queer conformer of the $\pi\pi^*$ state stands out with squared SOCMEs of 21.6 and 20.1 cm^{-2}, respectively. The SOC of the states with planar ligand orientation, both $\pi\pi^*$ and $n\pi^*$, is least pronounced.

A difference between $\pi\pi^*$ and $n\pi^*$ states can be seen when considering the ratios between S and T SOCMEs. Only for the $n\pi^*$ state, a higher SOC for the transition from triplet to singlet, compared to the transition from singlet to triplet is seen. For the $\pi\pi^*$ states, the behaviour is exactly the opposite. With corresponding VIBES rates, this can be reflected in the (r)ISC, where in the case of the $\pi\pi^*$ states the rISC would be less pronounced than the ISC.

The ISC and rISC rates at 77 K and 298 K are shown in the tables 4.6 and 4.7. The values at both temperatures are very similar to completely identical. Only one exception stands out: in the case of the orthogonal conformer, where the rISC rate at 77 K is almost 3 orders of magnitude smaller. All other rate constants are fairly hight, ranging from $10^7 - 10^{10}$ s^{-1}.

Table 4.6: ISC and rISC rates of the LLCT $\pi\pi^*$ and $n\pi^*$ states at of Zn-BDT 77 K.

State	Ligand Orientation	ISC [s^{-1}]	rISC [s^{-1}]
LLCT ($\pi\pi^*$)	planar	$1.4{\cdot}10^9$	$3.3{\cdot}10^7$
	queer	$3.7{\cdot}10^{10}$	$6.7{\cdot}10^9$
	ortho	$3.7{\cdot}10^9$	$6.2{\cdot}10^4$
LLCT ($n\pi^*$)	planar	$3.4{\cdot}10^9$	$1.5{\cdot}10^9$

The best rate constants are shown for the queer conformer of the $\pi\pi^*$ state and the $n\pi^*$ state. They have the highest values and a good ratio between ISC and rISC. In both cases, the ISC rate is about twice as large as the rISC rate.

Table 4.7: ISC and rISC rates of the LLCT $\pi\pi^*$ and $n\pi^*$ states at of Zn-BDT 298 K.

State	Ligand Orientation	ISC [s^{-1}]	rISC [s^{-1}]
LLCT ($\pi\pi^*$)	planar	$2.0{\cdot}10^9$	$7.8{\cdot}10^7$
	queer	$3.7{\cdot}10^{10}$	$6.7{\cdot}10^9$
	ortho	$4.6{\cdot}10^9$	$1.0{\cdot}10^7$
LLCT ($n\pi^*$)	planar	$3.4{\cdot}10^9$	$1.4{\cdot}10^9$

ISC and rISC Rates - Different Characters

Furthermore, the question is unresolved, which state is populated after excitation and from which state emission processes occur. One way to answer this question is to consider the (r)ISC rates between states of different character ($\pi\pi^*/n\pi^*$). The resulting rate constants are shown for all three conformers in the following figures. The equilibrium arrows reflect which states are preferably populated. Associated rate constants are located near the arrows.

First, the overview of the (r)ISC constants at 77 K:

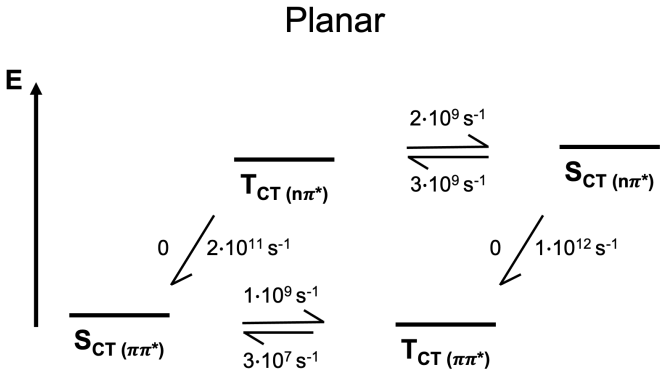

Fig. 4.10: (r)ISC rates of the LLCT states for the planar conformers of Zn-BDT at 77 K.

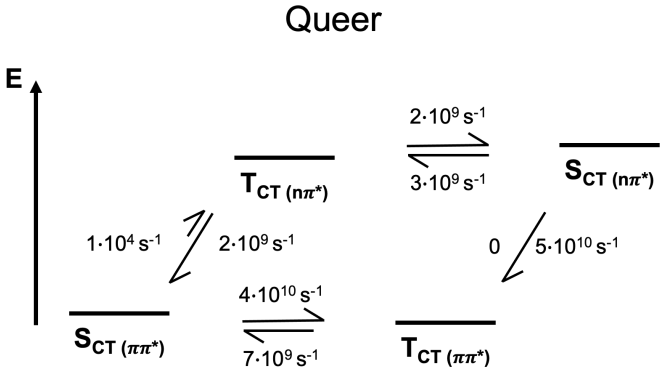

Fig. 4.11: (r)ISC rates of the LLCT states for the queer conformers of Zn-BDT at 77 K.

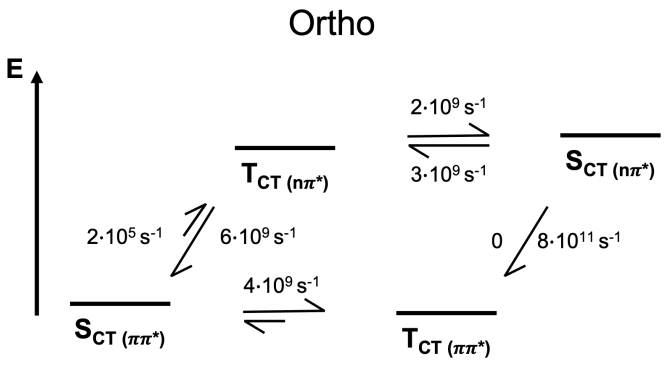

Fig. 4.12: (r)ISC rates of the LLCT states for the ortho conformers of Zn-BDT at 77 K.

At 77 K, the preferred population of the $\pi\pi^*$ states is evident. For all conformers, there are fast ISC rates from S-CT($n\pi^*$) to T-CT($\pi\pi^*$) and rISC from T-CT($n\pi^*$) to S-CT($\pi\pi^*$). Corresponding back reactions have very low rate constants. Thus, in this case only the lower-lying LLCT ($\pi\pi^*$) states would be occupied and relaxation back to the ground state would only occur from these states. This is optimal for the TADF properties of Zn-BDT, since the S-LLCT($\pi\pi^*$) state of all conformers has a higher fluorescence rate than the corresponding $n\pi^*$ state.
Together with the high rISC rate, the low phosphorescence and the high fluorescence rate, delayed fluorescence from the S1 state is the preferred relaxation process. In this case, the queer conformer shows the best TADF properties, with a high fluorescence rate, the lowest phosphorescence rate and the best ratio of ISC and rISC.

At 298 K, a different behaviour is observed. The rate constants for the forward reaction to the LLCT ($\pi\pi^*$) states have hardly changed, however, the rate constants for the reverse reactions to the LLCT ($n\pi^*$) states have increased significantly. In the case of the planar conformer, the rISC rates that were very slow at 77 K have increased to 10^8 or 10^7 s^{-1}. The ratio is still several orders of magnitude in favour of the $\pi\pi^*$ states, but this behaviour is not as pronounced for the other conformers. For the queer and orthogonal conformer, a similar distribution (resulting from ISC and rISC rates in the same magnitude) between the T-CT($n\pi^*$) and S-CT($\pi\pi^*$) state exists. Therefore, the only equilibrium position favouring the $\pi\pi^*$ states is between S-CT($n\pi^*$) and T-CT($\pi\pi^*$) caused by larger ISC from S-CT($n\pi^*$) to T-CT($\pi\pi^*$) then rISC from S-CT($n\pi^*$) to T-CT($\pi\pi^*$) (compare figure 4.14 and 4.15). In the case of the orthogonal conformer, the population of the T-CT($\pi\pi^*$ state) is still 10000 times higher than that of the S-CT($n\pi^*$), but for the queer conformer it is only 100 times higher. However, even this ratio should be sufficient for the equilibrium to be on the side of the $\pi\pi^*$ states for all conformers and for emission to occur from the S-LLCT($\pi\pi^*$).

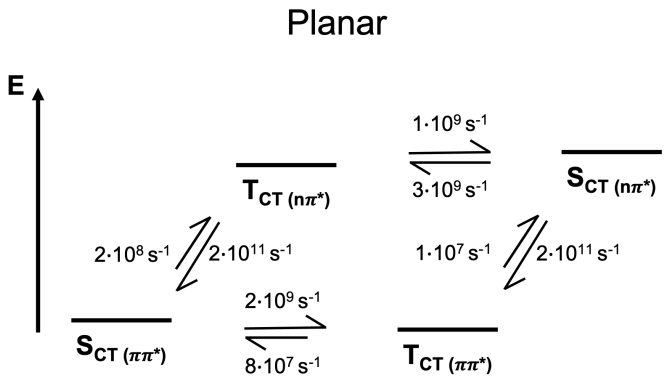

Fig. 4.13: (r)ISC rates of the LLCT states for the planar conformers of Zn-BDT at 298 K.

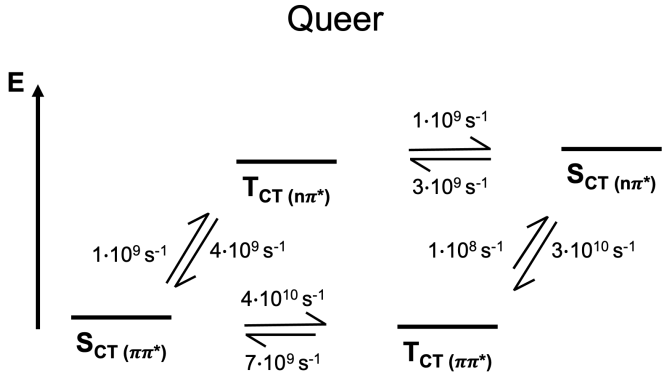

Fig. 4.14: (r)ISC rates of the LLCT states for the queer conformers of Zn-BDT at 298 K.

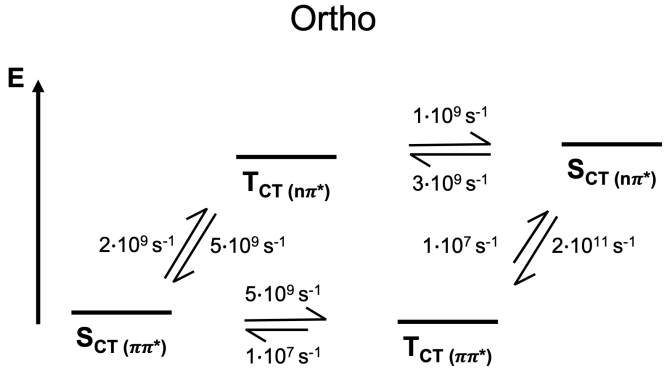

Fig. 4.15: (r)ISC rates of the LLCT states for the ortho conformers of Zn-BDT at 298 K.

4.1.4 Emission

Due to large displacements that persist even in Vertical Hessian calculations, satisfactory spectra could not be calculated for the orthogonal conformer (see appendix). However, by neglecting two frequencies with the highest displacement values a better result was obtained, that is displayed in the figure below together with the other two conformers and the experimental spectrum.

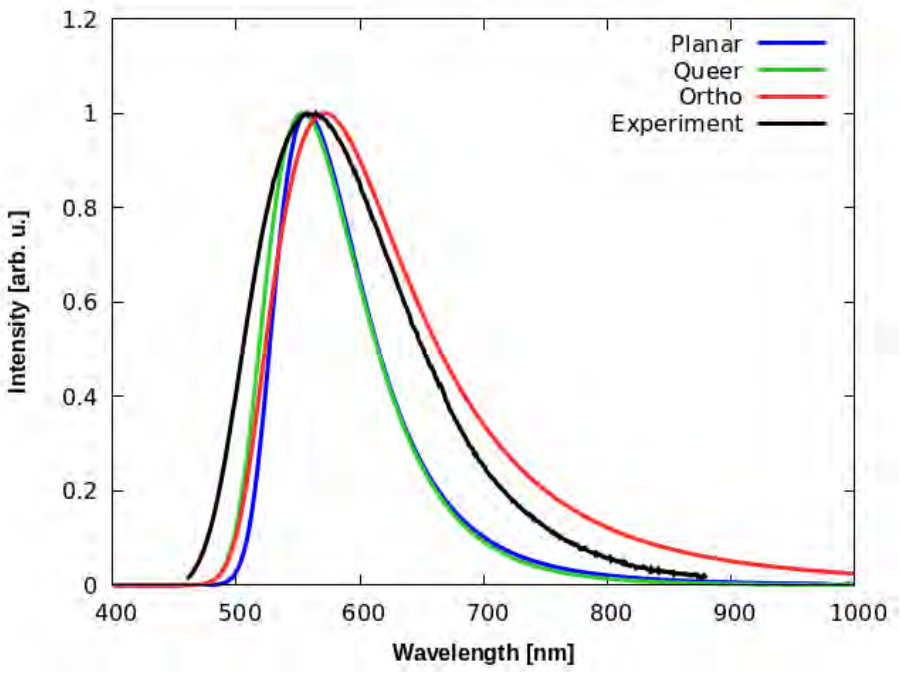

Fig. 4.16: Emission spectrum from the S-LLCT ($\pi\pi^*$) state for all conformers of Zn-BDT and the experimental spectrum at 298 K. The experimental spectrum was measured in solid state by Mrózek and Steffen et al. from TU Dortmund. Results have not been published yet.

The emission spectra of the planar and queer conformer are almost identical in terms of their energy level and shape. They have emission maxima at 557 nm and 553 nm respectively and are thus slightly blue-shifted compared to the orthogonal conformer with a maximum at 571 nm. The spectrum of the orthogonal conformer is much broader than that of the other two conformers.

The experimentally measured spectrum has an emission maximum at 564 nm, in the middle of the calculated spectra and could very well be caused by the superposition of the individual conformers. The shape of the experimental spectrum is broader and shows the strongest similarity to the orthogonal conformer.

Due to the position of the emission maximum of around 560 nm, the emission from the S-LLCT ($\pi\pi^*$) state generates light that is perceived by the human eye as yellow.

4.2 Zn-BDO

4.2.1 Ground State

Ground State Minima

A scan with a fixed dihedral angle built up by N-C-Zn-O (compare figure 4.17) that is decisive for the ligand arrangement towards each other was also performed on the Zn-BDO. All calculations were performed in DCM utilizing the PCM model. The calculated DFT/MRCI energies, shown in figure 4.17, reveal the existence of multiple conformers with near degenerated energies. In the range of 0-40 degrees, there is only a slight increase in energy and five stationary points within a range 1.5 kJ/mol can be observed. A significantly increased energy is observed at angles greater than 40 degrees, with distinctive minima for angles of 60 and 90 degrees standing out. The overall lowest-lying energy minima from the scan are at 0 and 90 degrees. For comparison with the Zn-BDT, a conformer with a queer ligand position is also of interest.

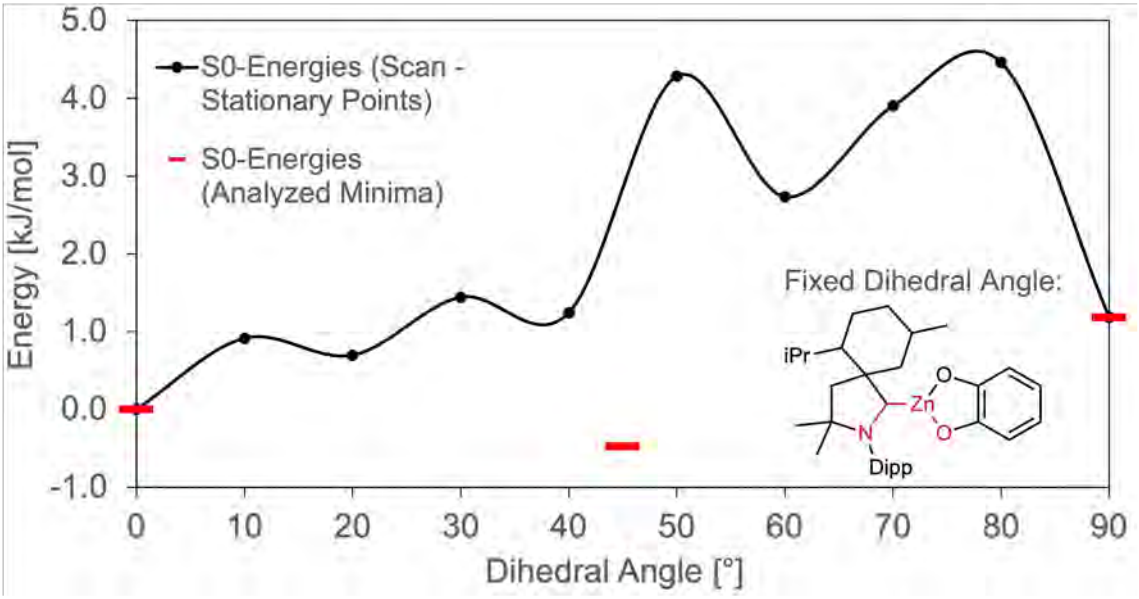

Fig. 4.17: Relative DFT/MRCI energies of the Zn-BDO with different ligand positions. The S0 energies of the identified stationary points are marked in blue, the S0 energies of calculated minima are marked in red.

The results of the scan were used as starting points for minima with a planar, queer, and orthogonal ligand arrangement. The resulting optimized minima structures are marked with red bars in figure 4.17. The minima of the planar and orthogonal conformers were identical to their stationary points and therefore lie on the curve of the torsion path. For the queer conformer, a lower-lying minimum was found. Due to the newly detected minimum, the queer conformer is now lower in energy than the planar and orthogonal one. The specific dihedral angles of the conformers, their ground state energies, and their energy differences are summarized in table 4.8. All three conformers are very close

in energy, with a maximum energy difference of 1.7 kJ/mol. Since the energy barriers between the conformers are also low, it can be assumed that all conformers are present at RT.

Table 4.8: Summary of the conformer names, dihedral angles, and S0 DFT/MRCI energies of the optimized minima of Zn-BDO, as well as the energy difference compared to the most favourable conformer.

Conformer Name	Dihedral Angle	S0-Energy [Hartree]	ΔE [kJ/mol]
planar	0	-1715.921531	0.5
queer	45	-1715.921711	0
ortho	90	-1715.921081	1.7

Excitations

As for the Zn-BDT, the S1 and T1 for all three conformers are a $\pi\pi^*$ states. They are characterized by a charge transfer from the BDO ligand to the carbene carbon atom of the CAAC ligand. Yet again, the same orbitals are involved in the singlet and triplet state. The difference densities of both states at the geometry of the queer conformer are shown in figure 4.18 (a and e).

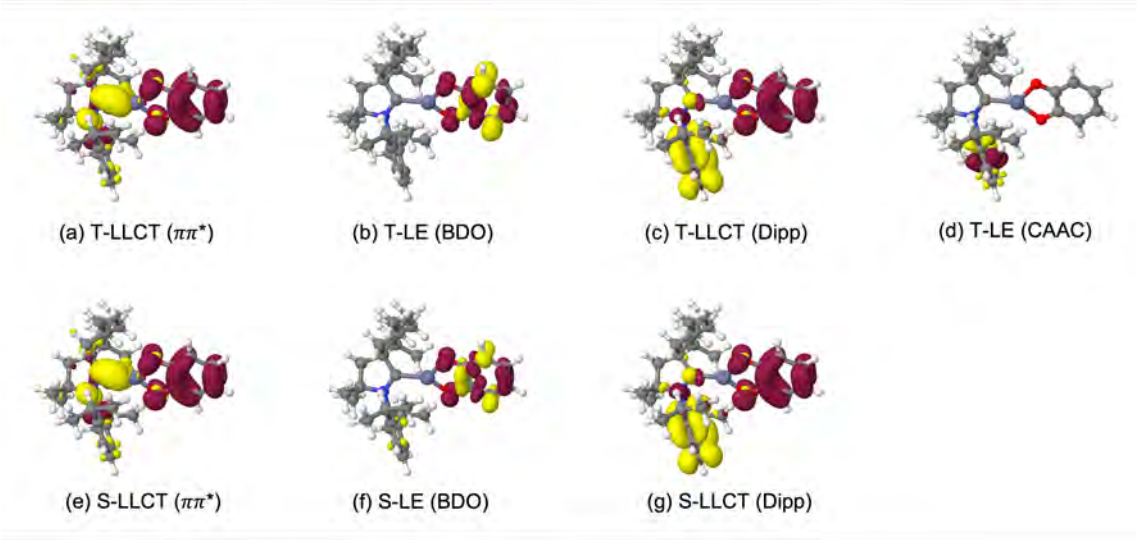

Fig. 4.18: DFT/MRCI difference densities (±0.002) of low-lying excited states at the ground state geometry of the queer conformer of Zn-BDO. Red indicates a loss and yellow indicates an increase in electron density.

Locally excited (LE) states are significantly higher in energy at the ground state geometry of the three conformers. The energetic differences of all states presented in figure 4.18 are illustrated in figure 4.19. The lowest LE is a triplet state that is characterized by a redistribution of charge on the BDO ligand. It is 1.13 to 0.94 eV above the T1-LLCT ($\pi\pi^*$) for the different conformers. The lowest locally excited singlet state is even higher, with a distance of 1.85 to 1.66 eV. Pictures of the difference densities of these two states

are also shown in figure 4.18 (b and f).
The lowest state with a local excitation on the CAAC ligand is 1.38 to 1.23 eV above the lowest triplet state (T1-LLCT ($\pi\pi^*$)). The corresponding singlet state is a lot higher in engery and is therefore omitted.
Contrary to the Zn-BDT, a LLCT ($n\pi^*$) state involving a non-bonding orbital is not among the lowest 10 excitations, however another LLCT state was found. The LLCT (Dipp) is characterised by a shift of electron density from the BDO ligand to the Dipp moiety of the CAAC ligand. The respective triplet and singlet LLCT (Dipp) lie very close to each other and are 1.6 to 1.4 eV above the lowest excited triplet state.

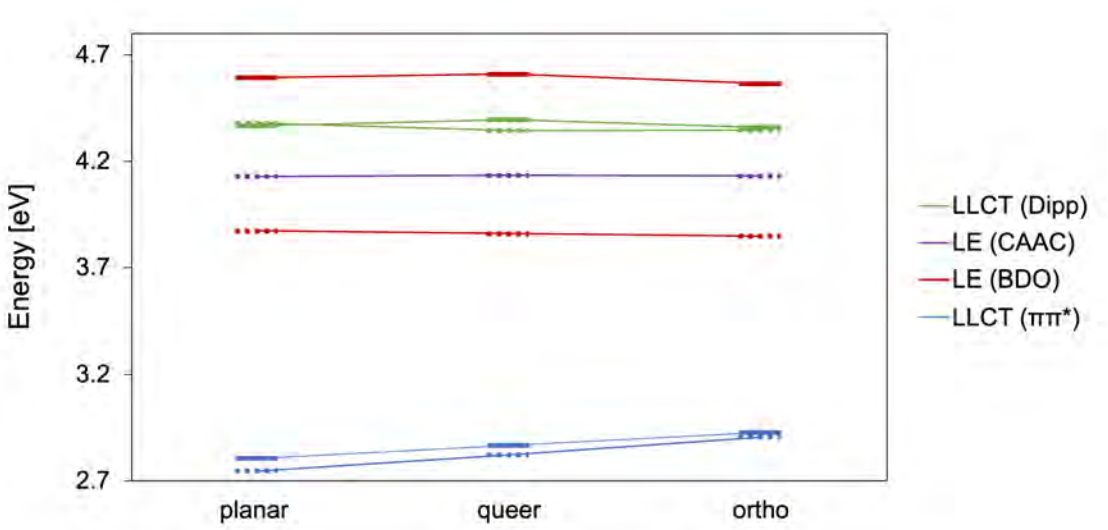

Fig. 4.19: Vertical excitation energies based on the ground state geometry of each conformer of Zn-BDO. Singlet states are represented by solid lines, triplet states by dashed lines.

With the exception of a slight increase in energy of the LLCT ($\pi\pi^*$) states, there are hardly any changes between the conformers.
There is also no states involving charge transfer to the zinc atom in Zn-BDO. Among the first ten excitations, there are no LMCT or MC state for any of the conformers.

Absorption

The planar and queer conformer show similar absorption characteristics. The absorption spectra are characterized primarily by 3 bands. The spectrum of the orthogonal conformer, however, has one band less, which is the lowest-energy band for the other conformers. For the planar and queer conformers this slightly wider band with a maximum at 442 and 432, respectively, originates from the S1 LLCT ($\pi\pi^*$) state.
The band with the second lowest energy is similar for all conformers and is caused by a strongly absorbing local excitation on the BDO ligand and has its maximum at around 270 nm. In the case of the planar and queer conformer, this is the most intense band.

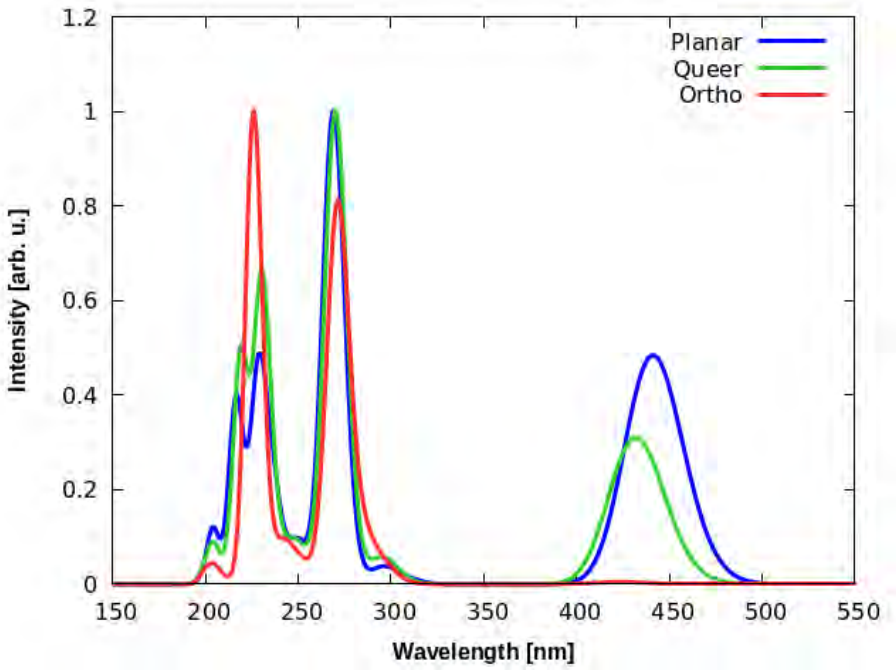

Fig. 4.20: Absorption spectra of all three conformers of Zn-BDO.

In the case of the next band, there are again striking differences between the orthogonal conformer and the other two. The band of the planar and queer conformers is divided into two almost equally high, mutually overlapping peaks with maxima at 228 and 218 nm. They are caused by another state of local excitation on the BDO, as well as a charge transfer from the BDO to the zinc atom. For the orthogonal conformer, only one sharp, pronounced peak is visible with a maximum at 225 nm and characterized by a mixed state with charge transfer from the BDO ligand to the CAAC ligand and metal atom.

4.2.2 Excited States

Optimized Geometries

For further characterization of the photophysical properties two singlets (LLCT ($\pi\pi^*$) and LLCT (Dipp)) and three triplets (LLCT ($\pi\pi^*$), LE (BDO) and LE (CAAC)) were optimized. In the following, the differences between the geometries of the excited and ground states will be discussed. A detailed summary of the dihedral angles, S0-energies, and energy differences can be found in table 4.9.

Comparison to the Ground State Geometries

For the singlet and triplet LLCT ($\pi\pi^*$) states, three energetically close conformers are again relevant. Compared to the ground state geometry, they differ mainly in the twist of the ligands with respect to each other. The queer conformer shows the smallest deviations, with the singlet and triplet state separated by only 2° from the ground state at an angle of 47°. The orthogonal conformer has a deviation of 8° and 7° for the singlet and triplet state, respectively. However, the difference is greatest for the planar conformer, with the singlet state having a dihedral angle of 24° and the triplet state having a dihedral angle of 14° compared to the 0° of the ground state.

All three remaining excited state geometries are similar to the orthogonal conformer in the ground state.
The T-LE (BDO) remains unchanged in terms of the CAAC ligand but shows geometrical differences on the BDO ligand. Similar to the BDT, the chalkogen atoms are twisted out of the benzylplane. Also, a slight bending of the benzene ring can be seen, which is no longer in exact orthogonal alignment with the CAAC ligand. Differences are illustrated in figure 4.21.

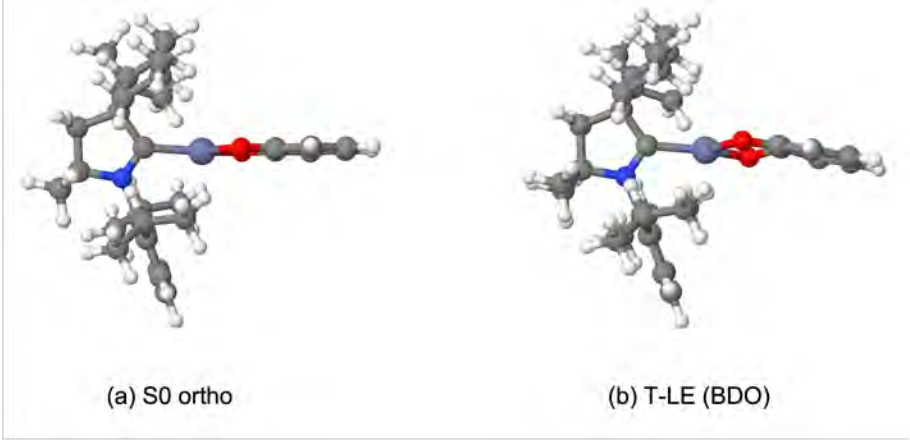

Fig. 4.21: Comparison of the geometry of the ortho conformer of the ground state to that of T-LE (BDO) for Zn-BDO.

The geometry of the local excitation on the CAAC ligand has a slightly altered dihedral angle with an angle of 83 degrees compared to the 90 degrees of the orthogonal conformer. Changes to the CAAC ligand are primarily on the Dipp residue, where, due to the redistribution of charge, the planarity of the six-ring is lost.

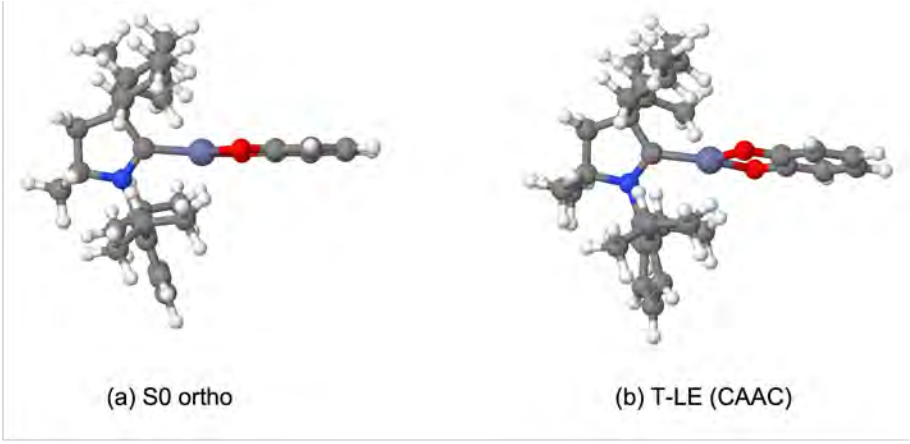

Fig. 4.22: Comparison of the geometry of the ortho conformer of the ground state to that of T-LE (CAAC) for Zn-BDO.

The geometry of the LLCT (Dipp) state has similarities with the LLCT ($n\pi^*$) of Zn-BDT in terms of a bending of the BDO ligand. However, for the LLCT (Dipp), the positions of the oxygen atoms and the benzene ring hardly change, but a displacement of the zinc atom occurs. It moves towards the Dipp residue of the CAAC ligand, causing its alignment to change. In the case of the orthogonal conformer of the ground state, the Dipp residue leans towards the BDO ligand. Due to the change in position of the zinc atom, the Dipp residue now leans to the opposite direction, as shown in the following figure.

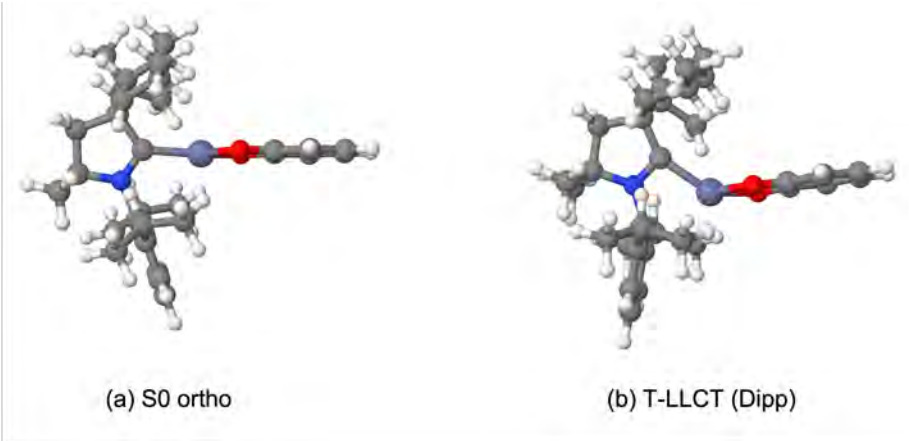

Fig. 4.23: Comparison of the geometry of the ortho conformer of the ground state to that of T-LLCT (Dipp) for Zn-BDO.

Comparison of the Energies of the Excited State Geometries

After comparing the ground state energies of the excited state geometries (see table 4.9) it can be seen, that the planar S-LLCT ($\pi\pi^*$) geometry has the overall lowest S0 energy. The ground state energies of the other S-LLCT ($\pi\pi^*$) geometries are a little bit higher with 4.5 and 9 kJ/mol above the S0 energy of the planar S-LLCT ($\pi\pi^*$) for the queer and orthogonal conformer. With a distance of 13 to 20 kJ/mol, the S0 energies of the conformers of the same triplet state are slightly higher. The order of the conformers is swapped, with the orthogonal one now having the most favourable ground state energy of the triplet states and the queer one having the least favourable. The S0 energy of the LE (BDO) geometry is only slightly above the T-LLCT ($\pi\pi^*$) geometries with a distance of 25 kJ/mol to the most favourable geometry. The ground state energies of the LE (CAAC) and LLCT (Dipp) geometries are significantly higher, at 55 and 87 kJ/mol, respectively.

Table 4.9: Dihedral angles, S0 energies and energy differences compared to the most favourable S0 energy (S-LLCT ($\pi\pi^*$) planar) of the optimized excited state geometries of Zn-BDO.

Optimized State	Angle (Orientation)	ΔE [kJ/mol]
S-LLCT ($\pi\pi^*$)	24° (planar)	0
	47° (queer)	4.5
	82° (ortho)	9.0
S-LLCT (Dipp)	(ortho - bend)	86.7
T-LLCT ($\pi\pi^*$)	14° (planar)	18.8
	47° (queer)	20.3
	83° (ortho)	12.7
T-LE (BDO)	(ortho - twisted)	25.3
T-LE (CAAC)	83° (ortho)	55.2

Adiabatic Excitation Energies

Excitation and adiabatic excitation energies of the Zn-BDO are presented in the figure 4.24.

With an energy gain of 1 eV upon excitation at the corresponding optimized geometry, the S and T LLCT ($\pi\pi^*$) states are the overall lowest. The S-LLCT (Dipp) state also experiences a significant stabilisation of 1.4 eV compared to the ground state. However, with a distance of 3.0 eV to the S0 state, the S-LLCT (Dipp) state is still 1.2 eV above the LLCT ($\pi\pi^*$)s. The locally excited states experience smaller energy lowerings of 0.4 and 0.6 eV for LE (BDO) and LE (CAAC), respectively, and thus still lie above the S-LLCT (Dipp) state at their optimized geometry.

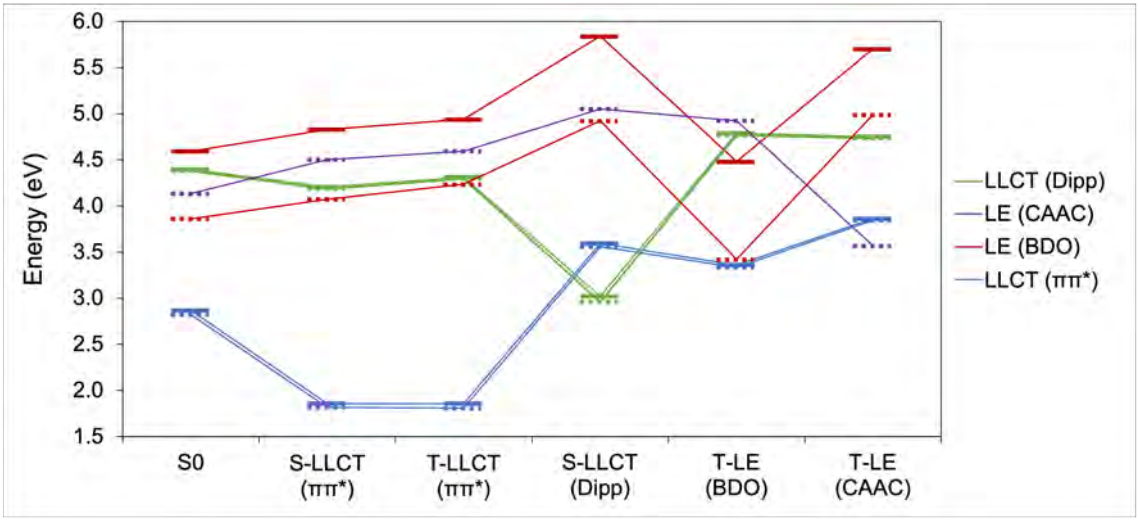

Fig. 4.24: Excitation energies for all optimized state geometries of Zn-BDO. For the S0, S- and T-LLCT ($\pi\pi^*$) geometries the results of the queer conformers are shown. Similar diagrams for the other conformers hardly differ and can be taken from the appendix. Singlet states are represented by solid lines, triplet states by dashed lines.

The LLCT ($\pi\pi^*$) states are thus by far the energetically lowest states with a minimum distance of 1.2 eV to the others. Since the other states are far above, it can be interpreted from figure 4.24 that these do not play a role in the photophysical properties of the Zn-BDO. Thus, it can be assumed that after excitation following Kasha's rule, only the LLCT ($\pi\pi^*$) states will be populated. Therefore, the photoluminescence of Zn-BDO can be described using a three-state model (S1, T1 and S0).

Small ΔE_{S-T}s of the LLCT ($\pi\pi^*$) states can be inferred from figure 4.24. A detailed list of these is given in table 4.10. For Zn-BDO, tiny energy gaps of 114 to 401 cm^{-1} are also observed for all conformers. Thus, the deviation between the conformers is greater than for Zn-BDT, resulting in both smaller and larger ΔE_{S-T}s.

Table 4.10: ΔE_{S-T}s of the LLCT ($\pi\pi^*$) states of Zn-BDO.

Ligand Orientation	planar	queer	ortho
ΔE_{S-T} [cm^{-1}]	114	401	194

4.2.3 Rate Constants

Comparison with the Zn-BDT show that the oxygen atoms cause a weaker SOC than the sulfur atoms. Again, the queer conformer shows the largest SOCMEs.

Table 4.11: SOCMEs, ISC and rISC rates of the LLCT ($\pi\pi^*$) states of Zn-BDO at 77 and 298 K.

Ligand Orientation	$\sum$SOCME^2 [cm^{-2}]		k_{ISC} [s^{-1}]		k_{rISC} [s^{-1}]	
	S	T	77 K	298 K	77 K	298 K
planar	1.25	0.36	$2.2{\cdot}10^9$	$7.1{\cdot}10^8$	$8.6{\cdot}10^7$	$6.2{\cdot}10^7$
queer	5.80	3.97	$5.0{\cdot}10^9$	$2.3{\cdot}10^9$	$1.0{\cdot}10^5$	$6.9{\cdot}10^6$
ortho	1.25	3.69	$2.0{\cdot}10^9$	$6.6{\cdot}10^8$	$1.1{\cdot}10^8$	$2.3{\cdot}10^8$

The SOCMEs in combination with the VIBEs rates lead to pronounced ISC rates of the order of 10^9 s^{-1}. The temperature dependency is low and the rates of all conformers at 298 K are about half to one third as large as the ones at 77 K. Differences of the ISC rates between conformers are also not pronounced. The queer conformer shows the highest rates, which are about three times as high as those of the other two conformer at 77 and 298K.
The rISC rates are slightly smaller than the ISC rates and are in the range of 10^5 to 10^8 s^{-1}. There is hardly any temperature dependency for the planar and orthogonal conformer. However, for the queer conformer, the rISC rates is about 70 times higher at 298 K than at 77 K. The rates of the queer conformer are particularly low at 77 K lying two to three orders of magnitude below the other conformers. At 298 K, the difference with a factor of 10 or 30 to the planar or orthogonal conformer is not quite as pronounced. The orthogonal conformer has the highest rISC rate of $2 \cdot 10^8$ s^{-1} and also the best ratio of ISC to rISC in terms of TADF properties.

Table 4.12: Fluorescence and Phosphorescence rates of the LLCT ($\pi\pi^*$) states of Zn-BDO at 77 and 298 K.

Ligand Orientation	k_F [s^{-1}]	k_P [s^{-1}]
planar	$7.3{\cdot}10^6$	0
queer	$4.9{\cdot}10^6$	4
ortho	$4.5{\cdot}10^5$	44

The fluorescence rates for Zn-BDO are somewhat lower than those of Zn-BDT. The planar conformer has the highest rate of $7 \cdot 10^6$ s^{-1} and is about 10 times larger than that of the orthogonal conformer with the lowest rate. The phosphorescence rates are tiny, so no radiation will occur from the T1.

A graphical summary of all important rate constants that highlight the TADF path using a three-state model is given in the figure below.

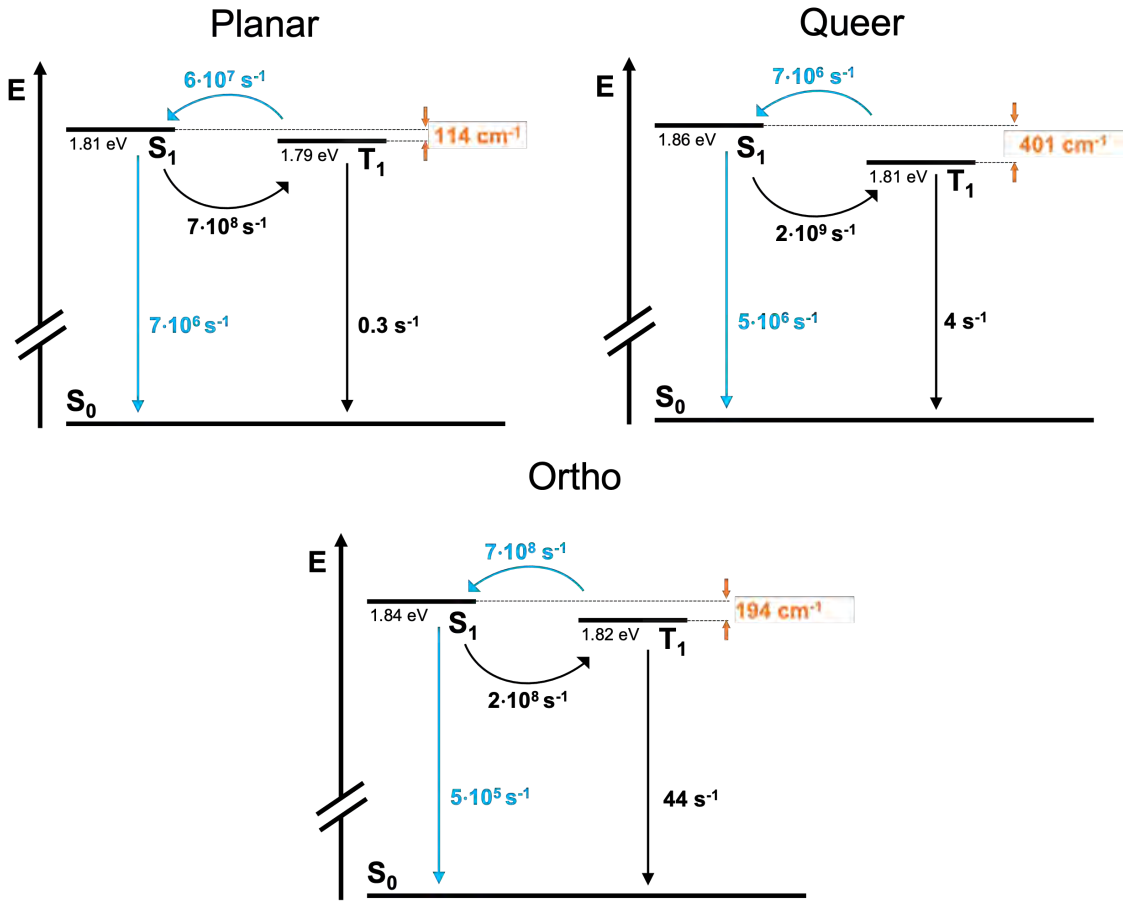

Fig. 4.25: Three-state model of all three conformers for the Zn-BDO at 298 K. It contains all TADF relevant rate constants, the energetic level of the S1 and T1 as well as the energetic difference of these states. The TADF path is represented in blue.

Despite conformational differences, the Zn-BDO qualifies as a suitable TADF emitter based on its photophysical properties. It has high (r)ISC and fluorescence rates, and very low phosphorescence rates. Among the conformers, the planar one stands out as the best. It has the highest fluorescence rate and a good ratio between ISC and rISC. The orthogonal conformer follows with the best ratio of (r)ISC, but the lowest fluorescence rate. The queer conformer has the least outstanding TADF properties when comparing the conformers due to a ratio of (r)ISC that is clearly on the side of ISC combined with a medium fluorescence rate compared to the other conformers.

4.2.4 Emission

Due to large displacements that persist even in Vertical Hessian calculations, satisfactory spectra could not be calculated for the planar and orthogonal conformer. However, by neglecting the frequency with the highest displacement value a better result was obtained for the planar conformer (see appendix). Neglecting modes did not lead to better results for the orthogonal conformer.

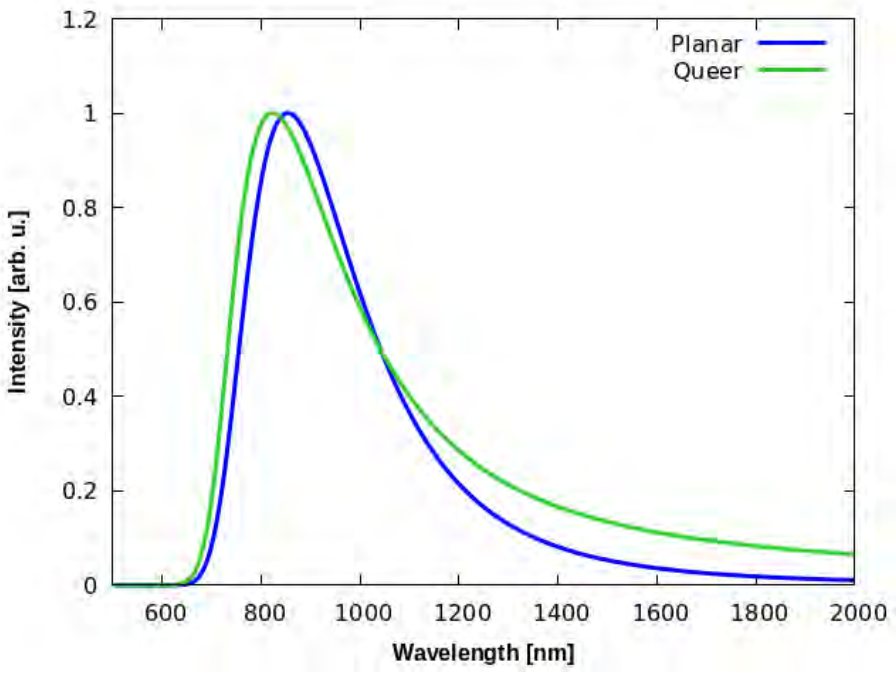

Fig. 4.26: Emission spectrum from the S-LLCT ($\pi\pi^*$) state for the planar and queer conformer of Zn-BDO at 298 K.

The spectra show emission by fluorescence emanating from the S-LLCT ($\pi\pi^*$) in the near-infrared region with a maximum at 853 and 821 nm for the planar and queer conformer. The emission of Zn-BDO is thus red-shifted compared to Zn-BDT, with a distance of about 260-290 nm.

5 Conclusion

The Zn-BDT has a low energy barrier for rotation of the BDT ligand, which allows for multiple conformers to exist in solution. Especially three conformers are energetically favourable, one with planar, queer and orthogonal position of the BDT and CAAC ligand towards each other.
Two singlet and triplet LLCT states, whose adiabatic excitation energies are close to each other qualify as emissive states. The lower one is characterized by a $\pi\pi^*$ excitation, the higher one by a $n\pi^*$ excitation. By considering the (r)ISC rates, it turns out that the equilibrium is on the side of the LLCT ($\pi\pi^*$) states. This behaviour is significantly more pronounced for 77K than for 298 K.
The singlet and triplet LLCT ($\pi\pi^*$) states have tiny energy gaps of about 200 cm^{-1} for all conformers. The SOC between the states is rather low in the one to two digit range, but they still exhibit high (r)ISC rates of up to 10^9 s^{-1} for rISC and up to 10^{10} s^{-1} for ISC. The temperature dependency of these rates is rather low.
The phosphorescence rates are very low, so that emission is only to be expected from the singlet state. With up to 10^7 s^{-1} for the planar conformer, the fluorescence rates are also high. The emission spectrum of the singlet LLCT ($\pi\pi^*$) shows a maximum at 560 nm and thus appears as yellow light to the viewer. The calculations match well with the experimentally measured absorption and emission spectra.
Despite minor conformer differences, Zn-BDT is characterized as a good TADF emitter material.

In comparison to Zn-BDT, Zn-BDO has many similarities, but also some differences. The BDO ligand in Zn-BDO is also able to rotate easily, leading to the presence of multiple conformers. Like Zn-BDT, a planar, queer and orthogonal conformer are favourable. However, Zn-BDO does not have a low-lying LLCT ($n\pi^*$) state. By considering the adiabatic excitation energies, only one singlet and triplet LLCT ($\pi\pi^*$) state qualifies as an emissive state. As with Zn-BDT, the LLCT states in Zn-BDO also have tiny energy gaps, with greater variations among the conformers compared to Zn-BDT, which results in both larger and smaller energy gaps. The SOCMEs are in the single digit region for all conformers and are thus somewhat lower for the Zn-BDO. This is also reflected in the (r)ISC rates which are an order of magnitude lower than those of the Zn-BDT with a maximum of 10^9 s^{-1} for the ISC rates.
The phosphorescence rates are again very low, so no emission is expected from the triplet LLCT ($\pi\pi^*$) state. The fluorescence rates are again about an order of magnitude lower for the Zn-BDO with a maximum of 10^6 s^{-1} for the planar conformer. The emission with a maximum at 821 nm for the queer conformer and a maximum of 853 for the planar conformer is in the near-infrared region and is red shifted by about 260 to 290 nm compared to the Zn-BDT.

Minor conformer differences are also present for the Zn-BDO, but again good TADF emitter properties exist for each conformer.

Bibliography

[1] Nakanotani, H.; Higuchi, T. *Nature Communications* **2014**, *5*, 4016.

[2] Wei, Q.; Fei, N.; Islam, A. *Advanced Optical Materials* **2018**, *6*, 1800512.

[3] Kawamura, Y.; Goushi, K.; Brooks, J. *Applied Physics Letters* **2005**, *86*, 071104.

[4] Sain, N.; Sharma, D.; Choudhary, P. *International Journal of Engineering Applied Sciences and Technology* **2020**, *4*, 587–591.

[5] Czerwieniec, R.; Leitl, M. J.; Homeier, H. H.; Yersin, H. *Coordination Chemistry Reviews* **2016**, *325*, 2–28.

[6] Bergmann, L.; Hedley, G. J.; Baumann, T.; Bräse, S.; Samuel, I. D. W. *Science Advances* **2016**, *2*, e1500889.

[7] Hamze, R.; Peltier, J. L.; Sylvinson, D.; Jung, M.; Cardenas, J.; Haiges, R.; Soleilhavoup, M.; Jazzar, R.; Djurovich, P. I.; Bertrand, G.; Thompson, M. E. *Science* **2019**, *363*, 601–606.

[8] Gernert, M.; Balles-Wolf, L.; Kerner, F.; Müller, U.; Schmiedel, A.; Holzapfel, M.; Marian, C. M.; Pflaum, J.; Lambert, C.; Steffen, A. *Journal of the American Chemical Society* **2020**, *142*, 8897–8909.

[9] Lüdtke, N.; Föller, J.; Marian, C. M. *Physical Chemistry Chemical Physics* **2020**, *22*, 23530–23544.

[10] Putscher, M.; Lüdtke, N.; Marian, C. M. *not submitted yet* **2022**,

[11] Lüdtke, N.; Steffen, A.; Marian, C. M. *Inorganic Chemistry* **2022**, *61*, 20896–20905.

[12] Šípoš, R.; Šima, J. *Revista Cubana de Física* **2020**, *37*, 125–130.

[13] Kasha, M. *Discussions Faraday Society* **1950**, *9*, 14–19.

[14] Murthy, K.; Virk, H. *Defect and Diffusion Forum* **2013**, *347*, 1–34.

[15] Püschner, D. *Quantitative Rechenverfahren der Theoretischen Chemie*; Springer Fachmedien Wiesbaden, 2017.

[16] Hohenberg, P.; Kohn, W. *Physical Review* **1964**, *136*, B864–B871.

[17] Kohn, W.; Sham, L. J. *Physical Review* **1965**, *140*, A1133–A1138.

[18] Mardirossian, N.; Head-Gordon, M. *Molecular Physics* **2017**, *115*, 2315–2372.

[19] Becke, A. D. *The Journal of Chemical Physics* **1993**, *98*, 1372–1377.

[20] Lee, C.; Yang, W.; Parr, R. G. *Physical Review B* **1988**, *37*, 785–789.

[21] Runge, E.; Gross, E. K. U. *Physical Review Letters* **1984**, *52*, 997–1000.

[22] Dreuw, A.; Head-Gordon, M. *Chemical Reviews* **2005**, *105*, 4009–4037.

[23] Dreuw, A.; Head-Gordon, M. *Journal of the American Chemical Society* **2004**, *126*, 4007–4016.

[24] Hirata, S.; Head-Gordon, M. *Chemical Physics Letters* **1999**, *314*, 291–299.

[25] Szabo, A.; Ostlund, N. S. *Modern Quantum Chemistry*; Dover Publications, 1996.

[26] Föller, J. *Quantum Chemical Investigation of Coinage Metal Complexes with Regard to their Application in OLEDs*; PhD thesis, Heinrich-Heine University Düsseldorf, 2018.

[27] Grimme, S.; Waletzke, M. *The Journal of Chemical Physics* **1999**, *111*, 5645–5655.

[28] Kleinschmidt, M.; Marian, C. M.; Waletzke, M.; Grimme, S. *The Journal of Chemical Physics* **2009**, *130*, 044708.

[29] Heil, A.; Kleinschmidt, M.; Marian, C. M. *The Journal of Chemical Physics* **2018**, *149*, 164106.

[30] Lyskov, I.; Kleinschmidt, M.; Marian, C. M. *The Journal of Chemical Physics* **2016**, *144*, 034104.

[31] Marian, C. M. *Reviews in Computational Chemistry*; John Wiley & Sons, Ltd, 2001; Chapter 3, pp 99–204.

[32] Marian, C. M. *WIREs Computational Molecular Science* **2012**, *2*, 187–203.

[33] Kleinschmidt, M.; Tatchen, J.; Marian, C. M. *Journal of Computational Chemistry* **2002**, *23*, 824–833.

[34] Etinski, M.; Tatchen, J.; Marian, C. M. *Phys. Chem. Chem. Phys.* **2014**, *16*, 4740–4751.

[35] Salzmann, S.; Martinez-Junza, V.; Zorn, B.; Braslavsky, S. E.; Mansurova, M.; Marian, C. M.; Gärtner, W. *The Journal of Physical Chemistry A* **2009**, *113*, 9365–9375.

[36] Kleinschmidt, M.; Tatchen, J.; Marian, C. M. *The Journal of Chemical Physics* **2006**, *124*, 124101.

[37] Tatchen, J.; Gilka, N.; Marian, C. M. *Physical Chemistry Chemical Phyics* **2007**, *9*, 5209–5221.

[38] Barone, V.; Bloino, J.; Biczysko, M.; Santoro, F. *Journal of Chemical Theory and Computation* **2009**, *5*, 540–554.

[39] Götze, J. P.; Karasulu, B.; Thiel, W. *The Journal of Chemical Physics* **2013**, *139*, 234108.

[40] Tomasi, J.; Mennucci, B.; Cammi, R. *Chemical Reviews* **2005**, *105*, 2999–3094.

[41] Amovilli, C.; Barone, V.; Cammi, R. *Advances in Quantum Chemistry* **1998**, *32*, 227–261.

[42] Cammi, R.; Cossi, M.; Mennucci, B. *International Journal of Quantum Chemistry* **1996**, *60*, 1165–1178.

[43] Miertuš, S.; Scrocco, E.; Tomasi, J. *Chemical Physics* **1981**, *55*, 117–129.

[44] Klamt, A.; Schüürmann, G. *Journal of the Chemical Society, Perkin Transaction 2* **1993**, 799–805.

[45] Frisch, M. J. et al. Gaussian 16 Revision A.03. 2016; Gaussian Inc. Wallingford CT.

[46] Schäfer, A.; Horn, H.; Ahlrichs, R. *The Journal of Chemical Physics* **1992**, *97*, 2571–2577.

[47] Rappoport, D.; Furche, F. *The Journal of Chemical Physics* **2010**, *133*, 134105.

[48] Figgen, D.; Rauhut, G.; Dolg, M.; Stoll, H. *Chemical Physics* **2005**, *311*, 227–244.

[49] Kleinschmidt, M.; Tatchen, J.; Marian, C. M. *Journal of Computational Chemistry* **2002**, *23*, 824–833.

[50] Kleinschmidt, M.; Marian, C. M. *Chemical Physics* **2005**, *311*, 71–79.

[51] Kleinschmidt, M.; Tatchen, J.; Marian, C. M. *The Journal of Chemical Physics* **2006**, *124*, 124101.

7 Appendix

7.1 Zn-BDT

7.1.1 Excitation Energies and Characterisations

Table 7.1: Vertical excitation energies and characterisations of the first ten singlet and triplet excited states of the planar S0 geometry for Zn-BDT.

	ΔE [eV]	Character		From	To
S0	0.00				
S1	3.16	LLCT	$\pi\pi^*$	BDT	CAAC (Carbene)
S2	3.75	LLCT	$\pi\pi^*$	BDT	CAAC (Carbene)
S3	4.14	LLCT	$n\pi^*$	BDT	CAAC (Carbene)
S4	4.36	LE	$\pi\pi^*$	BDT	BDT
S5	4.52	Ambiguous	π	BDT	Empty
S6	4.63	Mixed	$n\pi^*$	BDT/CAAC	CAAC (Carbene)
S7	4.65	LLCT	$\pi\pi^*$	BDT	CAAC (Dipp)
S8	4.83	Mixed	$\pi\pi^*$	BDT	BDT/CAAC
S9	4.91	Mixed	$\pi\pi^*$	BDT	BDT/CAAC
S10	4.97	LE	$\pi\pi^*$	CAAC	CAAC
T1	3.08	LLCT	$\pi\pi^*$	BDT	CAAC (Carbene)
T2	3.70	LLCT	$\pi\pi^*$	BDT	CAAC (Carbene)
T3	3.78	LE	$\pi\pi^*$	BDT	BDT
T4	4.03	LE	$\pi\pi^*$	BDT	BDT
T5	4.11	Mixed	$n\pi^*$	BDT/CAAC	CAAC (Carbene)
T6	4.12	LLCT	$n\pi^*$	BDT	CAAC
T7	4.15	LE	$\pi\pi^*$	CAAC	CAAC
T8	4.24	LE	$\pi\pi^*$	BDT	BDT
T9	4.43	Ambiguous	π	BDT	Empty
T10	4.53	Mixed	$n\pi^*$	BDT/CAAC	CAAC (Dipp)

Table 7.2: Vertical excitation energies and characterisations of the first ten singlet and triplet excited states of the queer S0 geometry for Zn-BDT.

	ΔE [eV]	Character		From	To
S0	0.00				
S1	3.22	LLCT	$\pi\pi^*$	BDT	CAAC (Carbene)
S2	3.82	LLCT	$\pi\pi^*$	BDT	CAAC (Carbene)
S3	4.24	LLCT	$n\pi^*$	BDT	CAAC (Carbene)
S4	4.37	LE	$\pi\pi^*$	BDT	BDT
S5	4.56	Ambiguous	π	BDT	Empty
S6	4.63	Mixed	$n\pi^*$	BDT/CAAC	CAAC
S7	4.73	LLCT	$\pi\pi^*$	BDT	CAAC (Dipp)
S8	4.85	Mixed	$\pi\pi^*$	BDT	BDT/CAAC
S9	4.90	Mixed	$\pi\pi^*$	BDT	BDT/CAAC
S10	5.00	LE	$\pi\pi^*$	CAAC	CAAC
T1	3.17	LLCT	$\pi\pi^*$	BDT	CAAC (Carbene)
T2	3.78	LE	$\pi\pi^*$	BDT	BDT
T3	3.79	LLCT	$\pi\pi^*$	BDT	CAAC (Carbene)
T4	4.03	LE	$\pi\pi^*$	BDT	BDT
T5	4.11	Mixed	$n\pi^*$	BDT/CAAC	CAAC
T6	4.18	LE	$\pi\pi^*$	CAAC	CAAC
T7	4.20	LLCT	$n\pi^*$	BDT	CAAC (Carbene)
T8	4.25	LE	$\pi\pi^*$	BDT	BDT
T9	4.47	Ambiguous	π	BDT	Empty
T10	4.64	LE	$\pi\pi^*$	CAAC	CAAC

Table 7.3: Vertical excitation energies and characterisations of the first ten singlet and triplet excited states of the orthogonal S0 geometry for Zn-BDT.

	ΔE [eV]	Character		From	To
S0	0.00				
S1	3.26	LLCT	$\pi\pi^*$	BDT	CAAC (Carbene)
S2	3.88	LLCT	$\pi\pi^*$	BDT	CAAC (Carbene)
S3	4.34	LLCT	$n\pi^*$	BDT	CAAC (Carbene)
S4	4.37	LE	$\pi\pi^*$	BDT	BDT
S5	4.54	Ambiguous	π	BDT	Empty
S6	4.68	Mixed	$n\pi^*$	BDT/CAAC	CAAC
S7	4.80	LLCT	$\pi\pi^*$	BDT	CAAC (Dipp)
S8	4.89	LE	$\pi\pi^*$	BDT	BDT
S9	4.96	LLCT	$\pi\pi^*$	BDT	CAAC (Dipp)
S10	5.05	LE	$\pi\pi^*$	CAAC	CAAC
T1	3.23	LLCT	$\pi\pi^*$	BDT	CAAC (Carbene)
T2	3.78	LE	$\pi\pi^*$	BDT	BDT
T3	3.85	LLCT	$\pi\pi^*$	BDT	CAAC (Carbene)
T4	4.03	LE	$\pi\pi^*$	BDT	BDT
T5	4.15	Mixed	$n\pi^*$	BDT/CAAC	CAAC
T6	4.20	LE	$\pi\pi^*$	CAAC	CAAC
T7	4.24	LE	$\pi\pi^*$	BDT	BDT
T8	4.27	LLCT	$n\pi^*$	BDT	CAAC (Carbene)
T9	4.44	Ambiguous	π	BDT	Empty
T10	4.67	LE	$\pi\pi^*$	CAAC	CAAC

Table 7.4: Energy difference to the S0 state of the planar S0 geometry and characterisations of the first ten singlet and triplet excited states of the planar S-LLCT $\pi\pi^*$ geometry for Zn-BDT.

	ΔE [eV]	Character		From	To
S0	0.47				
S1	2.40	LLCT	$\pi\pi^*$	BDT	CAAC (Carbene)
S2	3.30	LLCT	$\pi\pi^*$	BDT	CAAC (Carbene)
S3	3.59	LLCT	$n\pi^*$	BDT	CAAC (Carbene)
S4	4.52	Mixed	$n\pi^*/\pi\pi^*$	BDT/CAAC	CAAC
S5	4.55	Mixed	$n\pi^*/\pi\pi^*$	BDT/CAAC	CAAC
S6	4.62	LE	$\pi\pi^*$	BDT	BDT
S7	4.66	LE	$\pi\pi^*$	BDT	BDT
S8	4.68	Mixed	$n\pi^*/\pi\pi^*$	BDT/CAAC	CAAC (Carbene)
S9	4.70	LLCT	$\pi\pi^*$	BDT	CAAC (Dipp)
S10	4.90	LLCT	$\pi\pi^*$	BDT	CAAC (Dipp)
T1	2.34	LLCT	$\pi\pi^*$	BDT	CAAC (Carbene)
T2	3.27	LLCT	$\pi\pi^*$	BDT	CAAC (Carbene)
T3	3.55	LLCT	$n\pi^*$	BDT	CAAC (Carbene)
T4	3.95	LE	$\pi\pi^*$	BDT	BDT
T5	4.16	Mixed	$n\pi^*$	BDT/CAAC	CAAC
T6	4.28	LE	$\pi\pi^*$	BDT	BDT
T7	4.39	LE	$\pi\pi^*$	CAAC	CAAC
T8	4.54	LE	$\pi\pi^*$	CAAC	CAAC
T9	4.55	Mixed	$\pi\pi^*$	BDT/CAAC	CAAC
T10	4.63	Mixed	$\pi\pi^*$	BDT/CAAC	CAAC

Table 7.5: Energy difference to the S0 state of the queer S0 geometry and characterisations of the first ten singlet and triplet excited states of the queer S-LLCT $\pi\pi^*$ geometry for Zn-BDT.

	ΔE [eV]	Character		From	To
S0	0.50				
S1	2.46	LLCT	$\pi\pi^*$	BDT	CAAC (Carbene)
S2	3.36	LLCT	$\pi\pi^*$	BDT	CAAC (Carbene)
S3	3.67	LLCT	$n\pi^*$	BDT	CAAC (Carbene)
S4	4.54	Mixed	$n\pi^*/\pi\pi^*$	BDT/CAAC	CAAC
S5	4.62	LE	$\pi\pi^*$	CAAC	CAAC
S6	4.68	LE	$\pi\pi^*$	BDT	BDT
S7	4.72	LE	$\pi\pi^*$	BDT	BDT
S8	4.75	LE	$\pi\pi^*$	CAAC	CAAC
S9	4.80	LLCT	$\pi\pi^*$	BDT	CAAC (Dipp)
S10	4.97	LLCT	$\pi\pi^*$	BDT	CAAC (Dipp)
T1	2.41	LLCT	$\pi\pi^*$	BDT	CAAC (Carbene)
T2	3.33	LLCT	$\pi\pi^*$	BDT	CAAC (Carbene)
T3	3.62	LLCT	$n\pi^*$	BDT	CAAC (Carbene)
T4	3.98	LE	$\pi\pi^*$	BDT	BDT
T5	4.18	Mixed	$n\pi^*$	BDT/CAAC	CAAC
T6	4.34	LE	$\pi\pi^*$	BDT	BDT
T7	4.47	LE	$\pi\pi^*$	CAAC	CAAC
T8	4.61	LE	$\pi\pi^*$	CAAC	CAAC
T9	4.63	Ambiguous	π	BDT	Empty
T10	4.72	LE	$\pi\pi^*$	CAAC	CAAC

Table 7.6: Energy difference to the S0 state of the orthogonal S0 geometry and characterisations of the first ten singlet and triplet excited states of the orthogonal S-LLCT $\pi\pi^*$ geometry for Zn-BDT.

	ΔE [eV]	Character		From	To
S0	0.49				
S1	2.46	LLCT	$\pi\pi^*$	BDT	CAAC (Carbene)
S2	3.39	LLCT	$\pi\pi^*$	BDT	CAAC (Carbene)
S3	3.74	LLCT	$n\pi^*$	BDT	CAAC (Carbene)
S4	4.56	Mixed	$n\pi^*$	BDT/CAAC	CAAC
S5	4.65	LE	$\pi\pi^*$	CAAC	CAAC
S6	4.67	LE	$\pi\pi^*$	BDT	BDT
S7	4.71	Ambiguous	π	BDT	Empty
S8	4.78	LE	$\pi\pi^*$	CAAC	CAAC
S9	4.85	LLCT	$\pi\pi^*$	BDT	CAAC (Dipp)
S10	5.04	LLCT	$\pi\pi^*$	BDT	CAAC (Dipp)
T1	2.43	LLCT	$\pi\pi^*$	BDT	CAAC (Carbene)
T2	3.37	LLCT	$\pi\pi^*$	BDT	CAAC (Carbene)
T3	3.64	LLCT	$n\pi^*$	BDT	CAAC (Carbene)
T4	3.96	LE	$\pi\pi^*$	BDT	BDT
T5	4.17	Mixed	$n\pi^*$	BDT/CAAC	CAAC
T6	4.32	LE	$\pi\pi^*$	BDT	BDT
T7	4.49	LE	$\pi\pi^*$	CAAC	CAAC
T8	4.62	LE	$\pi\pi^*$	CAAC	CAAC
T9	4.62	Ambiguous	π	BDT	Empty
T10	4.76	LE	$\pi\pi^*$	CAAC	CAAC

Table 7.7: Energy difference to the S0 state of the planar S0 geometry and characterisations of the first ten singlet and triplet excited states of the planar T-LLCT $\pi\pi^*$ geometry for Zn-BDT.

	ΔE [eV]	Character		From	To
S0	0.52				
S1	2.46	LLCT	$\pi\pi^*$	BDT	CAAC (Carbene)
S2	3.36	LLCT	$\pi\pi^*$	BDT	CAAC (Carbene)
S3	3.64	LLCT	$n\pi^*$	BDT	CAAC (Carbene)
S4	4.57	LE	$\pi\pi^*$	CAAC	CAAC
S5	4.61	Mixed	$n\pi^*$	BDT/CAAC	CAAC
S6	4.68	LE	$\pi\pi^*$	BDT	BDT
S7	4.70	LE	$\pi\pi^*$	BDT	BDT
S8	4.73	Mixed	$n\pi^*/\pi\pi^*$	BDT/CAAC	CAAC
S9	4.75	LLCT	$\pi\pi^*$	BDT	CAAC (Dipp)
S10	4.96	LLCT	$\pi\pi^*$	BDT	CAAC (Dipp)
T1	2.38	LLCT	$\pi\pi^*$	BDT	CAAC (Carbene)
T2	3.33	LLCT	$\pi\pi^*$	BDT	CAAC (Carbene)
T3	3.61	LLCT	$n\pi^*$	BDT	CAAC (Carbene)
T4	4.00	LE	$\pi\pi^*$	BDT	BDT
T5	4.23	Mixed	$n\pi^*$	BDT/CAAC	CAAC
T6	4.33	LE	$\pi\pi^*$	BDT	BDT
T7	4.43	LE	$\pi\pi^*$	CAAC	CAAC
T8	4.59	LE	$\pi\pi^*$	CAAC	CAAC
T9	4.61	Ambiguous	π	BDT	Empty
T10	4.67	Mixed	$\pi\pi^*$	BDT/CAAC	CAAC

Table 7.8: Energy difference to the S0 state of the queer S0 geometry and characterisations of the first ten singlet and triplet excited states of the queer T-LLCT $\pi\pi^*$ geometry for Zn-BDT.

	ΔE [eV]	Character		From	To
S0	0.53				
S1	2.50	LLCT	$\pi\pi^*$	BDT	CAAC (Carbene)
S2	3.38	LLCT	$\pi\pi^*$	BDT	CAAC (Carbene)
S3	3.70	LLCT	nπ^*	BDT	CAAC (Carbene)
S4	4.58	Mixed	nπ^*	BDT/CAAC	CAAC
S5	4.65	LE	$\pi\pi^*$	CAAC	CAAC
S6	4.71	LE	$\pi\pi^*$	BDT	BDT
S7	4.77	LE	$\pi\pi^*$	BDT	BDT
S8	4.78	Mixed	n$\pi*/\pi\pi^*$	BDT/CAAC	CAAC
S9	4.83	LLCT	$\pi\pi^*$	BDT	CAAC (Dipp)
S10	5.01	LLCT	$\pi\pi^*$	BDT	CAAC (Dipp)
T1	2.44	LLCT	$\pi\pi^*$	BDT	CAAC (Carbene)
T2	3.35	LLCT	$\pi\pi^*$	BDT	CAAC (Carbene)
T3	3.66	LLCT	n$\pi*$	BDT	CAAC (Carbene)
T4	4.01	LE	$\pi\pi^*$	BDT	BDT
T5	4.22	Mixed	n$\pi*$	BDT/CAAC	CAAC
T6	4.37	LE	$\pi\pi^*$	BDT	BDT
T7	4.50	LE	$\pi\pi^*$	CAAC	CAAC
T8	4.63	LE	$\pi\pi^*$	CAAC	CAAC
T9	4.67	Ambiguous	π	BDT	Empty
T10	4.75	LE	$\pi\pi^*$	CAAC	CAAC

Table 7.9: Energy difference to the S0 state of the orthogonal S0 geometry and characterisations of the first ten singlet and triplet excited states of the orthogonal T-LLCT $\pi\pi^*$ geometry for Zn-BDT.

	ΔE [eV]	Character		From	To
S0	0.47				
S1	2.47	LLCT	$\pi\pi^*$	BDT	CAAC (Carbene)
S2	3.38	LLCT	$\pi\pi^*$	BDT	CAAC (Carbene)
S3	3.76	LLCT	n$\pi*$	BDT	CAAC (Carbene)
S4	4.56	Mixed	n$\pi*$	BDT/CAAC	CAAC
S5	4.64	LE	$\pi\pi^*$	BDT	BDT
S6	4.67	LE	$\pi\pi^*$	CAAC	CAAC
S7	4.71	LE	$\pi\pi^*$	BDT	BDT
S8	4.80	Mixed	n$\pi*/\pi\pi^*$	BDT/CAAC	CAAC
S9	4.84	LLCT	$\pi\pi^*$	BDT	CAAC (Dipp)
S10	5.03	LLCT	$\pi\pi^*$	BDT	CAAC (Dipp)
T1	2.44	LLCT	$\pi\pi^*$	BDT	CAAC (Carbene)
T2	3.36	LLCT	$\pi\pi^*$	BDT	CAAC (Carbene)
T3	3.66	LLCT	n$\pi*$	BDT	CAAC (Carbene)
T4	3.94	LE	$\pi\pi^*$	BDT	BDT
T5	4.15	Mixed	n$\pi*$	BDT/CAAC	CAAC
T6	4.29	LE	$\pi\pi^*$	BDT	BDT
T7	4.50	LE	$\pi\pi^*$	CAAC	CAAC
T8	4.62	Ambiguous	π	BDT	Empty
T9	4.62	LE	$\pi\pi^*$	CAAC	CAAC
T10	4.75	LE	$\pi\pi^*$	BDT	BDT

Table 7.10: Energy difference to the S0 state of the planar, queer and orthogonal S0 geometry and characterisations of the first ten singlet and triplet excited states of the S-LLCT nπ^* geometry for Zn-BDT.

	ΔE [eV]			Character		From	To
	planar	queer	ortho				
S0	0.97	0.93	0.95				
S1	2.63	2.59	2.61	LLCT	nπ^*	BDT	CAAC (Carbene)
S2	3.28	3.23	3.26	LLCT	$\pi\pi^*$	BDT	CAAC (Carbene)
S3	3.74	3.70	3.72	LLCT	$\pi\pi^*$	BDT	CAAC (Carbene)
S4	4.73	4.69	4.71	LMCT	nn	BDT	Zinc
S5	4.95	4.91	4.93	Mixed	nπ^*/$\pi\pi^*$	BDT/CAAC	CAAC
S6	4.96	4.92	4.94	LE	$\pi\pi^*$	CAAC	CAAC
S7	5.01	4.97	4.99	LLCT	nπ^*	BDT	CAAC (Dipp)
S8	5.01	4.97	4.99	Mixed	nπ^*/$\pi\pi^*$	BDT/CAAC	CAAC
S9	5.06	5.02	5.04	LE	nπ^*	BDT	BDT
S10	5.16	5.12	5.14	LE	nπ^*	BDT	BDT
T1	1.63	2.60	2.56	LLCT	nπ^*	BDT	CAAC (Carbene)
T2	2.23	3.19	3.15	LLCT	$\pi\pi^*$	BDT	CAAC (Carbene)
T3	2.73	3.70	3.66	LLCT	$\pi\pi^*$	BDT	CAAC (Carbene)
T4	3.66	4.63	4.59	LMCT	nn	BDT	Zinc
T5	3.78	4.75	4.71	Mixed	nπ^*/$\pi\pi^*$	BDT/CAAC	CAAC
T6	3.84	4.80	4.76	LE	$\pi\pi^*$	BDT	BDT
T7	3.88	4.84	4.80	LE	$\pi\pi^*$	CAAC	CAAC
T8	3.99	4.96	4.92	Mixed	nπ^*	BDT	BDT/CAAC
T9	4.00	4.96	4.92	LE	nπ^*	CAAC	CAAC
T10	4.05	5.02	4.98	LE	nπ^*	BDT	BDT

Table 7.11: Energy difference to the S0 state of the planar, queer and orthogonal S0 geometry and characterisations of the first ten singlet and triplet excited states of the T-LLCT nπ^* geometry for Zn-BDT.

	ΔE [eV]			Character		From	To
	planar	queer	ortho				
S0	0.97	0.93	0.95				
S1	2.63	2.59	2.61	LLCT	nπ^*	BDT	CAAC (Carbene)
S2	3.28	3.23	3.26	LLCT	$\pi\pi^*$	BDT	CAAC (Carbene)
S3	3.74	3.70	3.72	LLCT	$\pi\pi^*$	BDT	CAAC (Carbene)
S4	4.73	4.69	4.71	LMCT	nn	BDT	Zinc
S5	4.95	4.91	4.93	Mixed	nπ^*/$\pi\pi^*$	BDT/CAAC	CAAC
S6	4.96	4.92	4.94	LE	$\pi\pi^*$	CAAC	CAAC
S7	5.01	4.97	4.99	LLCT	nπ^*	BDT	CAAC (Dipp)
S8	5.01	4.97	4.99	Mixed	nπ^*/$\pi\pi^*$	BDT/CAAC	CAAC
S9	5.06	5.02	5.04	LE	nπ^*	BDT	BDT
S10	5.16	5.12	5.14	LE	nπ^*	BDT	BDT
T1	1.63	2.60	2.56	LLCT	nπ^*	BDT	CAAC (Carbene)
T2	2.23	3.19	3.15	LLCT	$\pi\pi^*$	BDT	CAAC (Carbene)
T3	2.73	3.70	3.66	LLCT	$\pi\pi^*$	BDT	CAAC (Carbene)
T4	3.66	4.63	4.59	LMCT	nn	BDT	Zinc
T5	3.78	4.75	4.71	Mixed	nπ^*/$\pi\pi^*$	BDT/CAAC	CAAC
T6	3.84	4.80	4.76	LE	$\pi\pi^*$	BDT	BDT
T7	3.88	4.84	4.80	LE	$\pi\pi^*$	CAAC	CAAC
T8	3.99	4.96	4.92	Mixed	nπ^*	BDT	BDT/CAAC
T9	4.00	4.96	4.92	LE	nπ^*	CAAC	CAAC
T10	4.05	5.02	4.98	LE	nπ^*	BDT	BDT

Table 7.12: Energy difference to the S0 state of the planar, queer and orthogonal S0 geometry and characterisations of the first ten singlet and triplet excited states of the T-LE-BDT geometry for Zn-BDT.

	ΔE [eV]			Character		From	To
	planar	queer	ortho				
S0	0.90	0.86	0.88				
S1	3.77	3.73	3.75	LLCT	$\pi\pi^*$	BDT	CAAC (Carbene)
S2	4.39	4.35	4.37	LE	$\pi\pi^*$	BDT	BDT
S3	4.74	4.70	4.72	LE	$\pi\pi^*$	BDT	BDT
S4	4.83	4.79	4.81	LLCT	$\pi\pi^*$	BDT	CAAC (Carbene)
S5	5.06	5.02	5.04	Ambiguous	π	BDT	Empty
S6	5.28	5.24	5.26	LLCT	$n\pi^*$	BDT	CAAC (Carbene)
S7	5.31	5.27	5.29	LLCT	$\pi\pi^*$	BDT	CAAC (Dipp)
S8	5.42	5.38	5.40	Mixed	$\pi\pi^*$	BDT/CAAC	CAAC
S9	5.45	5.41	5.43	LLCT	$\pi\pi^*$	BDT	CAAC (Dipp)
S10	5.48	5.44	5.46	LE	$\pi\pi^*$	BDT	BDT
T1	3.23	3.19	3.21	LE	$\pi\pi^*$	BDT	BDT
T2	3.71	3.67	3.69	LLCT	$\pi\pi^*$	BDT	CAAC (Carbene)
T3	4.51	4.47	4.49	LE	$\pi\pi^*$	BDT	BDT
T4	4.75	4.71	4.73	LLCT	$\pi\pi^*$	BDT	CAAC (Carbene)
T5	4.93	4.89	4.91	LE	$\pi\pi^*$	BDT	BDT
T6	4.95	4.91	4.93	Mixed	$\pi\pi^*$	BDT/CAAC	CAAC
T7	5.03	4.99	5.01	LE	$\pi\pi^*$	BDT	BDT
T8	5.09	5.05	5.07	LE	$n\pi^*$	CAAC	CAAC
T9	5.25	5.21	5.24	LLCT	$n\pi^*$	BDT	CAAC (Carbene)
T10	5.29	5.25	5.27	LLCT	$\pi\pi^*$	BDT	CAAC (Dipp)

Table 7.13: Energy difference to the S0 state of the planar, queer and orthogonal S0 geometry and characterisations of the first ten singlet and triplet excited states of the T-LE-CAAC geometry for Zn-BDT.

	ΔE [eV]			Character		From	To
	planar	queer	ortho				
S0	0.93	0.89	0.91				
S1	4.03	3.99	4.01	LLCT	$\pi\pi^*$	BDT	CAAC (Carbene)
S2	4.64	4.60	4.62	LLCT	$\pi\pi^*$	BDT	CAAC (Carbene)
S3	5.02	4.98	5.00	LLCT	$\pi\pi^*$	BDT	CAAC (Dipp)
S4	5.07	5.03	5.05	LLCT	$n\pi^*$	BDT	CAAC (Carbene)
S5	5.12	5.08	5.10	LE	$\pi\pi^*$	CAAC	CAAC
S6	5.31	5.27	5.29	LE	$\pi\pi^*$	BDT	BDT
S7	5.35	5.31	5.33	LE	$\pi\pi^*$	CAAC	CAAC
S8	5.50	5.46	5.48	Ambiguous	π	BDT	Empty
S9	5.54	5.50	5.52	Mixed	$n\pi^*$	BDT/CAAC	CAAC
S10	5.69	5.65	5.67	LLCT	$\pi\pi^*$	BDT	CAAC (Dipp)
T1	3.60	3.56	3.58	LE	$\pi\pi^*$	CAAC	CAAC
T2	3.98	3.94	3.96	LLCT	$\pi\pi^*$	BDT	CAAC (Carbene)
T3	4.61	4.57	4.59	LLCT	$\pi\pi^*$	BDT	CAAC (Carbene)
T4	4.71	4.67	4.69	LE	$\pi\pi^*$	BDT	BDT
T5	4.94	4.90	4.92	Mixed	$n\pi^*$	BDT/CAAC	CAAC
T6	4.96	4.92	4.94	Mixed	$n\pi^*/\pi\pi^*$	BDT/CAAC	BDT/CAAC
T7	5.01	4.96	4.99	LLCT	$n\pi^*$	BDT	CAAC (Carbene)
T8	5.04	5.00	5.02	LLCT	$n\pi^*$	BDT	CAAC (Carbene)
T9	5.18	5.14	5.16	LE	$\pi\pi^*$	BDT	BDT
T10	5.19	5.15	5.17	LE	$\pi\pi^*$	CAAC	CAAC

Excitation Energy Diagrams

In the following two diagrams excitation energies for all optimized state geometries of Zn-BDT are shown. For the S0, S- and T-LLCT ($\pi\pi^*$) geometries the results of the planar conformer are presented in figure 7.1 and the orthogonal conformer in figure 7.2.

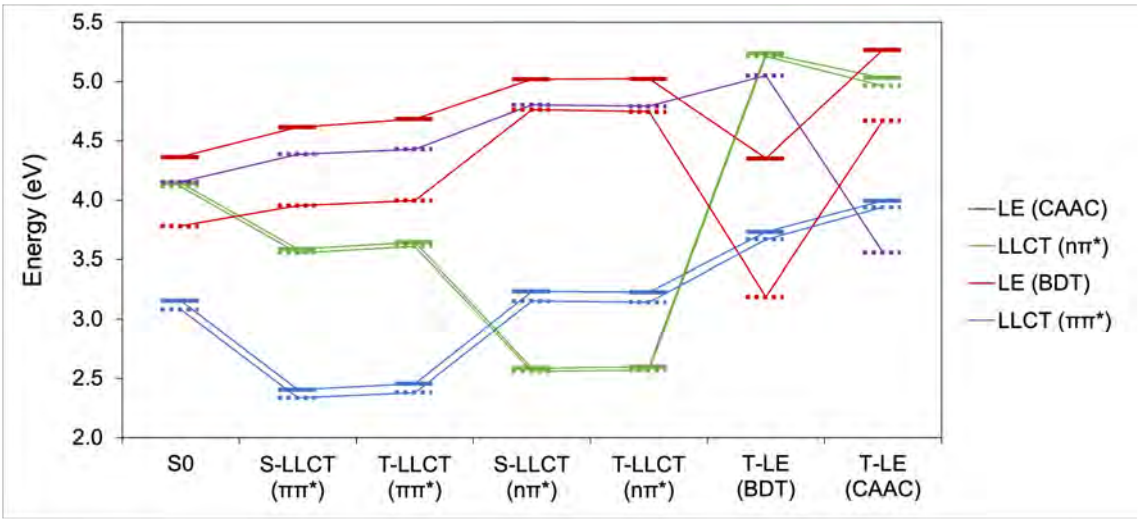

Fig. 7.1: Excitation energy diagram of the planar conformer for Zn-BDT. Singlet states are represented by solid lines, triplet states by dashed lines.

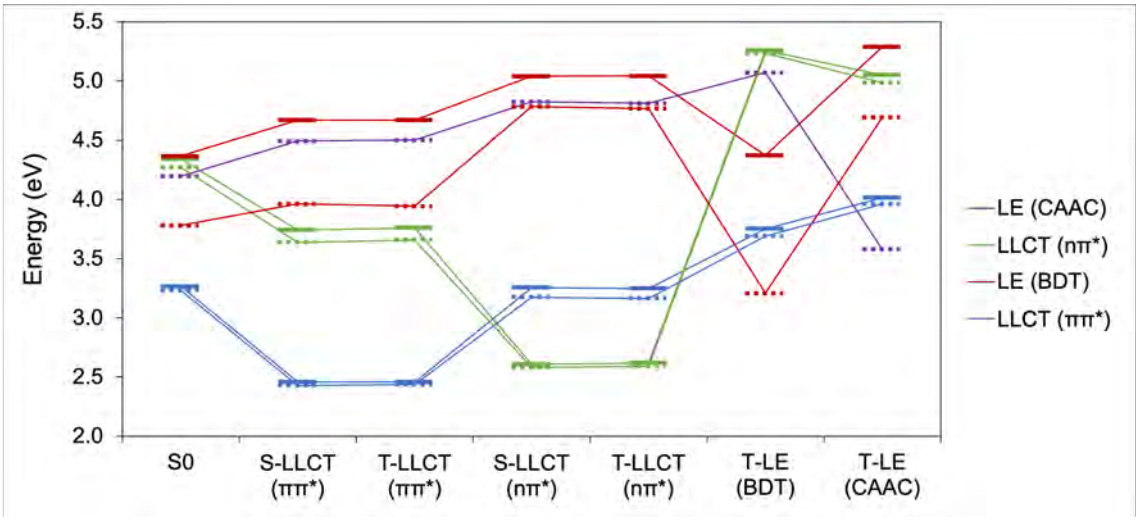

Fig. 7.2: Excitation energy diagram of the orthogonal conformer for Zn-BDT. Singlet states are represented by solid lines, triplet states by dashed lines.

7.1.2 Geometries

Table 7.14: Optimized planar ground state geometry (S0-planar) of Zn-BDT.

Atom	x	y	z	Atom	x	y	z
Zn	1.591797	7.556923	12.319013	H	4.624040	3.016644	15.494218
S	0.866501	7.065522	10.208485	H	4.172486	2.780662	13.801286
S	0.618427	9.632668	12.379712	C	2.419803	9.786369	15.903690
N	3.390217	5.460936	13.388112	H	2.874268	9.834540	16.904031
C	3.870183	5.703945	15.676074	H	1.955309	10.762610	15.720818
H	4.747314	5.996842	16.255760	C	4.101150	8.139773	15.080583
H	3.235577	5.119702	16.343478	H	4.626958	8.145405	16.043375
C	-0.544125	8.720325	8.572031	H	4.867510	7.946152	14.320858
H	-0.462802	7.891689	7.875100	C	1.359893	8.696336	15.874769
C	-1.211804	9.872206	8.191359	H	0.831213	8.738378	14.918353
H	-1.650108	9.941042	7.200277	H	0.606690	8.898498	16.644187
C	4.228095	5.241403	11.068070	C	-0.124901	3.938105	12.348298
C	5.746967	4.990233	14.129954	H	-0.412011	3.432841	11.418970
H	5.999372	4.428880	13.228328	H	-0.143981	5.013988	12.157526
H	6.327425	4.568983	14.956436	H	-0.882134	3.705927	13.106107
H	6.056909	6.029447	14.004191	C	5.234687	6.376786	11.199967
C	-1.313476	10.932620	9.085988	H	5.194517	6.756685	12.220327
H	-1.832255	11.844604	8.806434	C	3.109878	6.938156	15.142394
C	2.330665	3.242611	10.587697	C	2.340274	3.864332	11.833932
H	1.584967	2.483479	10.379840	C	3.510640	9.530134	14.872065
C	1.253523	3.473580	12.825928	H	3.050058	9.586076	13.879868
H	1.448078	3.983689	13.769730	C	0.843750	6.219915	16.291315
C	3.242470	3.580025	9.604386	H	1.305084	5.238474	16.135903
H	3.217343	3.078903	8.642131	C	2.753792	6.544163	13.715088
C	4.168237	4.578211	9.843918	C	4.887592	7.547545	10.274659
H	4.856316	4.860758	9.055073	H	4.965819	7.254612	9.221512
C	3.320742	4.847997	12.071964	H	5.586767	8.374949	10.443623
C	4.267893	4.852806	14.472508	H	3.871195	7.914628	10.436375
C	6.672066	5.927281	10.920112	C	4.607211	10.586039	14.924396
H	6.966270	5.059719	11.516901	H	4.192707	11.587202	14.758333
H	7.368271	6.743763	11.143741	H	5.370858	10.407728	14.157635
H	6.805353	5.664713	9.864892	H	5.106748	10.587416	15.902049
C	1.221808	1.968618	13.105494	C	0.323134	6.222866	17.728687
H	0.507290	1.753904	13.908465	H	-0.138339	7.183853	17.986651
H	2.198524	1.580096	13.407551	H	1.131403	6.036007	18.445365

Atom	x	y	z	Atom	x	y	z
H	0.897732	1.407016	12.222439	H	-0.436696	5.445198	17.868939
C	-0.066217	9.661973	10.745505	C	-0.325675	6.309645	15.314987
C	0.037822	8.586784	9.839321	H	-1.009748	5.468475	15.475916
C	-0.744717	10.819153	10.343514	H	-0.003389	6.261686	14.271011
H	-0.821511	11.645098	11.044141	H	-0.900906	7.232164	15.445984
C	3.968688	3.377297	14.694865	C	1.940701	7.301724	16.110376
H	2.939082	3.207096	15.013222	H	2.459978	7.356192	17.076667

Table 7.15: Optimized queer ground state geometry (S0-queer) of Zn-BDT.

Atom	x	y	z	Atom	x	y	z
Zn	1.585936	7.602213	12.354441	H	4.785896	3.075201	15.428583
S	0.184753	6.998921	10.646816	H	4.299499	2.841086	13.745382
S	1.495390	9.844978	11.889668	C	2.308041	9.736644	16.033282
N	3.373010	5.486372	13.391352	H	2.768529	9.758658	17.031735
C	3.874450	5.712420	15.674466	H	1.818339	10.707219	15.890364
H	4.742309	6.015242	16.262840	C	4.031900	8.169116	15.140337
H	3.255930	5.093052	16.325495	H	4.567969	8.158850	16.097407
C	-0.929677	8.676928	8.817773	H	4.795376	8.027736	14.366577
H	-1.355092	7.759044	8.423656	C	1.275925	8.622220	15.970883
C	-1.211691	9.883422	8.199422	H	0.729973	8.693939	15.025334
H	-1.855537	9.905991	7.325359	H	0.528355	8.770648	16.758195
C	4.129391	5.276702	11.035951	C	-0.129918	3.826046	12.499710
C	5.757911	5.131768	14.081953	H	-0.428013	3.311732	11.579085
H	6.026975	4.581225	13.178866	H	-0.211010	4.900878	12.320635
H	6.379786	4.753199	14.898868	H	-0.846200	3.554012	13.283552
H	5.998919	6.187435	13.942351	C	5.113157	6.437044	11.111386
C	-0.664267	11.057613	8.706238	H	5.079924	6.856128	12.117416
H	-0.873022	12.013463	8.235318	C	3.079155	6.936734	15.169198
C	2.262842	3.231529	10.639977	C	2.313011	3.854227	11.884426
H	1.528445	2.453156	10.466184	C	3.395340	9.545313	14.984770
C	1.285481	3.425027	12.922380	H	2.922798	9.612264	14.000393
H	1.496589	3.946985	13.856306	C	0.832787	6.114827	16.281520
C	3.121644	3.588679	9.617114	H	1.315228	5.158179	16.052024
H	3.066963	3.085492	8.657165	C	2.725080	6.557849	13.736371
C	4.033597	4.607209	9.816917	C	4.728802	7.559630	10.141174

Atom	x	y	z	Atom	x	y	z
H	4.681846	4.902675	8.999649	H	4.821273	7.230587	9.100202
C	3.275336	4.866118	12.079249	H	5.398148	8.416585	10.279624
C	4.296560	4.903571	14.451363	H	3.703346	7.906123	10.289506
C	6.555599	6.008743	10.821615	C	4.457592	10.634167	15.056493
H	6.883918	5.174566	11.446788	H	4.008956	11.625669	14.924822
H	7.236117	6.850195	10.995420	H	5.217016	10.503301	14.276257
H	6.672306	5.704474	9.775649	H	4.968220	10.622854	16.028421
C	1.328141	1.920085	13.204013	C	0.342703	6.012553	17.725656
H	0.666488	1.678972	14.043924	H	-0.130271	6.946101	18.054447
H	2.333764	1.569725	13.452350	H	1.168729	5.795519	18.413017
H	0.979377	1.345143	12.339170	H	-0.400085	5.212955	17.829443
C	0.448562	9.790779	10.460940	C	-0.357997	6.238760	15.335768
C	-0.103916	8.600748	9.946488	H	-1.009235	5.363409	15.439016
C	0.153381	11.001665	9.822456	H	-0.052142	6.287623	14.287016
H	0.581438	11.916295	10.221367	H	-0.962455	7.125953	15.552059
C	4.087814	3.410572	14.654734	C	1.897373	7.235346	16.146161
H	3.079819	3.176075	14.999194	H	2.414547	7.269270	17.114338

Table 7.16: Optimized orthogonal ground state geometry (S0-ortho) of Zn-BDT.

Atom	x	y	z	Atom	x	y	z
Zn	1.179492	-0.019319	-0.045352	H	-5.159028	0.315034	-0.031031
S	2.450926	-0.740747	-1.803754	H	-4.353397	-1.232529	-0.312890
S	2.947244	0.149599	1.410710	C	0.775348	4.096128	1.147595
N	-1.763309	-0.271608	0.267959	H	0.108683	4.934136	1.398515
C	-2.834474	1.807206	0.466649	H	1.801618	4.467992	1.252070
H	-3.321645	2.379841	1.257793	C	-0.871612	2.395743	1.941301
H	-3.240608	2.170119	-0.478805	H	-1.579040	3.172741	2.256377
C	5.127269	-1.227011	-1.757209	H	-1.023604	1.554441	2.627321
H	4.964253	-1.508961	-2.792962	C	0.527624	3.658059	-0.286721
C	6.400767	-1.304181	-1.218573	H	1.286987	2.923252	-0.572348
H	7.228685	-1.644706	-1.833027	H	0.672529	4.510076	-0.960722
C	-1.292779	-2.555681	1.120864	C	-0.816922	-1.367779	-3.448123
C	-3.545693	-0.055418	2.025692	H	-0.658645	-2.371956	-3.857602
H	-3.697744	-1.131243	2.126183	H	0.105211	-1.065396	-2.946859
H	-4.500563	0.435424	2.237095	H	-0.989755	-0.686369	-4.288899

Atom	x	y	z	Atom	x	y	z
H	-2.828256	0.276573	2.778567	C	-1.021147	-2.105175	2.549582
C	6.605114	-0.943669	0.109291	H	-1.161433	-1.026057	2.605463
H	7.595648	-0.997674	0.550774	C	-1.299832	1.983859	0.500984
C	-1.636832	-3.573084	-1.461147	C	-1.760040	-2.199719	-1.265685
H	-1.751604	-3.978020	-2.460260	C	0.536079	2.953491	2.124993
C	-2.014663	-1.341480	-2.496388	H	1.268424	2.170405	1.903856
H	-2.143538	-0.307074	-2.176808	C	-1.218521	2.843856	-1.989906
C	-1.362061	-4.431991	-0.413206	H	-2.005967	2.083131	-2.031612
H	-1.272670	-5.498980	-0.590098	C	-0.783536	0.579317	0.216296
C	-1.185496	-3.920677	0.858037	C	0.425386	-2.391025	2.963264
H	-0.948197	-4.597472	1.671070	H	0.632661	-3.467164	2.964267
C	-1.601313	-1.699805	0.043690	H	0.600291	-2.019200	3.979940
C	-3.126578	0.316183	0.607401	H	1.148711	-1.904448	2.303504
C	-1.969609	-2.760974	3.558972	C	0.750546	3.384467	3.569974
H	-3.022185	-2.653489	3.282884	H	1.767659	3.766692	3.715442
H	-1.830843	-2.309980	4.548247	H	0.605271	2.546742	4.262768
H	-1.761546	-3.832229	3.655910	H	0.049076	4.180416	3.852818
C	-3.278179	-1.762611	-3.252852	C	-1.794465	4.100701	-2.641342
H	-3.489230	-1.045425	-4.054392	H	-1.078874	4.931533	-2.598491
H	-4.156376	-1.814935	-2.603538	H	-2.714028	4.425751	-2.140410
H	-3.150599	-2.745297	-3.719906	H	-2.030646	3.922482	-3.697012
C	4.238103	-0.426285	0.343386	C	-0.059762	2.312520	-2.829405
C	4.031162	-0.793820	-1.001217	H	-0.416730	2.063601	-3.835429
C	5.532355	-0.512827	0.871693	H	0.387741	1.406515	-2.411922
H	5.689147	-0.230687	1.908367	H	0.737670	3.055315	-2.939361
C	-4.217893	-0.147630	-0.345171	C	-0.886847	3.113657	-0.495870
H	-4.029230	0.160351	-1.374301	H	-1.553192	3.929871	-0.187021

Table 7.17: Optimized planar excited singlet LLCT ($\pi\pi^*$) state geometry (S-LLCT $\pi\pi^*$ planar) of Zn-BDT.

Atom	x	y	z	Atom	x	y	z
Zn	0.859819	0.383777	0.057729	H	-5.237404	-0.973676	0.093547
S	2.308736	-1.493979	-0.283305	H	-4.054634	-2.288934	0.051881
S	2.738275	1.816300	-0.065725	C	-0.475795	4.329634	0.787668

Atom	x	y	z	Atom	x	y	z
N	-1.832487	-0.626413	0.445129	H	-1.310040	5.027233	0.952675
C	-3.378120	1.118138	0.327041	H	0.446020	4.921949	0.852364
H	-4.058295	1.652784	0.995615	C	-1.752503	2.414186	1.731107
H	-3.802955	1.192635	-0.675894	H	-2.617948	3.068147	1.914246
C	4.901100	-1.516179	-0.976374	H	-1.767072	1.652407	2.517539
H	4.756047	-2.589227	-1.029749	C	-0.597235	3.707257	-0.594733
C	6.118628	-0.968114	-1.260241	H	0.307821	3.128153	-0.803870
H	6.951022	-1.604406	-1.540508	H	-0.624306	4.501310	-1.350676
C	-0.756685	-2.545409	1.560711	C	-0.396302	-1.764207	-3.058311
C	-3.657259	-0.595989	2.173201	H	0.076302	-2.712235	-3.342079
H	-3.554928	-1.650497	2.440946	H	0.355459	-1.152434	-2.550816
H	-4.707386	-0.318419	2.317262	H	-0.692165	-1.246885	-3.978965
H	-3.057016	-0.001532	2.865145	C	-0.650507	-1.836414	2.902129
C	6.293559	0.433099	-1.191755	H	-1.084978	-0.844382	2.786815
H	7.261183	0.867248	-1.419880	C	-1.955798	1.724037	0.352099
C	-0.713565	-3.925364	-0.864854	C	-1.212665	-2.623619	-0.839415
H	-0.672425	-4.462138	-1.807006	C	-0.498619	3.267537	1.878984
C	-1.616416	-1.993418	-2.162978	H	0.380147	2.622184	1.742345
H	-2.037933	-1.011591	-1.949548	C	-2.030372	2.340793	-2.212791
C	-0.259088	-4.545684	0.285188	H	-2.602468	1.408215	-2.184201
H	0.120926	-5.562037	0.245902	C	-1.061320	0.499025	0.196416
C	-0.268718	-3.850230	1.480438	C	0.809394	-1.644368	3.326771
H	0.120532	-4.328464	2.373373	H	1.298930	-2.605932	3.521342
C	-1.276943	-1.939928	0.395216	H	0.858772	-1.054099	4.249882
C	-3.267357	-0.362867	0.710903	H	1.395130	-1.126994	2.560653
C	-1.400829	-2.568506	4.018770	C	-0.404856	3.876531	3.271581
H	-2.442072	-2.774071	3.755358	H	0.505225	4.479386	3.379681
H	-1.396594	-1.966378	4.935370	H	-0.387610	3.099914	4.046157
H	-0.923602	-3.526792	4.254605	H	-1.263967	4.529927	3.473359
C	-2.665721	-2.815861	-2.915063	C	-2.861851	3.347115	-3.007708
H	-3.008785	-2.269672	-3.802075	H	-2.372579	4.329380	-3.040662
H	-3.539185	-3.033750	-2.293104	H	-3.854417	3.485529	-2.562151
H	-2.255048	-3.772027	-3.259595	H	-3.002296	3.014438	-4.043692
C	3.971250	0.716692	-0.529930	C	-0.741769	2.021998	-2.967988
C	3.788043	-0.710467	-0.608202	H	-0.980802	1.582378	-3.944190
C	5.249524	1.243793	-0.839319	H	-0.129283	1.299070	-2.421214
H	5.386740	2.317904	-0.787555	H	-0.139101	2.918618	-3.151854
C	-4.196961	-1.220981	-0.145052	C	-1.839221	2.825673	-0.749823
H	-4.049873	-1.040419	-1.211496	H	-2.693310	3.485275	-0.538675

Table 7.18: Optimized queer excited singlet LLCT ($\pi\pi^*$) state geometry (S-LLCT $\pi\pi^*$ queer) of Zn-BDT.

Atom	x	y	z	Atom	x	y	z
Zn	0.875320	0.292289	0.124899	H	-5.277715	-0.909430	0.262842
S	2.318501	-1.340907	-0.843760	H	-4.128170	-2.253015	0.223618
S	2.797306	1.586879	0.670210	C	-0.357290	4.295007	0.702848
N	-1.851279	-0.643005	0.463968	H	-1.173826	5.025956	0.797254
C	-3.336817	1.139977	0.291332	H	0.580473	4.860820	0.774679
H	-4.031964	1.722994	0.901648	C	-1.727969	2.466088	1.688761
H	-3.718728	1.164138	-0.731844	H	-2.582074	3.149463	1.806020
C	4.932311	-1.165647	-1.429370	H	-1.790867	1.748027	2.511697
H	4.777985	-2.137107	-1.885057	C	-0.445112	3.605490	-0.649587
C	6.159447	-0.569289	-1.471748	H	0.450344	2.989129	-0.790695
H	6.989344	-1.067156	-1.961441	H	-0.417125	4.360322	-1.444467
C	-0.775988	-2.587305	1.546147	C	-0.644511	-1.823495	-3.120103
C	-3.618115	-0.459173	2.242157	H	-0.202310	-2.777877	-3.430607
H	-3.572765	-1.504764	2.556163	H	0.148879	-1.215026	-2.677121
H	-4.642327	-0.107776	2.409734	H	-1.003419	-1.312084	-4.021568
H	-2.955668	0.123122	2.884992	C	-0.661381	-1.906819	2.901313
C	6.349708	0.702369	-0.881764	H	-1.066587	-0.900690	2.802994
H	7.325781	1.173895	-0.921418	C	-1.901836	1.714823	0.338240
C	-0.812925	-3.954343	-0.886202	C	-1.314786	-2.654798	-0.836156
H	-0.810375	-4.488266	-1.830820	C	-0.458304	3.293130	1.844714
C	-1.797947	-2.036047	-2.137721	H	0.402853	2.616314	1.779101
H	-2.201379	-1.051550	-1.905145	C	-1.874038	2.201963	-2.252630
C	-0.310325	-4.577327	0.241976	H	-2.358169	1.223576	-2.179890
H	0.072987	-5.591534	0.183886	C	-1.039786	0.462135	0.243640
C	-0.286430	-3.889792	1.441274	C	0.795411	-1.768307	3.355285
H	0.127121	-4.374256	2.319752	H	1.255022	-2.747094	3.535395
C	-1.327031	-1.969585	0.400385	H	0.844793	-1.202530	4.293507
C	-3.268595	-0.320570	0.756212	H	1.410868	-1.245837	2.616817
C	-1.450668	-2.643758	3.988283	C	-0.402734	3.972149	3.206567
H	-2.490816	-2.819330	3.699692	H	0.520785	4.553054	3.321344
H	-1.450552	-2.061970	4.918002	H	-0.441166	3.237799	4.020554
H	-1.000721	-3.618431	4.210477	H	-1.248289	4.660384	3.337488
C	-2.900356	-2.863045	-2.805126	C	-2.798973	3.102239	-3.071073

Atom	x	y	z	Atom	x	y	z
H	-3.306705	-2.324183	-3.669642	H	-2.392062	4.119373	-3.147985
H	-3.726397	-3.076042	-2.120033	H	-3.792128	3.177008	-2.611807
H	-2.515021	-3.822287	-3.169879	H	-2.928164	2.719733	-4.091287
C	4.021560	0.749315	-0.183995	C	-0.575527	1.970303	-3.025606
C	3.821096	-0.536089	-0.804783	H	-0.799036	1.488131	-3.985036
C	5.310332	1.336944	-0.260972	H	0.115284	1.315038	-2.486135
H	5.457232	2.309966	0.193639	H	-0.054351	2.908658	-3.245641
C	-4.256335	-1.191799	-0.015371	C	-1.711487	2.759568	-0.809081
H	-4.160638	-1.063274	-1.094597	H	-2.545538	3.459714	-0.658223

Table 7.19: Optimized orthogonal excited singlet LLCT ($\pi\pi^*$) state geometry (S-LLCT $\pi\pi^*$ ortho) of Zn-BDT.

Atom	x	y	z	Atom	x	y	z
Zn	1.079243	-0.000996	0.081254	H	-5.194814	0.280793	0.207435
S	2.437013	-0.966061	-1.621118	H	-4.402991	-1.283867	-0.024643
S	3.043786	0.112838	1.474085	C	0.831936	4.085186	1.055509
N	-1.805625	-0.304036	0.326752	H	0.217202	4.972792	1.266025
C	-2.820619	1.789026	0.421109	H	1.879285	4.400229	1.148828
H	-3.347795	2.438150	1.125682	C	-0.921179	2.524722	1.891932
H	-3.198576	2.032816	-0.574268	H	-1.586130	3.370122	2.123827
C	5.082023	-1.427491	-1.679413	H	-1.138282	1.747341	2.630659
H	4.878624	-1.799461	-2.677031	C	0.555367	3.604773	-0.360255
C	6.357605	-1.423570	-1.191817	H	1.269519	2.815300	-0.624478
H	7.172628	-1.794938	-1.803663	H	0.746327	4.423693	-1.063951
C	-1.264351	-2.593240	1.088971	C	-0.884030	-1.206801	-3.429174
C	-3.465741	0.078476	2.175226	H	-0.674695	-2.188755	-3.870291
H	-3.675024	-0.976629	2.366107	H	0.026793	-0.858644	-2.934847
H	-4.372061	0.644334	2.418491	H	-1.107582	-0.513096	-4.248311
H	-2.676052	0.402733	2.855708	C	-1.007146	-2.173905	2.527605
C	6.622171	-0.933646	0.109448	H	-1.146191	-1.095726	2.591428
H	7.638179	-0.932305	0.489096	C	-1.289319	1.999327	0.475726
C	-1.587636	-3.531113	-1.518499	C	-1.757684	-2.170787	-1.266122
H	-1.699220	-3.902716	-2.531862	C	0.511650	3.007599	2.081573
C	-2.061659	-1.271629	-2.453693	H	1.189477	2.164081	1.900303
H	-2.216320	-0.263025	-2.073155	C	-1.199585	2.794454	-2.040430

Atom	x	y	z	Atom	x	y	z
C	-1.275566	-4.419808	-0.505337	H	-1.897820	1.953010	-2.063015
H	-1.151925	-5.476773	-0.721208	C	-0.749375	0.597399	0.211927
C	-1.109323	-3.945923	0.782417	C	0.431235	-2.472028	2.961388
H	-0.846070	-4.642685	1.571488	H	0.630834	-3.549899	2.979317
C	-1.624282	-1.693785	0.058945	H	0.606476	-2.087456	3.973638
C	-3.100707	0.307465	0.704219	H	1.166728	-2.007107	2.297555
C	-1.973275	-2.847037	3.508070	C	0.750353	3.485922	3.507419
H	-3.019308	-2.717375	3.215872	H	1.787041	3.817218	3.645630
H	-1.847886	-2.427939	4.513790	H	0.553144	2.687752	4.233760
H	-1.780979	-3.924281	3.574542	H	0.093913	4.331044	3.753845
C	-3.326151	-1.702559	-3.202500	C	-1.903246	3.981775	-2.696430
H	-3.583774	-0.960459	-3.967872	H	-1.271561	4.879666	-2.666360
H	-4.184130	-1.809713	-2.532084	H	-2.843499	4.221381	-2.185053
H	-3.181396	-2.661577	-3.713350	H	-2.135529	3.776194	-3.748925
C	4.257750	-0.456926	0.421016	C	-0.005255	2.372211	-2.894989
C	3.990472	-0.944688	-0.909768	H	-0.351416	2.060418	-3.887701
C	5.601484	-0.465881	0.885394	H	0.533411	1.528320	-2.454609
H	5.798345	-0.091443	1.883395	H	0.706409	3.192543	-3.040721
C	-4.271656	-0.201670	-0.132359	C	-0.879031	3.106369	-0.550986
H	-4.148224	0.030022	-1.191503	H	-1.517785	3.957363	-0.274683

Table 7.20: Optimized planar excited triplet LLCT ($\pi\pi^*$) state geometry (T-LLCT $\pi\pi^*$ planar) of Zn-BDT.

Atom	x	y	z	Atom	x	y	z
Zn	0.842202	0.391835	-0.012883	H	-5.242961	-0.962972	0.119943
S	2.279456	-1.476352	-0.351336	H	-4.064071	-2.280283	0.045644
S	2.696519	1.830113	-0.166293	C	-0.443286	4.317211	0.744356
N	-1.832910	-0.627047	0.422900	H	-1.265010	5.026230	0.922949
C	-3.377153	1.122133	0.354129	H	0.487048	4.898134	0.787171
H	-4.037285	1.648889	1.048530	C	-1.722586	2.420958	1.722286
H	-3.829599	1.212931	-0.635164	H	-2.578429	3.084761	1.914849
C	4.912774	-1.514837	-0.862156	H	-1.731651	1.663562	2.513405
H	4.766400	-2.587081	-0.925582	C	-0.601673	3.691395	-0.633048
C	6.150155	-0.972896	-1.050280	H	0.291955	3.101249	-0.861119
H	6.998782	-1.612957	-1.265488	H	-0.636797	4.482923	-1.391204

Atom	x	y	z	Atom	x	y	z
C	-0.737530	-2.542051	1.527967	C	-0.447228	-1.766596	-3.095405
C	-3.628223	-0.614242	2.180524	H	0.026532	-2.713857	-3.379981
H	-3.516189	-1.670745	2.436615	H	0.306265	-1.146786	-2.600452
H	-4.677228	-0.343359	2.344030	H	-0.757932	-1.255970	-4.014947
H	-3.019890	-0.022945	2.868318	C	-0.608695	-1.828701	2.865255
C	6.327670	0.428434	-0.964901	H	-1.049109	-0.838833	2.755736
H	7.313166	0.856029	-1.115466	C	-1.953074	1.724692	0.351742
C	-0.732980	-3.927861	-0.895148	C	-1.230948	-2.625857	-0.864532
H	-0.706686	-4.466725	-1.836677	C	-0.457155	3.260855	1.841726
C	-1.653982	-1.996006	-2.182209	H	0.409734	2.602396	1.691197
H	-2.071586	-1.013969	-1.962171	C	-2.089607	2.336190	-2.213727
C	-0.261604	-4.545760	0.249422	H	-2.657364	1.401701	-2.167918
H	0.116679	-5.562654	0.206869	C	-1.057368	0.499931	0.189637
C	-0.251992	-3.847392	1.443110	C	0.858180	-1.627460	3.259774
H	0.150755	-4.323821	2.331033	H	1.360527	-2.585956	3.436525
C	-1.277282	-1.939658	0.369505	H	0.922571	-1.042720	4.185546
C	-3.262038	-0.364180	0.714996	H	1.418881	-1.097954	2.483616
C	-1.333207	-2.560995	3.998693	C	-0.327586	3.875812	3.228720
H	-2.378098	-2.773677	3.756072	H	0.591859	4.467954	3.315029
H	-1.315125	-1.955041	4.912613	H	-0.303797	3.102838	4.006767
H	-0.845892	-3.515409	4.229605	H	-1.174286	4.540769	3.444810
C	-2.714956	-2.818071	-2.918002	C	-2.949537	3.340815	-2.980088
H	-3.071026	-2.272327	-3.800147	H	-2.463856	4.324338	-3.027324
H	-3.579099	-3.034824	-2.282746	H	-3.927384	3.476389	-2.502260
H	-2.310158	-3.774820	-3.267927	H	-3.122789	3.009191	-4.011435
C	3.961333	0.724776	-0.494813	C	-0.826221	2.021767	-3.012457
C	3.778923	-0.702234	-0.578632	H	-1.098168	1.590566	-3.983863
C	5.265876	1.245164	-0.695557	H	-0.197398	1.294217	-2.491419
H	5.404337	2.318420	-0.632389	H	-0.228703	2.919201	-3.209162
C	-4.206725	-1.209760	-0.136755	C	-1.854728	2.821555	-0.756519
H	-4.074712	-1.017421	-1.203256	H	-2.696886	3.489416	-0.524654

Table 7.21: Optimized queer excited triplet LLCT ($\pi\pi^*$) state geometry (T-LLCT $\pi\pi^*$ queer) of Zn-BDT.

Atom	x	y	z	Atom	x	y	z
Zn	0.878205	0.285312	0.150457	H	-5.277484	-0.885166	0.210938
S	2.313197	-1.352819	-0.807655	H	-4.137831	-2.236943	0.171261
S	2.786200	1.581661	0.681530	C	-0.333889	4.286231	0.729700
N	-1.851329	-0.645390	0.452339	H	-1.147863	5.021117	0.815528
C	-3.323616	1.148853	0.282660	H	0.605673	4.847645	0.812060
H	-4.021274	1.729388	0.892423	C	-1.725555	2.466146	1.701852
H	-3.695339	1.187019	-0.743761	H	-2.576724	3.155050	1.807223
C	4.885612	-1.104593	-1.536193	H	-1.803493	1.749094	2.524693
H	4.719550	-2.055316	-2.029672	C	-0.410092	3.598321	-0.624559
C	6.108577	-0.501997	-1.589178	H	0.485385	2.980529	-0.758743
H	6.924180	-0.972780	-2.127347	H	-0.373170	4.354335	-1.417898
C	-0.790187	-2.584424	1.560893	C	-0.628793	-1.863138	-3.114107
C	-3.636342	-0.467624	2.212382	H	-0.185151	-2.821098	-3.411418
H	-3.599556	-1.516475	2.516355	H	0.161426	-1.249827	-2.672863
H	-4.660615	-0.112910	2.372138	H	-0.982912	-1.361887	-4.023241
H	-2.978028	0.105229	2.867909	C	-0.681634	-1.894288	2.912039
C	6.315631	0.739717	-0.942432	H	-1.075769	-0.884822	2.802556
H	7.289728	1.214675	-0.988737	C	-1.886045	1.715162	0.350952
C	-0.814938	-3.972359	-0.859999	C	-1.313059	-2.670754	-0.824747
H	-0.807447	-4.514356	-1.799987	C	-0.452835	3.285643	1.871380
C	-1.787091	-2.063057	-2.135038	H	0.404768	2.603133	1.816919
H	-2.188499	-1.075052	-1.914475	C	-1.829612	2.192287	-2.239753
C	-0.323017	-4.587408	0.277037	H	-2.292664	1.204066	-2.163521
H	0.056845	-5.603520	0.230470	C	-1.026838	0.458041	0.271145
C	-0.305758	-3.889727	1.470687	C	0.772227	-1.767056	3.379376
H	0.098888	-4.368436	2.356417	H	1.218630	-2.749008	3.574922
C	-1.331316	-1.974553	0.405422	H	0.817931	-1.192041	4.312176
C	-3.269917	-0.316497	0.732053	H	1.400834	-1.259157	2.641872
C	-1.486573	-2.616159	3.997898	C	-0.408783	3.965996	3.233004
H	-2.525825	-2.784985	3.702741	H	0.516726	4.541605	3.357908
H	-1.488721	-2.027364	4.923205	H	-0.461037	3.232797	4.047274
H	-1.046866	-3.592941	4.231035	H	-1.251774	4.659315	3.353385

Atom	x	y	z	Atom	x	y	z
C	-2.889126	-2.892869	-2.799500	C	-2.774160	3.071233	-3.058716
H	-3.288716	-2.361677	-3.671884	H	-2.386257	4.095283	-3.141484
H	-3.719637	-3.095493	-2.116755	H	-3.766795	3.130143	-2.595988
H	-2.505280	-3.857267	-3.152045	H	-2.900117	2.681880	-4.076746
C	4.005774	0.753950	-0.186295	C	-0.528690	1.983606	-3.015361
C	3.795793	-0.513783	-0.838453	H	-0.747488	1.504915	-3.977750
C	5.294640	1.343040	-0.264098	H	0.170174	1.333406	-2.480123
H	5.452494	2.296061	0.227682	H	-0.019881	2.929915	-3.230057
C	-4.255304	-1.172592	-0.058941	C	-1.676916	2.756344	-0.796661
H	-4.147065	-1.034393	-1.135848	H	-2.509249	3.460535	-0.655743

Table 7.22: Optimized orthogonal excited triplet LLCT ($\pi\pi^*$) state geometry (T-LLCT $\pi\pi^*$ ortho) of Zn-BDT.

Atom	x	y	z	Atom	x	y	z
Zn	0.906627	0.205751	0.210753	H	-5.249799	-0.830752	0.883120
S	2.439308	-1.042316	-1.089169	H	-4.102232	-2.117945	1.275490
S	2.764457	1.445142	1.097723	C	-0.347014	4.179160	-0.632605
N	-1.818042	-0.547940	0.875461	H	-1.171794	4.892079	-0.779844
C	-3.307544	1.077995	0.135734	H	0.583865	4.741225	-0.782673
H	-3.990548	1.841530	0.518185	C	-1.665346	2.787175	0.959847
H	-3.710980	0.744643	-0.823222	H	-2.528597	3.463777	0.873945
C	5.000518	-0.485795	-1.684753	H	-1.687052	2.385805	1.977265
H	4.889642	-1.291323	-2.401647	C	-0.453939	3.062792	-1.658990
C	6.191670	0.172270	-1.566031	H	0.437743	2.427583	-1.591956
H	7.032102	-0.112332	-2.189965	H	-0.439919	3.493684	-2.666951
C	-0.726774	-2.065033	2.492767	C	-0.729700	-2.796451	-2.172128
C	-3.526427	0.259992	2.529956	H	-0.251252	-3.783068	-2.153770
H	-3.479003	-0.614028	3.184145	H	0.037429	-2.041509	-1.981749
H	-4.541439	0.667547	2.595975	H	-1.119359	-2.631254	-3.183851
H	-2.836852	1.014234	2.912848	C	-0.566050	-0.990436	3.555537
C	6.334789	1.226142	-0.632041	H	-0.963633	-0.059830	3.152621
H	7.283506	1.744502	-0.544254	C	-1.872984	1.624878	-0.053601
C	-0.843158	-4.133513	0.623616	C	-1.337286	-2.878893	0.270768
H	-0.871291	-4.940345	-0.101344	C	-0.409495	3.632896	0.786451
C	-1.859486	-2.701384	-1.145707	H	0.467397	2.991212	0.934068

Atom	x	y	z	Atom	x	y	z
H	-2.272633	-1.696737	-1.224403	C	-1.931905	1.214640	-2.657442
C	-0.311706	-4.372993	1.878378	H	-2.378618	0.308194	-2.238620
H	0.063546	-5.358840	2.135928	C	-1.014220	0.401928	0.251874
C	-0.250110	-3.341019	2.796044	C	0.905962	-0.744266	3.901376
H	0.184656	-3.527668	3.772527	H	1.357969	-1.620965	4.380055
C	-1.307948	-1.835067	1.224493	H	0.992476	0.094980	4.602327
C	-3.225240	-0.129571	1.078300	H	1.504879	-0.502440	3.017316
C	-1.332343	-1.327021	4.838833	C	-0.344526	4.740857	1.829276
H	-2.382898	-1.561495	4.644416	H	0.568352	5.338586	1.715167
H	-1.297420	-0.480879	5.535721	H	-0.352625	4.331647	2.847166
H	-0.890147	-2.191274	5.348096	H	-1.202283	5.420198	1.736001
C	-2.964986	-3.702119	-1.492562	C	-2.919465	1.778008	-3.678489
H	-3.400453	-3.459770	-2.469507	H	-2.545764	2.716230	-4.110241
H	-3.770488	-3.696276	-0.751780	H	-3.892763	1.989824	-3.219327
H	-2.576168	-4.725154	-1.553834	H	-3.082954	1.075683	-4.505504
C	4.025526	0.928924	0.069585	C	-0.661994	0.758815	-3.374752
C	3.880927	-0.146401	-0.880343	H	-0.910572	-0.019581	-4.106298
C	5.280745	1.589923	0.155547	H	0.069424	0.334705	-2.681742
H	5.383579	2.398099	0.870660	H	-0.181030	1.577697	-3.921375
C	-4.238190	-1.203512	0.687955	C	-1.722256	2.222382	-1.490293
H	-4.179724	-1.458560	-0.371214	H	-2.551604	2.940887	-1.556371

Table 7.23: Optimized excited singlet LLCT ($n\pi^*$) state geometry (S-LLCT $n\pi^*$) of Zn-BDT.

Atom	x	y	z	Atom	x	y	z
Zn	-0.225399	3.792147	0.678535	H	0.903917	1.250888	-4.894898
S	-1.502664	5.811585	0.971328	H	0.340650	2.925649	-4.797796
S	-0.914185	3.829200	2.984046	C	1.442066	0.179333	2.165659
N	0.515098	3.078234	-2.008071	H	1.925201	-0.784801	1.949168
C	1.105922	0.823096	-2.124148	H	1.396280	0.268943	3.258545
H	2.008901	0.224510	-2.269419	C	2.295385	1.198727	0.059677
H	0.269148	0.215862	-2.474570	H	2.798744	0.257057	-0.202904
C	-0.296349	7.755569	2.589947	H	2.907856	2.004743	-0.358101
H	-0.531114	8.499946	1.835784	C	0.036829	0.186049	1.584240
C	0.366636	8.115689	3.758694	H	-0.492026	1.079230	1.934092

Atom	x	y	z	Atom	x	y	z
H	0.651691	9.150991	3.915782	H	-0.525688	-0.666045	1.984196
C	0.911271	5.494901	-2.331494	C	-3.390644	3.667310	-1.725171
C	2.598095	2.500093	-3.291889	H	-3.957200	4.581274	-1.939317
H	2.631491	3.434728	-3.856042	H	-2.954071	3.765416	-0.726386
H	3.034896	1.717443	-3.921872	H	-4.099730	2.831429	-1.699034
H	3.227022	2.604405	-2.404942	C	2.325659	5.451315	-1.773109
C	0.660435	7.158930	4.724345	H	2.539724	4.423034	-1.484242
H	1.174437	7.447668	5.635520	C	0.905793	1.203151	-0.637859
C	-1.718762	5.797835	-3.218535	C	-1.288519	4.537687	-2.807238
H	-2.744769	5.930182	-3.545659	C	2.290157	1.300570	1.580835
C	-2.314171	3.415140	-2.784637	H	1.826050	2.252905	1.869476
H	-1.800494	2.497164	-2.501561	C	-1.411867	-0.063651	-0.511587
C	-0.867044	6.888113	-3.211265	H	-1.430246	0.360993	-1.520082
H	-1.219235	7.860544	-3.541789	C	0.329323	2.613199	-0.726986
C	0.430036	6.733032	-2.758166	C	2.465847	6.313217	-0.513127
H	1.084581	7.597747	-2.724411	H	2.324154	7.376724	-0.738431
C	0.054740	4.373779	-2.400183	H	3.470400	6.196334	-0.088635
C	1.157880	2.119042	-2.942502	H	1.739461	6.039412	0.258270
C	3.374517	5.897002	-2.796988	C	3.707768	1.297153	2.137264
H	3.291031	5.354717	-3.742939	H	3.703184	1.382610	3.230868
H	4.384100	5.733604	-2.401225	H	4.295122	2.133042	1.737481
H	3.278972	6.965927	-3.020148	H	4.230590	0.367267	1.877280
C	-2.971284	3.192858	-4.149482	C	-1.752752	-1.547327	-0.648532
H	-3.612709	2.303890	-4.119218	H	-1.707047	-2.055492	0.323611
H	-2.230251	3.049053	-4.941764	H	-1.054228	-2.057456	-1.322768
H	-3.603301	4.041842	-4.434416	H	-2.765771	-1.686493	-1.045825
C	-0.370084	5.470709	3.368683	C	-2.516292	0.648382	0.266810
C	-0.662838	6.429304	2.400950	H	-3.470282	0.545222	-0.264424
C	0.294135	5.830324	4.533929	H	-2.311829	1.717469	0.369365
H	0.516260	5.082378	5.288349	H	-2.653145	0.224923	1.268124
C	0.390190	1.976088	-4.254232	C	0.024391	0.112179	0.055225
H	-0.626780	1.613635	-4.092336	H	0.556554	-0.818084	-0.189250

Table 7.24: Optimized excited triplet LLCT ($n\pi^*$) state geometry (T-LLCT $n\pi^*$) of Zn-BDT.

Atom	x	y	z	Atom	x	y	z
Zn	-0.209163	3.796751	0.679548	H	0.907972	1.256165	-4.897623
S	-1.491061	5.804194	0.968278	H	0.353764	2.933797	-4.797800
S	-0.893313	3.825296	2.989843	C	1.445245	0.172790	2.160051
N	0.519988	3.077466	-2.006927	H	1.927459	-0.790886	1.939452
C	1.099906	0.820268	-2.127391	H	1.402823	0.259575	3.253290
H	1.998324	0.215000	-2.273129	C	2.292339	1.197556	0.054237
H	0.258364	0.220462	-2.479349	H	2.797108	0.257752	-0.211979
C	-0.320956	7.759556	2.596590	H	2.902049	2.005954	-0.362713
H	-0.563402	8.501572	1.842516	C	0.038356	0.182049	1.582901
C	0.334247	8.127179	3.767242	H	-0.487363	1.076330	1.934666
H	0.605622	9.165872	3.926071	H	-0.524583	-0.669288	1.983819
C	0.916895	5.493780	-2.333540	C	-3.385196	3.666076	-1.717968
C	2.604657	2.492319	-3.287385	H	-3.951852	4.580613	-1.929365
H	2.644084	3.427163	-3.850655	H	-2.945944	3.762100	-0.720220
H	3.039057	1.708147	-3.917096	H	-4.094524	2.830401	-1.691892
H	3.232076	2.592687	-2.399006	C	2.333344	5.449698	-1.780519
C	0.637560	7.173136	4.732707	H	2.547500	4.421645	-1.490700
H	1.145193	7.467452	5.645677	C	0.901356	1.199671	-0.640985
C	-1.715867	5.798373	-3.211592	C	-1.284979	4.537698	-2.802660
H	-2.742822	5.931379	-3.535395	C	2.290817	1.295895	1.575529
C	-2.310950	3.415445	-2.779919	H	1.825992	2.247070	1.866898
H	-1.797278	2.496676	-2.499442	C	-1.416793	-0.063320	-0.508862
C	-0.863463	6.888174	-3.207134	H	-1.437674	0.363219	-1.516529
H	-1.216307	7.860865	-3.536173	C	0.323226	2.609240	-0.730308
C	0.435166	6.732116	-2.759094	C	2.479327	6.313614	-0.522563
H	1.090540	7.596280	-2.727841	H	2.339181	7.377018	-0.749380
C	0.059228	4.373353	-2.399154	H	3.484947	6.195347	-0.100990
C	1.161765	2.117665	-2.942547	H	1.754564	6.042173	0.251206
C	3.378379	5.892814	-2.809428	C	3.709945	1.293117	2.127982
H	3.289831	5.350181	-3.754733	H	3.708153	1.376203	3.221768
H	4.389452	5.728177	-2.418034	H	4.295055	2.130736	1.728506
H	3.283393	6.961721	-3.032869	H	4.233414	0.364543	1.864593
C	-2.970426	3.195852	-4.144089	C	-1.761083	-1.545992	-0.647415
H	-3.611651	2.306729	-4.114429	H	-1.712656	-2.056149	0.323548

Atom	x	y	z	Atom	x	y	z
H	-2.230773	3.053787	-4.938008	H	-1.066134	-2.056100	-1.325355
H	-3.603077	4.045291	-4.426193	H	-2.775882	-1.682347	-1.041122
C	-0.368448	5.472828	3.373129	C	-2.516427	0.649881	0.275107
C	-0.668489	6.428475	2.404743	H	-3.471933	0.554289	-0.254765
C	0.288217	5.840312	4.540278	H	-2.306053	1.717232	0.383243
H	0.516998	5.094773	5.295059	H	-2.653263	0.221694	1.274410
C	0.396556	1.982609	-4.256536	C	0.021365	0.109236	0.053796
H	-0.622796	1.625399	-4.098274	H	0.551597	-0.821480	-0.193130

Table 7.25: Optimized excited triplet LE_BDT state geometry of Zn-BDT.

Atom	x	y	z	Atom	x	y	z
Zn	0.967994	0.189838	-0.123472	H	-5.268250	-0.882654	0.273821
S	2.349289	-1.105676	-1.457571	H	-4.115869	-2.218320	0.169097
S	2.718195	1.247653	1.010254	C	-0.334898	4.291304	0.526040
N	-1.823305	-0.598637	0.403463	H	-1.167153	4.989737	0.696377
C	-3.345453	1.179595	0.338616	H	0.584123	4.889280	0.527811
H	-3.952541	1.753837	1.040858	C	-1.549134	2.407757	1.621519
H	-3.826131	1.264974	-0.637766	H	-2.405678	3.051306	1.857621
C	4.951974	-0.332188	-1.827456	H	-1.500238	1.664090	2.424388
H	4.845007	-0.704433	-2.843564	C	-0.505445	3.610275	-0.821954
C	6.212442	0.075869	-1.375628	H	0.393757	3.025568	-1.042067
H	7.060184	0.075932	-2.052186	H	-0.568567	4.368916	-1.610335
C	-0.748186	-2.527817	1.533902	C	-0.799037	-1.915155	-3.183363
C	-3.548464	-0.501291	2.227950	H	-0.327626	-2.869681	-3.443052
H	-3.438048	-1.550790	2.506418	H	-0.017156	-1.244335	-2.819006
H	-4.585215	-0.213198	2.426753	H	-1.215791	-1.485228	-4.101728
H	-2.907195	0.106778	2.868263	C	-0.581174	-1.818064	2.870497
C	6.403725	0.426555	0.019050	H	-1.000234	-0.815941	2.785823
H	7.409432	0.623323	0.381037	C	-1.894498	1.708114	0.273524
C	-0.870457	-3.969643	-0.861121	C	-1.370010	-2.670363	-0.840911
H	-0.895763	-4.532884	-1.787190	C	-0.295419	3.274380	1.658022
C	-1.908395	-2.104813	-2.147385	H	0.583517	2.639769	1.504542
H	-2.323048	-1.116501	-1.951089	C	-2.040669	2.179770	-2.311901
C	-0.334120	-4.555860	0.270642	H	-2.558442	1.219887	-2.205628
H	0.048630	-5.570535	0.230873	C	-1.073791	0.432395	0.159150

Atom	x	y	z	Atom	x	y	z
C	-0.272557	-3.835870	1.448192	C	0.892988	-1.656077	3.254631
H	0.168042	-4.296083	2.325420	H	1.379050	-2.628827	3.388076
C	-1.315432	-1.960004	0.375976	H	0.969230	-1.114663	4.204880
C	-3.275089	-0.291493	0.741512	H	1.461994	-1.095418	2.508022
C	-1.315184	-2.545070	4.002628	C	-0.148180	3.939518	3.020030
H	-2.361992	-2.750975	3.762067	H	0.763145	4.547384	3.060307
H	-1.289076	-1.939167	4.915586	H	-0.091062	3.195893	3.824037
H	-0.834621	-3.502925	4.230732	H	-1.000921	4.598207	3.230905
C	-3.024834	-2.972819	-2.735210	C	-2.988013	3.106705	-3.072385
H	-3.475914	-2.468208	-3.597350	H	-2.555995	4.110390	-3.175536
H	-3.816527	-3.178883	-2.009084	H	-3.948924	3.209010	-2.554277
H	-2.636065	-3.934946	-3.086515	H	-3.187583	2.726326	-4.081119
C	3.992463	0.237257	0.384113	C	-0.799790	1.907769	-3.159926
C	3.855459	-0.346116	-0.988220	H	-1.093130	1.420486	-4.096645
C	5.352292	0.475877	0.865270	H	-0.083696	1.246439	-2.664719
H	5.494282	0.727938	1.913472	H	-0.274776	2.832513	-3.421062
C	-4.255238	-1.153657	-0.040130	C	-1.763727	2.742204	-0.887646
H	-4.191289	-0.988127	-1.115985	H	-2.593059	3.427195	-0.667869

Table 7.26: Optimized excited triplet LE_CAAC state geometry of Zn-BDT.

Atom	x	y	z	Atom	x	y	z
Zn	0.945098	0.390986	-0.056672	H	-5.258605	-0.846133	0.216155
S	2.331131	-1.121999	-1.064926	H	-4.122898	-2.195376	0.079451
S	2.651594	1.672404	0.791643	C	-0.447760	4.373312	0.499710
N	-1.821789	-0.545267	0.401193	H	-1.278830	5.074061	0.666084
C	-3.400872	1.191387	0.488690	H	0.468497	4.974278	0.461146
H	-3.954931	1.689639	1.286140	C	-1.608316	2.499440	1.674669
H	-3.969040	1.346175	-0.429683	H	-2.473841	3.129920	1.913147
C	5.051519	-1.089929	-1.023096	H	-1.531312	1.772720	2.492379
H	4.944689	-1.987389	-1.624759	C	-0.649696	3.650465	-0.822865
C	6.316492	-0.625950	-0.703762	H	0.240343	3.052011	-1.045499
H	7.193692	-1.160738	-1.055250	H	-0.726448	4.384230	-1.633046
C	-0.599711	-2.461716	1.338079	C	-0.535507	-2.182883	-3.087149
C	-3.487084	-0.647744	2.237390	H	-0.269061	-3.235735	-3.238069
H	-3.343250	-1.715855	2.416405	H	0.310606	-1.686281	-2.606295

Atom	x	y	z	Atom	x	y	z
H	-4.517182	-0.397786	2.510037	H	-0.683708	-1.727060	-4.073642
H	-2.818459	-0.085652	2.894801	C	-0.227572	-1.809816	2.654100
C	6.449990	0.524941	0.066272	H	-0.590127	-0.779432	2.640490
H	7.433157	0.905214	0.326558	C	-1.970243	1.761919	0.352977
C	-1.576930	-4.141408	-0.773498	C	-1.655383	-2.669951	-0.884962
H	-2.098749	-4.755975	-1.499255	C	-0.375817	3.395818	1.665461
C	-1.818288	-2.060920	-2.251700	H	0.514618	2.777191	1.524118
H	-2.021706	-0.992890	-2.127920	C	-2.243473	2.212956	-2.231582
C	-0.827134	-4.702530	0.196651	H	-2.884453	1.334337	-2.097698
H	-0.706269	-5.779736	0.263975	C	-1.104325	0.519355	0.202275
C	-0.203357	-3.863640	1.175160	C	1.288369	-1.763380	2.877177
H	0.488649	-4.296612	1.885888	H	1.709886	-2.769189	2.981954
C	-1.314838	-1.895723	0.329482	H	1.503818	-1.219295	3.803712
C	-3.273010	-0.304531	0.767229	H	1.816993	-1.263126	2.061721
C	-0.884139	-2.527096	3.840563	C	-0.225766	4.109621	3.002313
H	-1.970174	-2.597102	3.737278	H	0.672277	4.738282	3.010083
H	-0.666165	-1.984003	4.767223	H	-0.141669	3.394404	3.829427
H	-0.492354	-3.543865	3.954565	H	-1.090234	4.756063	3.203160
C	-2.985721	-2.670521	-3.039117	C	-3.060406	3.224282	-3.035587
H	-3.159843	-2.087893	-3.950857	H	-2.503788	4.158064	-3.183583
H	-3.916636	-2.687041	-2.464580	H	-4.000144	3.472164	-2.528245
H	-2.763965	-3.697402	-3.349625	H	-3.307990	2.827403	-4.027073
C	4.028505	0.734032	0.188157	C	-1.040182	1.753164	-3.051411
C	3.892835	-0.431680	-0.591938	H	-1.382077	1.289612	-3.983902
C	5.315355	1.188898	0.501309	H	-0.432123	1.009106	-2.528546
H	5.416001	2.088085	1.101456	H	-0.386405	2.589442	-3.321076
C	-4.239588	-1.119426	-0.078371	C	-1.909367	2.783274	-0.827134
H	-4.131488	-0.899989	-1.142247	H	-2.734774	3.463694	-0.579123

7.1.3 Emission Spectra

The emission spectrum of the planar conformer is shown in the figure below. The red spectrum is composed of all modes and significantly broadened. By neglecting two of the 246 modes the spectrum becomes considerably narrower. Thus, the shape of the spectrum agrees much better with the experimental spectrum and calculated spectra of the other conformers. The two modes were selected because of their high displacement values.

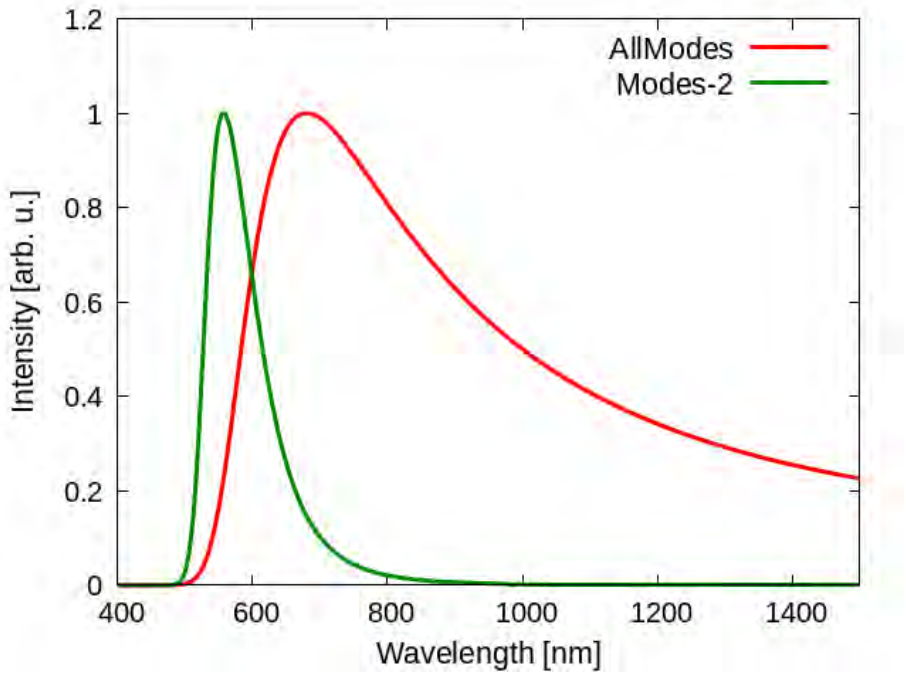

Fig. 7.3: Emission spectra of the planar S-LLCT $\pi\pi^*$ state at 298K for Zn-BDT.

7.2 Zn-BDO

7.2.1 Excitation Energies and Characterisations

Table 7.27: Vertical excitation energies and characterisations of the first ten singlet and triplet excited states of the planar S0 geometry for Zn-BDO.

	ΔE [eV]	Character		From	To
S0	0.00				
S1	2.81	LLCT	$\pi\pi^*$	BDO	CAAC (Carbene)
S2	4.02	LLCT	$\pi\pi^*$	BDO	CAAC (Carbene)
S3	4.19	Ambiguous	π	BDO	Empty
S4	4.37	LLCT	$\pi\pi^*$	BDO	CAAC (Dipp)
S5	4.58	LLCT	$\pi\pi^*$	BDO	CAAC (Dipp)
S6	4.61	LE	$\pi\pi^*$	BDT	BDO
S7	4.72	Mixed	$n\pi^*$	BDO/CAAC	CAAC
S8	4.94	LE	$\pi\pi^*$	CAAC	CAAC
S9	5.00	LE	$\pi\pi^*$	CAAC	CAAC
S10	5.18	LMCT		BDO	Zinc
T1	2.75	LLCT	$\pi\pi^*$	BDO	CAAC (Carbene)
T2	3.87	LE	$\pi\pi^*$	BDO	BDO
T3	3.95	LE	$\pi\pi^*$	BDO	BDO
T4	3.99	LLCT	$\pi\pi^*$	BDO	CAAC
T5	4.13	LE	$\pi\pi^*$	CAAC	CAAC
T6	4.13	Ambiguous	π	BDO	Empty
T7	4.26	Mixed	$n\pi^*$	BDO/CAAC	CAAC
T8	4.35	LLCT	$\pi\pi^*$	BDO	CAAC (Dipp)
T9	4.56	LLCT	$\pi\pi^*$	BDO	CAAC (Dipp)
T10	4.60	Mixed	$n\pi^*$	BDO/CAAC	BDO/CAAC

Table 7.28: Vertical excitation energies and characterisations of the first ten singlet and triplet excited states of the queer S0 geometry for Zn-BDO.

	ΔE [eV]	Character		From	To
S0	0.00				
S1	2.87	LLCT	$\pi\pi^*$	BDO	CAAC (Carbene)
S2	4.08	LLCT	$\pi\pi^*$	BDO	CAAC (Carbene)
S3	4.20	Ambiguous	π	BDO	Empty
S4	4.40	LLCT	$\pi\pi^*$	BDO	CAAC (Dipp)
S5	4.58	LLCT	$\pi\pi^*$	BDO	CAAC (Dipp)
S6	4.59	LE	$\pi\pi^*$	BDO	BDO
S7	4.74	Mixed	$n\pi^*$	BDO/CAAC	CAAC
S8	4.95	LE	$\pi\pi^*$	CAAC	CAAC
S9	5.07	LE	$\pi\pi^*$	CAAC	CAAC
S10	5.21	LMCT		BDO	Zinc
T1	2.82	LLCT	$\pi\pi^*$	BDO	CAAC (Carbene)
T2	3.86	LE	$\pi\pi^*$	BDO	BDO
T3	3.95	LE	$\pi\pi^*$	BDO	BDO
T4	4.06	LLCT	$\pi\pi^*$	BDO	CAAC
T5	4.13	LE	$\pi\pi^*$	CAAC	CAAC
T6	4.15	Ambiguous	π	BDO	Empty
T7	4.27	Mixed	$n\pi^*$	BDO/CAAC	CAAC
T8	4.38	LLCT	$\pi\pi^*$	BDO	CAAC (Dipp)
T9	4.56	LLCT	$\pi\pi^*$	BDO	CAAC (Dipp)
T10	4.58	LE	$\pi\pi^*$	BDO	BDO

Table 7.29: Vertical excitation energies and characterisations of the first ten singlet and triplet excited states of the orthogonal S0 geometry for Zn-BDO.

	ΔE [eV]	Character		From	To
S0	0.00				
S1	2.93	LLCT	$\pi\pi^*$	BDO	CAAC (Carbene)
S2	4.15	LLCT	$\pi\pi^*$	BDO	CAAC (Carbene)
S3	4.21	Ambiguous	π	BDO	Empty
S4	4.36	LLCT	$\pi\pi^*$	BDO	CAAC (Dipp)
S5	4.55	LLCT	$\pi\pi^*$	BDO	CAAC (Dipp)
S6	4.57	LE	$\pi\pi^*$	BDO	BDO
S7	4.79	Mixed	$n\pi^*$	BDO/CAAC	CAAC
S8	4.97	LE	$\pi\pi^*$	CAAC	CAAC
S9	5.12	LE	$\pi\pi^*$	CAAC	CAAC
S10	5.17	LMCT		BDO	Zinc
T1	2.91	LLCT	$\pi\pi^*$	BDO	CAAC (Carbene)
T2	3.85	LE	$\pi\pi^*$	BDO	BDO
T3	3.95	LE	$\pi\pi^*$	BDO	BDO
T4	4.11	LLCT	$\pi\pi^*$	BDO	CAAC
T5	4.13	LE	$\pi\pi^*$	CAAC	CAAC
T6	4.18	LLCT	$\pi\pi^*$	BDO	CAAC
T7	4.33	Mixed	$n\pi^*$	BDO/CAAC	CAAC
T8	4.35	LLCT	$\pi\pi^*$	BDO	CAAC (Dipp)
T9	4.53	LLCT	$\pi\pi^*$	BDO	CAAC (Dipp)
T10	4.54	LE	$\pi\pi^*$	BDO	BDO

Table 7.30: Energy difference to the S0 state of the planar S0 geometry and characterisations of the first ten singlet and triplet excited states of the planar S-LLCT $\pi\pi^*$ geometry for Zn-BDO.

	ΔE [eV]	Character		From	To
S0	0.51				
S1	1.81	LLCT	$\pi\pi^*$	BDO	CAAC (Carbene)
S2	3.54	LLCT	$\pi\pi^*$	BDO	CAAC (Carbene)
S3	4.05	Ambiguous	π	BDO	Empty
S4	4.17	LLCT	$\pi\pi^*$	BDO	CAAC (Dipp)
S5	4.39	LLCT	$\pi\pi^*$	BDO	CAAC (Dipp)
S6	4.52	LLCT	$n\pi^*$	BDO	CAAC (Carbene)
S7	4.64	LE	$\pi\pi^*$	CAAC	CAAC
S8	4.74	LE	$\pi\pi^*$	CAAC	CAAC
S9	4.84	LE	$\pi\pi^*$	BDO	BDO
S10	4.90	LLCT	$n\pi^*$	BDO	CAAC (Carbene)
T1	1.75	LLCT	$\pi\pi^*$	BDO	CAAC (Carbene)
T2	3.51	LLCT	$\pi\pi^*$	BDO	CAAC
T3	3.98	Ambiguous	π	BDO	Empty
T4	4.05	LE	$\pi\pi^*$	BDO	BDO
T5	4.11	LE	$\pi\pi^*$	BDO	BDO
T6	4.15	LLCT	$\pi\pi^*$	BDO	CAAC (Dipp)
T7	4.29	Mixed	$n\pi^*$	BDO/CAAC	CAAC
T8	4.37	LLCT	$\pi\pi^*$	BDO	CAAC (Dipp)
T9	4.47	LLCT	$\pi\pi^*$	BDO	CAAC (Dipp)
T10	4.56	LE	$\pi\pi^*$	CAAC	CAAC

Table 7.31: Energy difference to the S0 state of the queer S0 geometry and characterisations of the first ten singlet and triplet excited states of the queer S-LLCT $\pi\pi^*$ geometry for Zn-BDO.

	ΔE [eV]	Character		From	To
S0	0.56				
S1	1.86	LLCT	$\pi\pi^*$	BDO	CAAC (Carbene)
S2	3.60	LLCT	$\pi\pi^*$	BDO	CAAC (Carbene)
S3	4.11	Ambiguous	π	BDO	Empty
S4	4.21	LLCT	$\pi\pi^*$	BDO	CAAC (Dipp)
S5	4.42	LLCT	$\pi\pi^*$	BDO	CAAC (Dipp)
S6	4.58	LLCT	$n\pi^*$	BDO	CAAC (Carbene)
S7	4.70	LE	$\pi\pi^*$	CAAC	CAAC
S8	4.79	LE	$\pi\pi^*$	CAAC	CAAC
S9	4.83	LE	$\pi\pi^*$	BDO	BDO
S10	4.97	LLCT	$n\pi^*$	BDO	CAAC (Carbene)
T1	1.82	LLCT	$\pi\pi^*$	BDO	CAAC (Carbene)
T2	3.58	LLCT	$\pi\pi^*$	BDO	CAAC
T3	4.02	LE	$\pi\pi^*$	BDO	BDO
T4	4.07	LE	$\pi\pi^*$	BDO	BDO
T5	4.15	LE	$\pi\pi^*$	BDO	BDO
T6	4.18	LLCT	$\pi\pi^*$	BDO	CAAC (Dipp)
T7	4.36	Mixed	$n\pi^*$	BDO/CAAC	CAAC
T8	4.40	LLCT	$\pi\pi^*$	BDO	CAAC (Dipp)
T9	4.50	LE	$\pi\pi^*$	CAAC	CAAC
T10	4.60	LE	$\pi\pi^*$	CAAC	CAAC

Table 7.32: Energy difference to the S0 state of the orthogonal S0 geometry and characterisations of the first ten singlet and triplet excited states of the orthogonal S-LLCT $\pi\pi^*$ geometry for Zn-BDO.

	ΔE [eV]	Character		From	To
S0	0.59				
S1	1.84	LLCT	$\pi\pi^*$	BDO	CAAC (Carbene)
S2	3.63	LLCT	$\pi\pi^*$	BDO	CAAC (Carbene)
S3	4.13	Ambiguous	π	BDO	Empty
S4	4.19	LLCT	$\pi\pi^*$	BDO	CAAC (Dipp)
S5	4.41	LLCT	$\pi\pi^*$	BDO	CAAC (Dipp)
S6	4.61	LLCT	$n\pi^*$	BDO	CAAC (Carbene)
S7	4.69	LE	$\pi\pi^*$	CAAC	CAAC
S8	4.77	LE	$\pi\pi^*$	BDO	BDO
S9	4.78	LE	$\pi\pi^*$	CAAC	CAAC
S10	4.97	LLCT	$n\pi^*$	BDO	CAAC (Carbene)
T1	1.81	LLCT	$\pi\pi^*$	BDO	CAAC (Carbene)
T2	3.61	LLCT	$\pi\pi^*$	BDO	CAAC
T3	4.05	LE	$\pi\pi^*$	BDO	BDO
T4	4.07	Ambiguous	π	BDO	Empty
T5	4.16	LE	$\pi\pi^*$	BDO	BDO
T6	4.17	LLCT	$\pi\pi^*$	BDO	CAAC (Dipp)
T7	4.37	Mixed	$n\pi^*$	BDO/CAAC	CAAC
T8	4.39	LLCT	$\pi\pi^*$	BDO	CAAC (Dipp)
T9	4.50	LE	$\pi\pi^*$	CAAC	CAAC
T10	4.60	LE	$\pi\pi^*$	CAAC	CAAC

Table 7.33: Energy difference to the S0 state of the planar S0 geometry and characterisations of the first ten singlet and triplet excited states of the planar T-LLCT $\pi\pi^*$ geometry for Zn-BDO.

	ΔE [eV]	Character		From	To
S0	0.70				
S1	1.86	LLCT	$\pi\pi^*$	BDO	CAAC (Carbene)
S2	3.63	LLCT	$\pi\pi^*$	BDO	CAAC (Carbene)
S3	4.20	Ambiguous	π	BDO	Empty
S4	4.29	LLCT	$\pi\pi^*$	BDO	CAAC (Dipp)
S5	4.51	LLCT	$\pi\pi^*$	BDO	CAAC (Dipp)
S6	4.61	LLCT	$n\pi^*$	BDO	CAAC (Carbene)
S7	4.73	LE	$\pi\pi^*$	CAAC	CAAC
S8	4.83	LE	$\pi\pi^*$	CAAC	CAAC
S9	4.99	LLCT	$n\pi^*$	BDO	CAAC (Carbene)
S10	5.00	LE	$\pi\pi^*$	BDO	BDO
T1	1.79	LLCT	$\pi\pi^*$	BDO	CAAC (Carbene)
T2	3.62	LLCT	$\pi\pi^*$	BDO	CAAC
T3	4.13	LMCT		BDO	Zinc
T4	4.22	LE	$\pi\pi^*$	BDO	BDO
T5	4.27	LLCT	$\pi\pi^*$	BDO	CAAC (Dipp)
T6	4.29	LE	$\pi\pi^*$	BDO	BDO
T7	4.44	Mixed	$n\pi^*$	BDO/CAAC	CAAC
T8	4.49	LLCT	$\pi\pi^*$	BDO	CAAC (Dipp)
T9	4.59	LLCT	$\pi\pi^*$	BDO	CAAC (Dipp)
T10	4.69	LE	$\pi\pi^*$	CAAC	CAAC

Table 7.34: Energy difference to the S0 state of the queer S0 geometry and characterisations of the first ten singlet and triplet excited states of the queer T-LLCT $\pi\pi^*$ geometry for Zn-BDO.

	ΔE [eV]	Character		From	To
S0	0.72				
S1	1.86	LLCT	$\pi\pi^*$	BDO	CAAC (Carbene)
S2	3.64	LLCT	$\pi\pi^*$	BDO	CAAC (Carbene)
S3	4.16	LMCT		BDO	Zinc
S4	4.31	LLCT	$\pi\pi^*$	BDO	CAAC (Dipp)
S5	4.52	LLCT	$\pi\pi^*$	BDO	CAAC (Dipp)
S6	4.60	LLCT	$n\pi^*$	BDO	CAAC (Carbene)
S7	4.76	LE	$\pi\pi^*$	CAAC	CAAC
S8	4.85	LE	$\pi\pi^*$	CAAC	CAAC
S9	4.94	Mixed	$n\pi^*$	BDO	BDO/Zinc
S10	4.99	LLCT	$n\pi^*$	BDO	CAAC (Carbene)
T1	1.81	LLCT	$\pi\pi^*$	BDO	CAAC (Carbene)
T2	3.63	LLCT	$\pi\pi^*$	BDO	CAAC
T3	4.07	LMCT		BDO	Zinc
T4	4.24	LE	$\pi\pi^*$	BDO	BDO
T5	4.30	LLCT	$\pi\pi^*$	BDO	CAAC (Dipp)
T6	4.30	LE	$\pi\pi^*$	BDO	BDO
T7	4.41	Mixed	$n\pi^*$	BDO/CAAC	CAAC
T8	4.51	LLCT	$\pi\pi^*$	BDO	CAAC (Dipp)
T9	4.59	LE	$\pi\pi^*$	CAAC	CAAC
T10	4.70	LE	$\pi\pi^*$	CAAC	CAAC

Table 7.35: Energy difference to the S0 state of the orthogonal S0 geometry and characterisations of the first ten singlet and triplet excited states of the orthogonal T-LLCT $\pi\pi^*$ geometry for Zn-BDO.

	ΔE [eV]	Character		From	To
S0	0.63				
S1	1.85	LLCT	$\pi\pi^*$	BDO	CAAC (Carbene)
S2	3.64	LLCT	$\pi\pi^*$	BDO	CAAC (Carbene)
S3	4.12	LMCT		BDO	Zinc
S4	4.23	LLCT	$\pi\pi^*$	BDO	CAAC (Dipp)
S5	4.44	LLCT	$\pi\pi^*$	BDO	CAAC (Dipp)
S6	4.61	LLCT	$n\pi^*$	BDO	CAAC (Carbene)
S7	4.72	LE	$\pi\pi^*$	CAAC	CAAC
S8	4.80	Mixed	$n\pi^*$	BDO	BDO/Zinc
S9	4.81	LE	$\pi\pi^*$	CAAC	CAAC
S10	4.98	LLCT	$n\pi^*$	BDO	CAAC (Carbene)
T1	1.82	LLCT	$\pi\pi^*$	BDO	CAAC (Carbene)
T2	3.62	LLCT	$\pi\pi^*$	BDO	CAAC
T3	4.03	Mixed	$n\pi^*$	BDO	BDO/Zinc
T4	4.11	LE	$\pi\pi^*$	BDO	BDO
T5	4.20	LE	$\pi\pi^*$	BDO	BDO
T6	4.21	LLCT	$\pi\pi^*$	BDO	CAAC (Dipp)
T7	4.36	Mixed	$n\pi^*$	BDO/CAAC	CAAC
T8	4.42	LLCT	$\pi\pi^*$	BDO	CAAC (Dipp)
T9	4.52	LE	$\pi\pi^*$	CAAC	CAAC
T10	4.62	LE	$\pi\pi^*$	CAAC	CAAC

Table 7.36: Energy difference to the S0 state of the planar, queer and orthogonal S0 geometry and characterisations of the first ten singlet and triplet excited states of the S-LLCT (Dipp) geometry for Zn-BDO.

	ΔE [eV]			Character		From	To
	planar	queer	ortho				
S0	1.41	1.41	1.39				
S1	3.02	3.02	3.00	LLCT	$\pi\pi^*$	BDO	CAAC (Dipp)
S2	3.59	3.59	3.58	LLCT	$\pi\pi^*$	BDO	CAAC (Carbene)
S3	4.81	4.80	4.79	LMCT		BDO	Zinc
S4	4.82	4.82	4.81	LLCT	$\pi\pi^*$	BDO	CAAC (Dipp)
S5	4.88	4.88	4.87	LLCT	$\pi\pi^*$	BDO	CAAC (Dipp)
S6	5.45	5.44	5.43	LLCT	$\pi\pi^*$	BDO	CAAC (Carbene)
S7	5.53	5.53	5.52	LMCT		BDO	Zinc
S8	5.60	5.60	5.58	LE	$\pi\pi^*$	CAAC	CAAC
S9	5.74	5.74	5.72	LLCT	$n\pi^*$	BDO	CAAC (Dipp)
S10	5.84	5.83	5.82	LE	$\pi\pi^*$	BDO	BDO
T1	2.96	2.96	2.94	LLCT	$\pi\pi^*$	BDO	CAAC (Dipp)
T2	3.56	3.55	3.54	LLCT	$\pi\pi^*$	BDO	CAAC (Carbene)
T3	4.70	4.70	4.69	Mixed	$\pi\pi^*$	BDO/CAAC	BDO/Zinc
T4	4.78	4.77	4.76	Mixed	$\pi\pi^*$	BDO/CAAC	BDO/Zinc
T5	4.80	4.80	4.78	LLCT	$\pi\pi^*$	BDO	CAAC (Dipp)
T6	4.85	4.84	4.83	LLCT	$\pi\pi^*$	BDO	CAAC (Dipp)
T7	4.92	4.92	4.91	LE	$\pi\pi^*$	BDO	BDO
T8	4.95	4.94	4.93	LE	$\pi\pi^*$	BDO	BDO
T9	5.05	5.05	5.03	LE	$\pi\pi^*$	CAAC	CAAC
T10	5.33	5.32	5.31	LLCT	$n\pi^*$	BDO	CAAC (Dipp)

Table 7.37: Energy difference to the S0 state of the planar, queer and orthogonal S0 geometry and characterisations of the first ten singlet and triplet excited states of the T-LE-BDO geometry for Zn-BDO.

	ΔE [eV]			Character		From	To
	planar	queer	ortho				
S0	0.78	0.77	0.76				
S1	3.36	3.36	3.34	LLCT	$\pi\pi^*$	BDO	CAAC (Carbene)
S2	4.48	4.48	4.46	LE	$\pi\pi^*$	BDO	BDO
S3	4.79	4.78	4.77	LLCT	$\pi\pi^*$	BDO	CAAC (Dipp)
S4	4.95	4.94	4.93	Mixed	$\pi\pi^*$	BDO	BDO/CAAC
S5	4.97	4.97	4.95	Mixed	$\pi\pi^*$	BDO	BDO/CAAC
S6	4.98	4.97	4.96	LLCT	$\pi\pi^*$	BDO	CAAC
S7	5.45	5.45	5.43	LE	$\pi\pi^*$	BDO	BDO
S8	5.57	5.56	5.55	Mixed	$n\pi^*$	BDO/CAAC	CAAC
S9	5.61	5.60	5.59	LMCT		BDO	Zinc
S10	5.74	5.73	5.72	LE	$\pi\pi^*$	CAAC	CAAC
T1	3.33	3.33	3.32	LLCT	$\pi\pi^*$	BDO	CAAC (Carbene)
T2	3.42	3.42	3.40	LE	$\pi\pi^*$	BDO	BDO
T3	4.61	4.60	4.59	LE	$\pi\pi^*$	BDO	BDO
T4	4.67	4.66	4.65	LE	$\pi\pi^*$	BDO	BDO
T5	4.77	4.76	4.75	LLCT	$\pi\pi^*$	BDO	CAAC (Dipp)
T6	4.92	4.92	4.91	LE	$\pi\pi^*$	CAAC	CAAC
T7	4.94	4.93	4.92	LLCT	$\pi\pi^*$	BDO	CAAC (Carbene)
T8	4.96	4.96	4.94	LLCT	$\pi\pi^*$	BDO	CAAC (Dipp)
T9	5.12	5.11	5.10	Mixed	$n\pi^*$	BDO/CAAC	CAAC
T10	5.17	5.17	5.16	LE	$\pi\pi^*$	BDO	BDO

Table 7.38: Energy difference to the S0 state of the planar, queer and orthogonal S0 geometry and characterisations of the first ten singlet and triplet excited states of the T-LE-CAAC geometry for Zn-BDO.

	ΔE [eV]			Character		From	To
	planar	queer	ortho				
S0	1.08	1.08	1.07				
S1	3.86	3.86	3.85	LLCT	$\pi\pi^*$	BDO	CAAC (Carbene)
S2	4.75	4.75	4.73	LE	$\pi\pi^*$	CAAC	CAAC
S3	5.10	5.10	5.09	LLCT	$\pi\pi^*$	BDO	CAAC (Carbene)
S4	5.22	5.22	5.21	LLCT	$\pi\pi^*$	BDO	CAAC (Dipp)
S5	5.34	5.34	5.32	Ambiguous	π	BDO	Empty
S6	5.39	5.39	5.38	LLCT	$\pi\pi^*$	BDO	CAAC
S7	5.70	5.70	5.68	LE	$\pi\pi^*$	BDO	BDO
S8	5.79	5.79	5.78	LLCT	$\pi\pi^*$	BDO	CAAC (Dipp)
S9	5.86	5.85	5.84	Mixed	$n\pi^*$	BDO/CAAC	CAAC
S10	5.91	5.91	5.89	LLCT	$\pi\pi^*$	BDO	CAAC
T1	3.57	3.56	3.55	LE	$\pi\pi^*$	CAAC	CAAC
T2	3.84	3.84	3.83	LLCT	$\pi\pi^*$	BDO	CAAC (Carbene)
T3	4.74	4.73	4.72	LLCT	$\pi\pi^*$	BDO	CAAC (Dipp)
T4	4.99	4.98	4.97	LE	$\pi\pi^*$	BDO	BDO
T5	5.07	5.07	5.06	LE	$\pi\pi^*$	BDO	BDO
T6	5.10	5.09	5.08	LLCT	$\pi\pi^*$	BDO	CAAC (Carbene)
T7	5.18	5.17	5.16	LE	$\pi\pi^*$	CAAC	CAAC
T8	5.30	5.30	5.28	Ambiguous	π	BDO	Empty
T9	5.35	5.34	5.33	Mixed	$n\pi^*$	BDO/CAAC	CAAC
T10	5.54	5.54	5.53	LLCT	$\pi\pi^*$	BDO	CAAC (Dipp)

Excitation Energy Diagrams

In the following two diagrams excitation energies for all optimized state geometries of Zn-BDT are shown. For the S0, S- and T-LLCT ($\pi\pi^*$) geometries the results of the planar conformer are presented in figure 7.4 and the orthogonal conformer in figure 7.5.

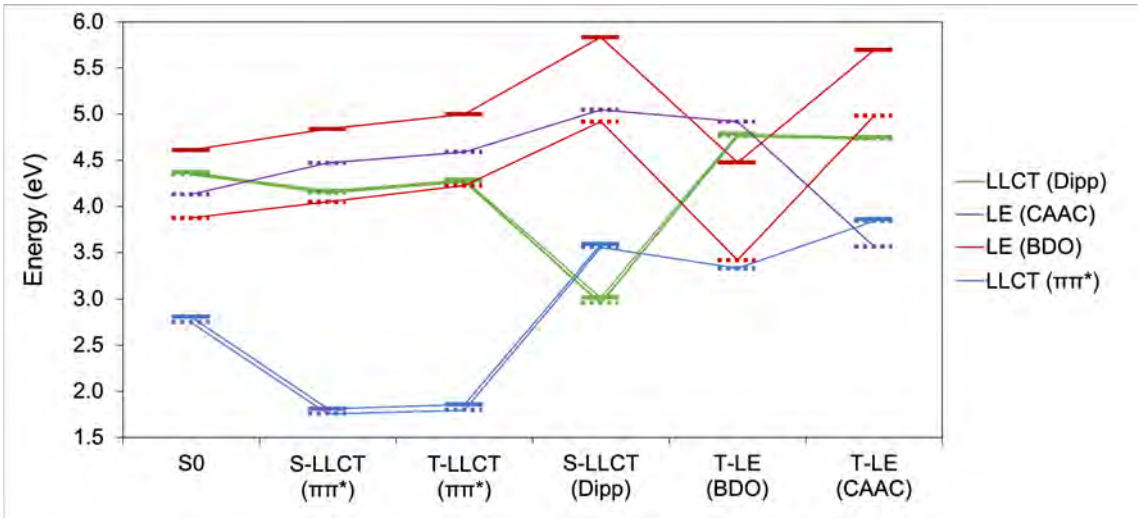

Fig. 7.4: Excitation energy diagram of the planar conformer for Zn-BDO. Singlet states are represented by solid lines, triplet states by dashed lines.

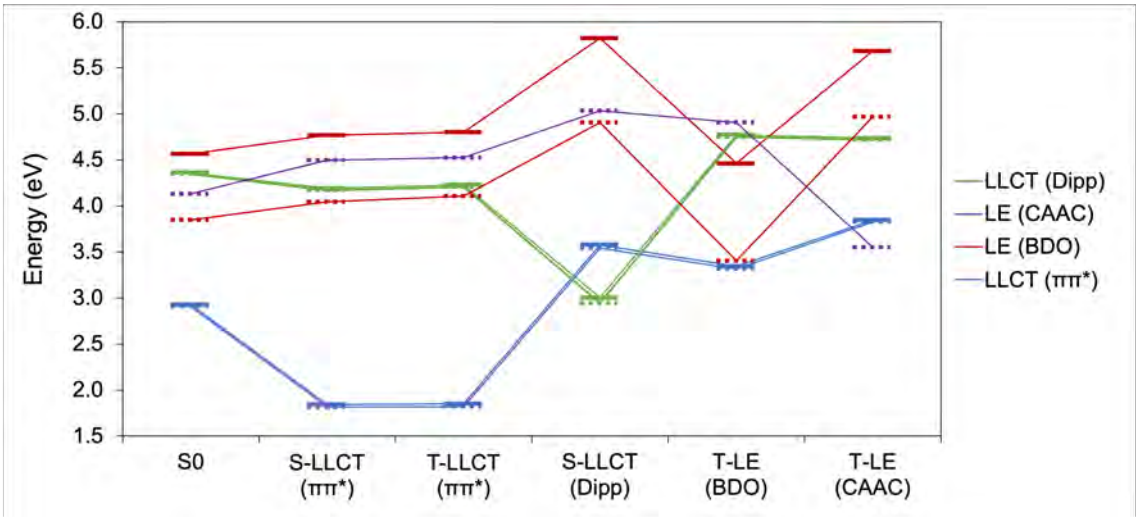

Fig. 7.5: Excitation energy diagram of the orthogonal conformer for Zn-BDO. Singlet states are represented by solid lines, triplet states by dashed lines.

7.2.2 Geometries

Table 7.39: Optimized planar ground state geometry (S0-planar) of Zn-BDO.

Atom	x	y	z	Atom	x	y	z
Zn	1.133163	0.045973	-0.168525	H	-5.073930	0.562879	-0.350783
O	2.087238	-1.541211	-0.629710	H	-4.295012	-0.961927	-0.791970
O	2.822859	0.914998	0.053887	C	0.995538	3.844742	1.457654
N	-1.750159	-0.207611	0.139023	H	0.419200	4.700797	1.838124
C	-2.791434	1.850693	0.628248	H	2.055286	4.105787	1.560029
H	-3.229141	2.250136	1.544972	C	-0.778392	2.220709	2.103059
H	-3.230817	2.412443	-0.197025	H	-1.403940	3.028804	2.502731
C	4.366103	-2.225279	-0.868765	H	-1.012132	1.333317	2.704047
H	4.050906	-3.227513	-1.147049	C	0.664184	3.608063	-0.007508
C	5.724178	-1.897512	-0.800003	H	1.345748	2.846101	-0.396620
H	6.472305	-2.652529	-1.026855	H	0.867545	4.519634	-0.580953
C	-1.320908	-2.528349	0.878899	C	-0.508585	-1.179559	-3.519184
C	-3.657590	-0.245759	1.764870	H	-0.387584	-2.164469	-3.984511
H	-3.814525	-1.322242	1.662807	H	0.377163	-0.997317	-2.903095
H	-4.627168	0.213895	1.980231	H	-0.534087	-0.430995	-4.319310
H	-3.003819	-0.058271	2.619510	C	-0.974576	-2.130059	2.306628
C	6.108699	-0.615500	-0.442887	H	-1.080104	-1.048765	2.400345
H	7.161813	-0.352816	-0.387022	C	-1.252345	1.995470	0.637677
C	-1.654221	-3.420362	-1.750132	C	-1.711011	-2.051399	-1.499518
H	-1.745968	-3.777029	-2.769913	C	0.681198	2.616251	2.301949
C	-1.800662	-1.116901	-2.696535	H	1.331366	1.805582	1.953821
H	-1.898072	-0.093494	-2.331655	C	-1.187310	3.156109	-1.727624
C	-1.462888	-4.334061	-0.730230	H	-2.083214	2.532331	-1.823234
H	-1.427426	-5.396470	-0.948931	C	-0.766377	0.631992	0.196061
C	-1.278308	-3.884770	0.564019	C	0.488629	-2.470054	2.618019
H	-1.077159	-4.604110	1.350005	H	0.634900	-3.555027	2.670285
C	-1.592195	-1.620779	-0.164301	H	0.773413	-2.049310	3.589545
C	-3.117634	0.361472	0.476255	H	1.172571	-2.086321	1.855454
C	-1.881177	-2.780801	3.354248	C	0.976098	2.845144	3.778396
H	-2.940946	-2.582500	3.173456	H	2.026772	3.119430	3.928269
H	-1.631033	-2.398922	4.350780	H	0.776700	1.944048	4.370994
H	-1.743994	-3.867477	3.377183	H	0.356683	3.656541	4.182512
C	-3.002958	-1.407303	-3.597464	C	-1.574924	4.545806	-2.232486
H	-3.065282	-0.653523	-4.390722	H	-0.740202	5.251216	-2.137580
H	-3.947051	-1.396902	-3.045414	H	-2.423056	4.952651	-1.669501

Atom	x	y	z	Atom	x	y	z
H	-2.910497	-2.384991	-4.082991	H	-1.859069	4.511717	-3.290774
C	3.782724	0.040814	-0.213393	C	-0.131958	2.549095	-2.648665
C	3.386330	-1.281057	-0.582635	H	-0.528137	2.470407	-3.667528
C	5.137483	0.348045	-0.152001	H	0.163919	1.541031	-2.343754
H	5.423819	1.357963	0.129853	H	0.773735	3.162772	-2.693368
C	-4.121280	0.106869	-0.638918	C	-0.799165	3.213743	-0.226254
H	-3.810772	0.558056	-1.583665	H	-1.395565	4.029566	0.203276

Table 7.40: Optimized queer ground state geometry (S0-queer) of Zn-BDO.

Atom	x	y	z	Atom	x	y	z
Zn	-1.119339	-0.172748	0.064285	H	4.973916	1.133306	0.553748
O	-1.979503	-1.611056	0.977553	H	4.420629	-0.542868	0.654204
O	-2.836652	0.309845	-0.639905	C	-1.511331	3.736585	-1.008002
N	1.792319	0.022818	-0.181616	H	-1.091983	4.735240	-1.199086
C	2.524753	2.261891	-0.189236	H	-2.595022	3.814190	-1.153471
H	2.939719	2.924349	-0.951328	C	0.565858	2.573197	-1.739827
H	2.832587	2.662782	0.776933	H	1.062220	3.528869	-1.950997
C	-4.187498	-2.502920	1.191215	H	0.987448	1.851714	-2.448991
H	-3.822363	-3.282749	1.854545	C	-1.212631	3.320310	0.423746
C	-5.542830	-2.429277	0.853098	H	-1.745567	2.386087	0.628461
H	-6.239333	-3.158897	1.257677	H	-1.627606	4.061189	1.114977
C	1.694382	-2.151689	-1.360027	C	0.700355	-1.767651	3.192893
C	3.693127	0.597517	-1.716535	H	0.711877	-2.826885	3.476049
H	4.002305	-0.443929	-1.832453	H	-0.200085	-1.595174	2.595521
H	4.588997	1.220909	-1.796223	H	0.629047	-1.177707	4.114240
H	3.027925	0.866460	-2.539432	C	1.350026	-1.535267	-2.708422
C	-5.989753	-1.428628	0.005717	H	1.328026	-0.451277	-2.598636
H	-7.041123	-1.363909	-0.261976	C	0.985961	2.186189	-0.289277
C	2.117004	-3.476740	1.066361	C	2.004709	-2.088564	1.077009
H	2.248351	-4.004638	2.004240	C	-0.925812	2.745373	-2.005024
C	1.976188	-1.394414	2.429692	H	-1.437999	1.790006	-1.852302
H	1.945670	-0.317461	2.263553	C	0.606954	2.993697	2.202726
C	2.041346	-4.199012	-0.110090	H	1.653568	2.683731	2.289142
H	2.133349	-5.280235	-0.093618	C	0.695885	0.709893	-0.111253
C	1.814178	-3.539054	-1.303289	C	-0.045139	-1.968698	-3.171760

Atom	x	y	z	Atom	x	y	z
H	1.713005	-4.116512	-2.215351	H	-0.081011	-3.047129	-3.362199
C	1.836802	-1.430518	-0.157192	H	-0.306056	-1.456065	-4.104766
C	3.064714	0.837387	-0.348684	H	-0.818918	-1.739358	-2.433682
C	2.371718	-1.876013	-3.796880	C	-1.165122	3.173718	-3.446862
H	3.393618	-1.617653	-3.506563	H	-2.236972	3.287447	-3.646716
H	2.132591	-1.330004	-4.716597	H	-0.769302	2.435029	-4.154505
H	2.353601	-2.944749	-4.037102	H	-0.680083	4.135569	-3.659362
C	3.206410	-1.698183	3.287463	C	0.505333	4.331621	2.936617
H	3.175354	-1.101680	4.206572	H	-0.517415	4.726392	2.923961
H	4.142210	-1.471509	2.768421	H	1.161771	5.084779	2.485215
H	3.235448	-2.752397	3.584169	H	0.798917	4.217784	3.986584
C	-3.734142	-0.550680	-0.182919	C	-0.225873	1.938647	2.926073
C	-3.273887	-1.582935	0.689810	H	0.091775	1.866207	3.972677
C	-5.084790	-0.494540	-0.509055	H	-0.109452	0.940283	2.493250
H	-5.421386	0.296415	-1.174224	H	-1.293160	2.184837	2.923543
C	4.096380	0.499676	0.717872	C	0.287663	3.173400	0.697076
H	3.728202	0.700720	1.725633	H	0.740285	4.134979	0.419656

Table 7.41: Optimized orthogonal ground state geometry (S0-ortho) of Zn-BDO.

Atom	x	y	z	Atom	x	y	z
Zn	1.128445	-0.008277	-0.154947	H	-5.068456	0.566423	-0.346944
O	2.298788	-0.259549	-1.645607	H	-4.301392	-0.982976	-0.717307
O	2.622655	-0.348497	0.990760	C	1.037615	3.847339	1.343007
N	-1.755026	-0.213630	0.186966	H	0.474970	4.718813	1.707481
C	-2.774863	1.874048	0.585341	H	2.100745	4.100724	1.430495
H	-3.204571	2.317474	1.485493	C	-0.752162	2.264446	2.040790
H	-3.211009	2.404660	-0.261992	H	-1.365669	3.092022	2.418548
C	4.589468	-0.839167	-2.008478	H	-0.994069	1.397985	2.668000
H	4.441045	-0.801624	-3.084526	C	0.688211	3.589340	-0.114643
C	5.841585	-1.154493	-1.470518	H	1.364350	2.827493	-0.515433
H	6.675740	-1.364151	-2.134876	H	0.886452	4.492224	-0.703069
C	-1.327776	-2.505734	1.011282	C	-0.518383	-1.287040	-3.457816
C	-3.675418	-0.159032	1.808146	H	-0.380395	-2.289652	-3.879546
H	-3.835223	-1.238541	1.757396	H	0.374589	-1.040794	-2.874546
H	-4.646429	0.313176	1.986174	H	-0.584565	-0.581527	-4.294359

Atom	x	y	z	Atom	x	y	z
H	-3.035169	0.068957	2.662831	C	-1.066265	-2.061433	2.444179
C	6.011441	-1.198134	-0.096569	H	-1.226264	-0.985616	2.507420
H	6.980647	-1.442413	0.330160	C	-1.234188	2.003169	0.583763
C	-1.584156	-3.483711	-1.597347	C	-1.682742	-2.109572	-1.390045
H	-1.653474	-3.873173	-2.606818	C	0.713079	2.646844	2.223780
C	-1.798699	-1.218996	-2.617948	H	1.349686	1.809192	1.913372
H	-1.908409	-0.185323	-2.287743	C	-1.165729	3.078825	-1.816756
C	-1.380560	-4.360556	-0.547896	H	-2.052376	2.438760	-1.888106
H	-1.309451	-5.427316	-0.734382	C	-0.764808	0.620228	0.186123
C	-1.236947	-3.868872	0.736299	C	0.389172	-2.318570	2.850779
H	-1.036284	-4.559622	1.547521	H	0.623056	-3.389191	2.820795
C	-1.593350	-1.635942	-0.066206	H	0.549276	-1.974386	3.879678
C	-3.117415	0.382892	0.498078	H	1.103656	-1.794859	2.208308
C	-2.003978	-2.734602	3.450476	C	1.014448	2.920819	3.691555
H	-3.058280	-2.620508	3.183212	H	2.069053	3.185891	3.829712
H	-1.857583	-2.297649	4.444864	H	0.805708	2.041590	4.312651
H	-1.795038	-3.807041	3.531561	H	0.406509	3.752932	4.069975
C	-3.010804	-1.562686	-3.487220	C	-1.576108	4.445834	-2.363191
H	-3.101382	-0.837122	-4.303728	H	-0.752359	5.166759	-2.289764
H	-3.946035	-1.552839	-2.920180	H	-2.430515	4.856358	-1.812349
H	-2.906092	-2.554172	-3.941488	H	-1.859203	4.375462	-3.419951
C	3.678115	-0.612570	0.232672	C	-0.103724	2.458053	-2.721690
C	3.503758	-0.566438	-1.184137	H	-0.512584	2.318551	-3.729040
C	4.930094	-0.927982	0.748696	H	0.239795	1.479199	-2.374641
H	5.048764	-0.959345	1.828652	H	0.777600	3.102024	-2.813023
C	-4.118647	0.089983	-0.610154	C	-0.775589	3.189562	-0.318363
H	-3.799817	0.496557	-1.572021	H	-1.366574	4.022565	0.084521

Table 7.42: Optimized planar excited singlet LLCT ($\pi\pi^*$) state geometry (S-LLCT $\pi\pi^*$ planar) of Zn-BDO.

Atom	x	y	z	Atom	x	y	z
Zn	0.888430	0.261405	0.002941	H	-5.232317	-0.887984	0.092252
O	2.327055	-1.046666	-0.437308	H	-4.099201	-2.246247	0.042131
O	2.448618	1.540578	-0.025523	C	-0.238090	4.211158	0.739521

Atom	x	y	z	Atom	x	y	z
N	-1.816350	-0.669488	0.433355	H	-1.033289	4.952493	0.907969
C	-3.299590	1.134209	0.332348	H	0.714249	4.754060	0.791794
H	-3.945123	1.689632	1.017998	C	-1.602625	2.370200	1.708298
H	-3.741046	1.232572	-0.661281	H	-2.431996	3.068176	1.896071
C	4.625520	-1.172373	-1.010779	H	-1.649070	1.613239	2.498532
H	4.565524	-2.243238	-1.167864	C	-0.403030	3.585150	-0.636736
C	5.794329	-0.481691	-1.189580	H	0.470139	2.957622	-0.840333
H	6.691979	-1.008344	-1.494938	H	-0.393589	4.373299	-1.399537
C	-0.795740	-2.613343	1.560111	C	-0.413090	-1.898651	-3.053529
C	-3.625842	-0.582983	2.170246	H	0.008194	-2.871108	-3.335748
H	-3.556657	-1.642360	2.429853	H	0.370395	-1.328901	-2.544963
H	-4.664623	-0.270894	2.325222	H	-0.676963	-1.366587	-3.975445
H	-2.999147	-0.014004	2.860354	C	-0.631887	-1.888588	2.887229
C	5.856592	0.924286	-0.983302	H	-1.018487	-0.877520	2.762796
H	6.800676	1.436191	-1.135197	C	-1.854592	1.684559	0.334760
C	-0.828438	-4.021318	-0.848831	C	-1.273286	-2.700464	-0.834909
H	-0.814178	-4.569001	-1.785479	C	-0.303517	3.156852	1.836594
C	-1.648001	-2.064339	-2.163542	H	0.538782	2.468836	1.687841
H	-2.027986	-1.063805	-1.958930	C	-1.932716	2.295649	-2.231601
C	-0.393551	-4.647305	0.305602	H	-2.559613	1.399225	-2.192759
H	-0.057487	-5.679406	0.275932	C	-1.015599	0.426447	0.171789
C	-0.364679	-3.938176	1.492349	C	0.845508	-1.765426	3.277294
H	0.012784	-4.421147	2.387795	H	1.286001	-2.747435	3.486214
C	-1.303443	-2.001241	0.392084	H	0.947143	-1.156899	4.184085
C	-3.239486	-0.353850	0.706979	H	1.443633	-1.298915	2.488742
C	-1.392693	-2.562168	4.032809	C	-0.160387	3.765912	3.224926
H	-2.450437	-2.710998	3.799456	H	0.781256	4.320961	3.318196
H	-1.330043	-1.949319	4.940131	H	-0.173026	2.992926	4.003305
H	-0.964257	-3.542834	4.270279	H	-0.981474	4.464107	3.434977
C	-2.729950	-2.844755	-2.913653	C	-2.712599	3.347340	-3.020216
H	-3.041726	-2.292916	-3.808697	H	-2.165442	4.298100	-3.064452
H	-3.616453	-3.013863	-2.294914	H	-3.688645	3.547173	-2.561780
H	-2.363285	-3.823162	-3.245087	H	-2.887389	3.019651	-4.052533
C	3.516346	0.964873	-0.393665	C	-0.675329	1.898265	-3.002449
C	3.451318	-0.485239	-0.614479	H	-0.953079	1.480057	-3.977845
C	4.749905	1.633133	-0.599448	H	-0.104369	1.133000	-2.468020
H	4.785171	2.704697	-0.439649	H	-0.017983	2.754967	-3.188907
C	-4.202386	-1.172938	-0.149970	C	-1.695454	2.774311	-0.773363
H	-4.050366	-0.993104	-1.216026	H	-2.509301	3.480363	-0.553774

Table 7.43: Optimized queer excited singlet LLCT ($\pi\pi^*$) state geometry (S-LLCT $\pi\pi^*$ queer) of Zn-BDO.

Atom	x	y	z	Atom	x	y	z
Zn	-1.051017	-0.189690	-0.008539	H	5.010656	1.131283	0.398122
O	-2.014758	-1.685536	0.898744	H	4.487221	-0.558095	0.448956
O	-2.906258	0.172107	-0.720591	C	-1.529256	3.767932	-0.965152
N	1.827726	-0.009096	-0.236512	H	-1.123125	4.780735	-1.104689
C	2.482395	2.233924	-0.135742	H	-2.612873	3.839311	-1.123466
H	2.925048	2.972751	-0.809367	C	0.580318	2.675165	-1.710789
H	2.757130	2.531707	0.877880	H	1.060147	3.654038	-1.860016
C	-4.171532	-2.635295	1.170288	H	1.021184	1.998147	-2.450203
H	-3.787192	-3.416490	1.815897	C	-1.241167	3.299227	0.453397
C	-5.502529	-2.540522	0.866162	H	-1.764323	2.350844	0.625993
H	-6.202705	-3.261422	1.273916	H	-1.669414	4.012858	1.167264
C	1.698336	-2.208171	-1.345898	C	0.703431	-1.611922	3.195273
C	3.631474	0.721216	-1.819204	H	0.655395	-2.664578	3.500493
H	3.989181	-0.293210	-2.015373	H	-0.193503	-1.392332	2.608896
H	4.488966	1.397800	-1.905498	H	0.677632	-0.999166	4.104743
H	2.912683	0.992355	-2.595463	C	1.406607	-1.611067	-2.713391
C	-5.993398	-1.505405	0.021335	H	1.400636	-0.527292	-2.606878
H	-7.055219	-1.464485	-0.195743	C	0.944493	2.175096	-0.283937
C	2.045962	-3.466413	1.121439	C	1.978175	-2.074767	1.078884
H	2.155451	-3.965754	2.078643	C	-0.907258	2.837182	-1.998606
C	1.979247	-1.321535	2.399505	H	-1.388432	1.856803	-1.897885
H	1.973502	-0.255574	2.173813	C	0.552955	2.877003	2.237339
C	1.960258	-4.227090	-0.031009	H	1.474619	2.290370	2.301570
H	2.019574	-5.310054	0.021877	C	0.642217	0.696483	-0.110014
C	1.771281	-3.597790	-1.248201	C	0.020707	-2.022817	-3.219931
H	1.669015	-4.200485	-2.144839	H	-0.040409	-3.104683	-3.386980
C	1.853159	-1.433854	-0.174020	H	-0.196413	-1.526286	-4.173401
C	3.038074	0.827496	-0.411760	H	-0.770046	-1.749930	-2.514240
C	2.457493	-1.988723	-3.760985	C	-1.146451	3.324808	-3.421350
H	3.473078	-1.748233	-3.434024	H	-2.218685	3.426239	-3.630161
H	2.268133	-1.451118	-4.697916	H	-0.725981	2.628404	-4.157442
H	2.426569	-3.061017	-3.986775	H	-0.680152	4.305371	-3.585880
C	3.209772	-1.626392	3.256660	C	0.814618	4.198982	2.959130

Atom	x	y	z	Atom	x	y	z
H	3.218271	-0.985703	4.146814	H	-0.057710	4.863034	2.896591
H	4.142692	-1.458004	2.710182	H	1.667875	4.730924	2.521307
H	3.209520	-2.666318	3.603603	H	1.029806	4.036095	4.022481
C	-3.759988	-0.631370	-0.241563	C	-0.504435	2.079909	2.999616
C	-3.257572	-1.687853	0.645237	H	-0.161528	1.899634	4.026023
C	-5.150400	-0.572264	-0.517335	H	-0.686374	1.103250	2.543020
H	-5.511619	0.218657	-1.164437	H	-1.458566	2.614906	3.064710
C	4.150141	0.476364	0.574900	C	0.255296	3.137434	0.733471
H	3.833944	0.616343	1.610499	H	0.703563	4.115277	0.507279

Table 7.44: Optimized orthogonal excited singlet LLCT ($\pi\pi^*$) state geometry (S-LLCT $\pi\pi^*$ ortho) of Zn-BDO.

Atom	x	y	z	Atom	x	y	z
Zn	1.072479	0.010608	-0.029392	H	-5.141333	0.286290	-0.082289
O	2.274712	-0.685241	-1.469725	H	-4.338044	-1.277522	-0.281642
O	2.794488	-0.087949	1.018850	C	0.843654	4.027074	1.183131
N	-1.773074	-0.305744	0.289349	H	0.227610	4.905535	1.425292
C	-2.810369	1.784182	0.382337	H	1.890124	4.333026	1.310188
H	-3.341869	2.395246	1.117144	C	-0.932510	2.442235	1.909151
H	-3.183931	2.080511	-0.599676	H	-1.593990	3.280145	2.175529
C	4.528605	-1.277027	-1.919931	H	-1.171135	1.626953	2.599959
H	4.298457	-1.534180	-2.947231	C	0.592287	3.612024	-0.258056
C	5.796104	-1.374357	-1.418022	H	1.300932	2.818635	-0.524252
H	6.604448	-1.718252	-2.053765	H	0.820066	4.450902	-0.926575
C	-1.190113	-2.525718	1.183089	C	-0.627257	-1.408043	-3.346974
C	-3.567052	-0.002137	2.018968	H	-0.419839	-2.408154	-3.747679
H	-3.726856	-1.073775	2.166439	H	0.258314	-1.072226	-2.800651
H	-4.522952	0.503056	2.197047	H	-0.779431	-0.733579	-4.198642
H	-2.858875	0.349753	2.772056	C	-0.946746	-1.997847	2.588182
C	6.083800	-1.029524	-0.065207	H	-1.164155	-0.931295	2.582564
H	7.103182	-1.121619	0.292956	C	-1.279863	1.995491	0.459601
C	-1.442105	-3.623576	-1.369355	C	-1.634081	-2.252424	-1.204415
H	-1.517101	-4.056331	-2.361689	C	0.501575	2.899821	2.148135
C	-1.869000	-1.415296	-2.451147	H	1.175741	2.059665	1.935401
H	-2.035396	-0.386600	-2.132952	C	-1.144228	2.926404	-2.009517

Atom	x	y	z	Atom	x	y	z
C	-1.144012	-4.444344	-0.296201	H	-1.969787	2.212021	-2.086201
H	-1.001664	-5.510566	-0.444956	C	-0.735037	0.612039	0.140573
C	-1.005904	-3.891075	0.963879	C	0.518469	-2.155625	3.006484
H	-0.741036	-4.533269	1.797635	H	0.815544	-3.210868	3.037425
C	-1.551713	-1.700065	0.094183	H	0.669152	-1.739937	4.010450
C	-3.094157	0.288408	0.591155	H	1.198649	-1.632126	2.327322
C	-1.847720	-2.667034	3.629864	C	0.718674	3.303761	3.600283
H	-2.905064	-2.620138	3.352615	H	1.755191	3.618671	3.773443
H	-1.731375	-2.175337	4.603234	H	0.502316	2.471775	4.281698
H	-1.586565	-3.723369	3.763487	H	0.064607	4.141041	3.877713
C	-3.087947	-1.877609	-3.253023	C	-1.621819	4.226587	-2.656018
H	-3.280401	-1.184816	-4.081302	H	-0.859892	5.013372	-2.579074
H	-3.990877	-1.927101	-2.636991	H	-2.533991	4.600226	-2.175178
H	-2.927324	-2.870568	-3.689064	H	-1.839154	4.082487	-3.721687
C	3.767760	-0.474272	0.308306	C	0.002732	2.332729	-2.824592
C	3.473629	-0.821814	-1.087386	H	-0.334373	2.131805	-3.849114
C	5.102263	-0.589932	0.777886	H	0.345226	1.385179	-2.399782
H	5.309416	-0.325981	1.808333	H	0.857835	3.015266	-2.891421
C	-4.194300	-0.193925	-0.352843	C	-0.846886	3.147620	-0.501557
H	-3.978191	0.061058	-1.392061	H	-1.480599	3.991992	-0.194171

Table 7.45: Optimized planar excited triplet LLCT ($\pi\pi^*$) state geometry (T-LLCT $\pi\pi^*$ planar) of Zn-BDO.

Atom	x	y	z	Atom	x	y	z
Zn	0.862443	0.307817	-0.020352	H	-5.218366	-0.912328	0.057239
O	2.279930	-1.063136	-0.311371	H	-4.070430	-2.258115	0.000565
O	2.419880	1.535894	-0.348376	C	-0.256896	4.216770	0.755460
N	-1.808967	-0.662530	0.428366	H	-1.044964	4.965522	0.924629
C	-3.310797	1.126458	0.343085	H	0.700098	4.751846	0.807066
H	-3.959791	1.664736	1.039328	C	-1.632841	2.382436	1.721459
H	-3.758856	1.234031	-0.646494	H	-2.462312	3.081996	1.902857
C	4.591285	-1.317943	-0.782771	H	-1.684483	1.625839	2.512021
H	4.519806	-2.398877	-0.764546	C	-0.431000	3.596042	-0.622876
C	5.769192	-0.675112	-1.026418	H	0.436501	2.964231	-0.837526
H	6.670915	-1.248669	-1.209343	H	-0.421480	4.388428	-1.381328

Atom	x	y	z	Atom	x	y	z
C	-0.762564	-2.590000	1.555048	C	-0.353626	-1.842291	-3.043993
C	-3.629452	-0.618903	2.153897	H	0.102693	-2.802118	-3.315071
H	-3.544012	-1.680094	2.402425	H	0.401823	-1.243065	-2.526258
H	-4.674387	-0.325980	2.305704	H	-0.620439	-1.322603	-3.972195
H	-3.016629	-0.047899	2.855055	C	-0.607376	-1.857160	2.878396
C	5.846549	0.751335	-1.046251	H	-1.013356	-0.854500	2.749787
H	6.804887	1.218205	-1.244400	C	-1.872794	1.695254	0.348108
C	-0.759144	-3.993791	-0.855908	C	-1.224261	-2.679847	-0.841685
H	-0.729067	-4.538976	-1.793775	C	-0.333169	3.165971	1.855781
C	-1.595241	-2.041032	-2.170212	H	0.504415	2.467754	1.718039
H	-1.995687	-1.049492	-1.961264	C	-1.984079	2.327221	-2.216071
C	-0.323943	-4.616001	0.300720	H	-2.592063	1.418007	-2.177300
H	0.026949	-5.643269	0.271514	C	-1.011061	0.450812	0.183930
C	-0.312184	-3.908349	1.488917	C	0.870458	-1.702709	3.254898
H	0.068309	-4.386577	2.385791	H	1.330968	-2.674330	3.470212
C	-1.276775	-1.984233	0.386813	H	0.969175	-1.082235	4.154111
C	-3.233740	-0.366559	0.696714	H	1.448457	-1.233548	2.452883
C	-1.349121	-2.537880	4.031767	C	-0.193899	3.779746	3.242393
H	-2.406640	-2.701216	3.806579	H	0.750455	4.329747	3.339155
H	-1.288391	-1.921321	4.936835	H	-0.215881	3.009816	4.023599
H	-0.905905	-3.511962	4.269550	H	-1.011889	4.483717	3.445110
C	-2.653512	-2.835624	-2.938515	C	-2.800977	3.375786	-2.971052
H	-2.964920	-2.283941	-3.833840	H	-2.271467	4.336802	-3.012236
H	-3.543961	-3.023813	-2.330820	H	-3.769864	3.551580	-2.488150
H	-2.266049	-3.805522	-3.271583	H	-2.993093	3.061072	-4.004402
C	3.492187	0.907275	-0.565427	C	-0.739593	1.965589	-3.025293
C	3.413119	-0.558964	-0.545219	H	-1.036601	1.575397	-4.006844
C	4.746082	1.525685	-0.822774	H	-0.149964	1.190524	-2.528010
H	4.793787	2.608027	-0.835640	H	-0.094619	2.833976	-3.200947
C	-4.183085	-1.183338	-0.178437	C	-1.726859	2.790977	-0.754976
H	-4.022618	-0.989430	-1.241054	H	-2.536072	3.497646	-0.520682

Table 7.46: Optimized queer excited triplet LLCT ($\pi\pi^*$) state geometry (T-LLCT $\pi\pi^*$ queer) of Zn-BDO.

Atom	x	y	z	Atom	x	y	z
Zn	-1.043318	-0.230400	-0.157823	H	4.990899	1.150349	0.413312
O	-1.985477	-1.816519	0.621127	H	4.491543	-0.547273	0.424303
O	-2.960636	0.357456	-0.426304	C	-1.507927	3.802522	-1.030568
N	1.831263	-0.020011	-0.281160	H	-1.065084	4.800277	-1.168165
C	2.452946	2.225202	-0.125121	H	-2.585349	3.909527	-1.210576
H	2.900164	2.989301	-0.766958	C	0.582288	2.654445	-1.737461
H	2.700662	2.496468	0.903079	H	1.080851	3.624064	-1.884490
C	-4.136502	-2.694659	1.101794	H	1.018978	1.966227	-2.468895
H	-3.719050	-3.588518	1.549877	C	-1.264987	3.327722	0.394265
C	-5.482917	-2.492171	1.013003	H	-1.828337	2.403355	0.556497
H	-6.168506	-3.238373	1.398809	H	-1.677070	4.061311	1.098044
C	1.779000	-2.228067	-1.372084	C	0.632672	-1.620875	3.133452
C	3.643775	0.767843	-1.827590	H	0.590492	-2.673373	3.439919
H	4.024487	-0.235023	-2.038737	H	-0.248346	-1.413771	2.519162
H	4.488612	1.462702	-1.891075	H	0.570424	-1.006076	4.039748
H	2.928976	1.038701	-2.607606	C	1.515401	-1.643499	-2.750546
C	-6.018974	-1.310253	0.416395	H	1.484234	-0.559616	-2.647514
H	-7.095832	-1.193107	0.367698	C	0.919049	2.152621	-0.305703
C	2.067134	-3.463968	1.112312	C	1.976662	-2.073975	1.058223
H	2.154381	-3.955256	2.075999	C	-0.896705	2.846481	-2.046618
C	1.926442	-1.313978	2.373907	H	-1.399348	1.876632	-1.940761
H	1.910271	-0.249498	2.142262	C	0.460886	2.801352	2.211537
C	2.034613	-4.233731	-0.036937	H	1.366916	2.192090	2.286178
H	2.112021	-5.315074	0.025640	C	0.629598	0.666566	-0.135258
C	1.875279	-3.615445	-1.263798	C	0.153663	-2.085369	-3.296780
H	1.813086	-4.225100	-2.159497	H	0.119286	-3.168951	-3.460893
C	1.881380	-1.442149	-0.201928	H	-0.044666	-1.596836	-4.258598
C	3.031323	0.834573	-0.425654	H	-0.662437	-1.825320	-2.615167
C	2.603825	-2.004806	-3.765084	C	-1.107461	3.321178	-3.478121
H	3.604880	-1.746264	-3.408344	H	-2.174437	3.445128	-3.701485
H	2.433916	-1.473229	-4.709208	H	-0.694368	2.605996	-4.200360
H	2.598453	-3.078149	-3.988150	H	-0.616409	4.288443	-3.649124

Atom	x	y	z	Atom	x	y	z
C	3.135891	-1.595126	3.268571	C	0.727626	4.093365	2.983639
H	3.110172	-0.947747	4.153601	H	-0.126015	4.780457	2.912996
H	4.081513	-1.417548	2.747277	H	1.607938	4.617597	2.592315
H	3.140720	-2.632343	3.623523	H	0.901962	3.892384	4.048057
C	-3.793303	-0.493116	-0.009711	C	-0.639379	2.003728	2.910649
C	-3.243488	-1.713229	0.593437	H	-0.328280	1.765275	3.935415
C	-5.204862	-0.337283	-0.084800	H	-0.839908	1.057010	2.400804
H	-5.599435	0.564940	-0.536931	H	-1.577204	2.566802	2.977760
C	4.137903	0.479680	0.566270	C	0.217716	3.110965	0.707673
H	3.807632	0.593815	1.600557	H	0.701549	4.080185	0.519248

Table 7.47: Optimized orthogonal excited triplet LLCT ($\pi\pi^*$) state geometry (T-LLCT $\pi\pi^*$ ortho) of Zn-BDO.

Atom	x	y	z	Atom	x	y	z
Zn	1.068957	-0.078697	0.063079	H	-5.142687	0.361322	-0.058774
O	2.298728	-0.846272	-1.312179	H	-4.382578	-1.222897	-0.269788
O	2.822844	0.134138	1.048169	C	0.970779	3.928639	1.096683
N	-1.791964	-0.324647	0.300941	H	0.400867	4.833511	1.354559
C	-2.774750	1.792315	0.422955	H	2.032637	4.191903	1.186267
H	-3.267083	2.403128	1.184738	C	-0.839279	2.415012	1.894597
H	-3.169417	2.119809	-0.540711	H	-1.464431	3.278775	2.166712
C	4.589025	-1.252971	-1.781623	H	-1.088353	1.616460	2.602101
H	4.360052	-1.644949	-2.765636	C	0.652473	3.525356	-0.335452
C	5.870314	-1.180175	-1.313471	H	1.328761	2.720299	-0.648498
H	6.692574	-1.520038	-1.933300	H	0.868082	4.366802	-1.005130
C	-1.287334	-2.574266	1.173389	C	-0.629956	-1.412972	-3.320987
C	-3.568777	0.011741	2.041172	H	-0.448075	-2.412478	-3.735303
H	-3.754273	-1.056275	2.183444	H	0.254813	-1.117345	-2.749895
H	-4.510884	0.539359	2.227506	H	-0.740755	-0.718436	-4.162722
H	-2.847193	0.342816	2.791589	C	-1.031425	-2.074370	2.586905
C	6.155597	-0.663206	-0.015277	H	-1.213762	-1.001245	2.597372
H	7.187165	-0.623552	0.316568	C	-1.237333	1.963094	0.461835
C	-1.557406	-3.631350	-1.394882	C	-1.701594	-2.256663	-1.213432
H	-1.638814	-4.048375	-2.393424	C	0.616712	2.824535	2.084921
C	-1.889260	-1.393953	-2.450217	H	1.255352	1.960081	1.866354

Atom	x	y	z	Atom	x	y	z
H	-2.029170	-0.365696	-2.118813	C	-1.159772	2.868368	-2.018340
C	-1.298705	-4.475494	-0.329668	H	-1.965200	2.128983	-2.063163
H	-1.193689	-5.544290	-0.490436	C	-0.731287	0.563627	0.140706
C	-1.150481	-3.942633	0.937927	C	0.426094	-2.285924	3.009287
H	-0.914126	-4.604127	1.765121	H	0.694263	-3.349117	3.012575
C	-1.612625	-1.723433	0.092180	H	0.583314	-1.900499	4.024073
C	-3.095334	0.301656	0.613981	H	1.124805	-1.763092	2.347989
C	-1.955408	-2.730306	3.617080	C	0.890522	3.239671	3.524488
H	-3.009815	-2.650863	3.336343	H	1.941882	3.520921	3.662796
H	-1.829533	-2.253825	4.596745	H	0.666914	2.424042	4.223263
H	-1.724460	-3.795014	3.738970	H	0.273723	4.102182	3.810188
C	-3.107638	-1.803237	-3.280795	C	-1.700170	4.155185	-2.640998
H	-3.260878	-1.092644	-4.102167	H	-0.958718	4.963343	-2.586813
H	-4.022774	-1.828961	-2.681227	H	-2.604221	4.499994	-2.124476
H	-2.974346	-2.795112	-3.728352	H	-1.952412	4.009712	-3.698840
C	3.808402	-0.268068	0.365817	C	-0.029729	2.310555	-2.881125
C	3.515037	-0.809150	-0.966571	H	-0.407834	2.077953	-3.884344
C	5.157936	-0.220988	0.806111	H	0.376043	1.387990	-2.458214
H	5.363263	0.176102	1.793260	H	0.789878	3.028479	-3.000317
C	-4.209187	-0.143056	-0.332541	C	-0.805054	3.096320	-0.523005
H	-3.985173	0.113174	-1.370018	H	-1.405737	3.958715	-0.199903

Table 7.48: Optimized excited singlet LLCT (Dipp) state geometry (S-LLCT Dipp) of Zn-BDO.

Atom	x	y	z	Atom	x	y	z
Zn	0.808523	-0.391339	-0.041747	H	-5.148412	-0.803611	-0.199435
O	2.073190	-0.218212	-1.610363	H	-4.002562	-2.155523	-0.276805
O	2.494020	0.152613	0.964893	C	0.042269	4.035551	0.594604
N	-1.761758	-0.588329	0.381294	H	-0.651241	4.871770	0.765149
C	-3.310849	1.195530	0.423929	H	1.052819	4.462457	0.589137
H	-3.849740	1.665520	1.250479	C	-1.476473	2.388675	1.679347
H	-3.872388	1.424550	-0.483525	H	-2.230378	3.163292	1.874154
C	4.270961	0.468143	-2.171332	H	-1.577359	1.654553	2.487859
H	4.086048	0.311431	-3.227726	C	-0.255251	3.389959	-0.750276
C	5.479909	0.910303	-1.709439	H	0.507373	2.629440	-0.953811

Atom	x	y	z	Atom	x	y	z
H	6.285231	1.111171	-2.407529	H	-0.165189	4.138582	-1.545668
C	-0.923496	-2.557925	1.699865	C	-0.163088	-2.439078	-2.921923
C	-3.634350	-0.745548	2.031138	H	0.037194	-3.504974	-3.085219
H	-3.511311	-1.821374	2.177284	H	0.687337	-2.015294	-2.381059
H	-4.691003	-0.498731	2.180476	H	-0.209227	-1.951409	-3.904208
H	-3.055372	-0.218432	2.793585	C	-0.546421	-1.758660	2.940338
C	5.705890	1.114986	-0.318819	H	-0.772083	-0.704754	2.752586
H	6.677905	1.466772	0.009240	C	-1.859433	1.722644	0.331735
C	-1.343260	-4.164870	-0.566639	C	-1.372947	-2.798723	-0.744120
H	-1.482519	-4.806708	-1.431793	C	-0.095814	3.034175	1.735021
C	-1.483127	-2.256242	-2.161818	H	0.660578	2.252380	1.589601
H	-1.676143	-1.181134	-2.104136	C	-2.011403	2.263575	-2.237564
C	-1.114991	-4.762113	0.675414	H	-2.783983	1.493103	-2.142099
H	-1.115872	-5.840812	0.782507	C	-1.045567	0.468254	0.191246
C	-0.910205	-3.931995	1.782875	C	0.959414	-1.856291	3.220345
H	-0.710756	-4.394314	2.745281	H	1.231723	-2.884410	3.487572
C	-1.095607	-1.923694	0.392822	H	1.240176	-1.205504	4.058273
C	-3.230723	-0.331448	0.621994	H	1.562719	-1.559012	2.357829
C	-1.306083	-2.170452	4.203825	C	0.151201	3.675209	3.093886
H	-2.390112	-2.157387	4.063686	H	1.149131	4.127336	3.139478
H	-1.061902	-1.489591	5.028295	H	0.079912	2.937400	3.902208
H	-1.025391	-3.179526	4.525786	H	-0.583911	4.465384	3.295398
C	-2.613789	-2.879773	-2.984068	C	-2.630421	3.398403	-3.052531
H	-2.702672	-2.368560	-3.950453	H	-1.933464	4.239701	-3.156416
H	-3.581195	-2.819242	-2.478188	H	-3.543703	3.777617	-2.579005
H	-2.416371	-3.936545	-3.196381	H	-2.891035	3.059551	-4.062330
C	3.451021	0.403121	0.175814	C	-0.859179	1.633386	-3.018546
C	3.217375	0.194453	-1.259844	H	-1.238108	1.192831	-3.948209
C	4.721593	0.874809	0.599744	H	-0.352516	0.839923	-2.461576
H	4.881699	1.028008	1.660799	H	-0.102878	2.376913	-3.293719
C	-4.101701	-1.072026	-0.381117	C	-1.648155	2.755568	-0.811703
H	-3.857188	-0.792861	-1.408873	H	-2.365988	3.552063	-0.572657

Table 7.49: Optimized excited triplet LE_BDT state geometry of Zn-BDO.

Atom	x	y	z	Atom	x	y	z
Zn	1.598693	7.480808	12.330896	H	4.749281	3.056844	15.361451
O	-0.080223	7.318624	11.433587	H	4.475011	2.935778	13.619070
O	1.782441	9.238644	11.536539	C	1.823804	9.550976	15.956590
N	3.516769	5.562118	13.341648	H	2.183837	9.614868	16.993497
C	3.790529	5.671370	15.677371	H	1.256587	10.469072	15.763210
H	4.596251	6.022938	16.324506	C	3.764647	8.159701	15.259454
H	3.190578	4.980840	16.271695	H	4.175338	8.186824	16.276467
C	-1.469065	8.584029	9.909324	H	4.627674	8.091614	14.586915
H	-2.268271	7.849877	9.965473	C	0.913421	8.342164	15.805991
C	-1.477854	9.579789	8.993021	H	0.443337	8.371974	14.817814
H	-2.295452	9.654837	8.279199	H	0.088139	8.413203	16.523072
C	4.540994	5.722801	11.096057	C	0.266174	3.866030	11.748442
C	5.837659	5.217650	14.244317	H	0.127875	3.398864	10.766314
H	6.200947	4.765979	13.318283	H	0.152669	4.947306	11.622976
H	6.385609	4.761384	15.074470	H	-0.539415	3.510247	12.401459
H	6.073029	6.283872	14.239494	C	5.399120	6.928135	11.453485
C	-0.431769	10.572019	8.950814	H	5.255257	7.153958	12.509378
H	-0.471990	11.358708	8.204443	C	2.928205	6.849276	15.168641
C	2.909531	3.627524	10.213807	C	2.759318	4.080498	11.522418
H	2.264396	2.835530	9.850379	C	3.022688	9.470686	15.019959
C	1.625894	3.487923	12.346686	H	2.653751	9.499394	13.987508
H	1.663762	3.917490	13.348673	C	0.671868	5.797133	16.020323
C	3.847808	4.179168	9.360937	H	1.263469	4.896372	15.821842
H	3.946470	3.808272	8.345825	C	2.738292	6.530775	13.701954
C	4.638232	5.226093	9.797544	C	4.969504	8.173265	10.669486
H	5.343183	5.678934	9.109492	H	5.083993	8.018305	9.590387
C	3.616887	5.107618	11.964829	H	5.605120	9.021532	10.950752
C	4.352402	4.945035	14.450538	H	3.930475	8.457626	10.864912
C	6.892111	6.670023	11.231126	C	3.964457	10.655035	15.195477
H	7.238385	5.761472	11.732322	H	3.439766	11.600300	15.014769
H	7.477276	7.513124	11.615594	H	4.807684	10.600982	14.496518
H	7.123668	6.571083	10.164855	H	4.372783	10.686581	16.214032
C	1.726351	1.966847	12.486191	C	0.045035	5.604342	17.400897
H	0.945357	1.602670	13.163543	H	-0.541721	6.482074	17.698773

Atom	x	y	z	Atom	x	y	z
H	2.694432	1.647732	12.882519	H	0.811120	5.437611	18.167111
H	1.579975	1.469088	11.521183	H	-0.629660	4.740369	17.405921
C	0.771935	9.452602	10.741237	C	-0.423713	5.843784	14.957278
C	-0.377192	8.497590	10.898182	H	-0.983803	4.901780	14.962219
C	0.707137	10.457848	9.810378	H	-0.035267	5.978456	13.942918
H	1.518726	11.177745	9.752901	H	-1.139628	6.650887	15.145951
C	4.145781	3.439673	14.532292	C	1.637905	7.011704	16.028479
H	3.105196	3.176505	14.731686	H	2.045885	7.063492	17.046624

Table 7.50: Optimized excited triplet LE_CAAC state geometry of Zn-BDO.

Atom	x	y	z	Atom	x	y	z
Zn	1.662256	7.506691	12.350377	H	4.585197	3.065220	15.515561
O	-0.012646	7.318733	11.459528	H	4.410573	2.878989	13.763682
O	1.789426	9.261527	11.589369	C	1.806481	9.562579	15.954249
N	3.565460	5.562466	13.381699	H	2.155627	9.633003	16.994563
C	3.845516	5.721886	15.713650	H	1.226183	10.471247	15.754852
H	4.677987	6.102988	16.308241	C	3.778159	8.204768	15.279818
H	3.270639	5.065152	16.368116	H	4.176434	8.243034	16.301645
C	-1.389942	8.608080	9.990664	H	4.651105	8.147243	14.618017
H	-2.119611	7.803640	9.947504	C	0.916749	8.339153	15.796184
C	-1.592689	9.796019	9.280063	H	0.453324	8.362623	14.804855
H	-2.489532	9.917075	8.678265	H	0.085145	8.396241	16.507338
C	4.451175	5.718364	11.100214	C	0.546700	4.022350	11.163004
C	5.850868	5.136216	14.262478	H	0.698638	3.550761	10.184524
H	6.180250	4.619292	13.356960	H	0.577057	5.110159	11.041703
H	6.404324	4.717479	15.108930	H	-0.460399	3.759181	11.509679
H	6.111628	6.195167	14.180558	C	5.256825	6.983941	11.318175
C	-0.651355	10.809941	9.346507	H	5.100643	7.315721	12.347045
H	-0.800889	11.735532	8.796851	C	2.967331	6.880146	15.182659
C	3.535090	3.050096	10.557351	C	2.993992	3.815470	11.699951
H	3.319684	1.989964	10.470770	C	3.014973	9.501137	15.028156
C	1.594107	3.526205	12.172118	H	2.653091	9.519136	13.993162
H	1.430257	4.076715	13.104515	C	0.719340	5.788407	16.005436
C	4.246600	3.696133	9.609467	H	1.331431	4.899116	15.817438
H	4.600391	3.180399	8.721248	C	2.794538	6.548023	13.715612

Atom	x	y	z	Atom	x	y	z
C	4.584622	5.072956	9.797017	C	4.808906	8.123327	10.398178
H	5.076744	5.611350	8.996808	H	4.911476	7.851768	9.341212
C	3.695651	5.077441	12.030813	H	5.442398	9.001078	10.572008
C	4.360410	4.933567	14.503759	H	3.773042	8.421850	10.585396
C	6.756836	6.724376	11.134316	C	3.932581	10.703595	15.208312
H	7.113985	5.900182	11.758620	H	3.392117	11.638402	15.019432
H	7.322625	7.623476	11.403771	H	4.783292	10.663080	14.517503
H	6.996122	6.484775	10.092379	H	4.330857	10.746475	16.230523
C	1.373349	2.040476	12.472286	C	0.076849	5.584718	17.377345
H	0.389739	1.897469	12.933811	H	-0.532031	6.450528	17.665574
H	2.129906	1.642231	13.156732	H	0.835110	5.434696	18.154713
H	1.393570	1.438164	11.557177	H	-0.580001	4.707032	17.374184
C	0.718156	9.470540	10.837708	C	-0.363831	5.811836	14.928050
C	-0.251991	8.425273	10.767668	H	-0.900838	4.856397	14.923924
C	0.500162	10.643433	10.123212	H	0.031732	5.962477	13.918475
H	1.247325	11.430482	10.184540	H	-1.101634	6.600342	15.111867
C	4.061388	3.445165	14.631755	C	1.661973	7.021262	16.025394
H	2.992492	3.259453	14.768678	H	2.055642	7.080619	17.048697

7.2.3 Emission Spectra

The emission spectrum of the planar conformer is shown in the figure below. The red spectrum is composed of all modes and lies in the region of negative energy. By neglecting one of the 246 modes the spectrum shift to higher and positive wavelength. Thus, the shape of the spectrum agrees much better with the spectrum of the queer conformer. The neglected mode was selected because of its high displacement value.

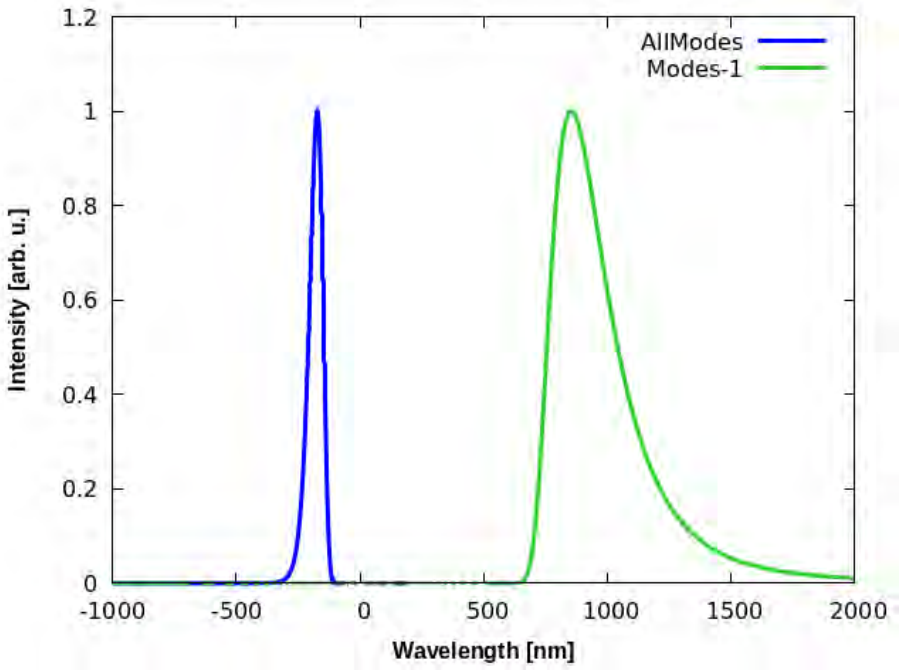

Fig. 7.6: Emission spectra of the planar S-LLCT $\pi\pi^*$ state at 298K for Zn-BDO.